國 立 交 通 大 學

電子工程學系電子研究所

博 士 論 文

銦錫氧化物電極與表面結構改進新穎氮化鎵發光元件特性之研究

Novel GaN-based Light-emitting Devices with Indium Tin Oxide Contacts and Surface Structure Modifications

研 究 生 ：朱 俊 宜

指導教授 ：張 國 明

中華民國九十六年一月

銦錫氧化物電極與表面結構改進新穎氮化鎵發光元件特性之研究

Novel GaN-based Light-emitting Devices with Indium Tin Oxide Contacts and Surface Structure Modifications

研 究 生：朱俊宜　　Student: Jiunn-Yi Chu

指導教授 ： 張國明 博士　　Advisor: Dr. Kow-Ming Chang

國立交通大學

電子工程學系電子研究所

博士論文

A Dissertation

Submitted to Department of Electronics Engineering & Institute of Electronics

College of Electrical and Computer Engineering

National Chiao Tung University

In Partial Fulfillment of Requirements

For the Degree of Doctor of Philosophy

In

Electronics Engineering

January 2007

Hsinchu, Taiwan, Republic of China

中 華 民 國 九 十 六 年 一 月

銦錫氧化物電極與表面結構改進新穎氮化鎵發光元件特性之研究

研究生：朱俊宜　　　　　　　　　　指導教授：張國明 博士

國立交通大學

電子工程系電子研究所

摘要

最近氮化鎵發光元件由於其多用途的應用和市場需求的迅速的發展吸引了眾人的目光，並使得相繼投入研究。自從氮化鎵發光二極體在西元一九九三年問世以來，高亮度氮化鎵發光二極體已成功地應用在行動電話鍵盤的發光模組、液晶顯示器背光源、照相機閃光燈和高色彩飽和度的戶外顯示器上。而這些發光元件更被視為將改變人們的生活模式並且舒緩嚴重的能源危機，不過依照目前元件的發光效率，氮化鎵發光二極體仍然比不上傳統的光源系統，因此氮化鎵發光二極體若要應用在固態照明上並且取代傳統的光源系統，許多限制了光輸出轉換效率的技術，譬如磊晶結構品質、P 型半導體的歐姆電極、出光效率、以及散熱問題等等必須得到長足的改善。

在這篇論文當中，提出了幾種方法來改進氮化鎵發光元件其出光效率，包含使用具有較低吸收係數的導電電極來取代原有的金屬電極以及元件表面結構上的修改。在論文第一部分，採用銦錫氧化物來取代傳統的鎳金電極，並分析其發

光元件的特性，銦錫氧化物為一具有高光穿透性的導電物質，不過由於銦錫氧化物與P型氮化鎵半導體的功函數差異甚大，因此使得銦錫氧化物在P型氮化鎵半導體上呈現蕭基接點的特性，因此在二者間插入一層薄的P型氮化鎵銦磊晶層，以降低其蕭基位能障，形成近似甌姆特性的接點。經由 XPS, XRD及 SIMS分析的結果，其介面形成機制主要是由於鎵原子的擴散並和氧化物的氧原子形成鍵結，造成鎵原子空缺，使得局部載子濃度的提高，進而提升內建電場強度和載子穿遂此介面的機率，因而降低此界面接觸電阻，形成近似歐姆接點。在分析此歐姆介面的主要電流傳導機制時，量測環境溫度對介面接觸電阻係數的影響，發現此介面電流的主要傳導機制和介面的合金條件相關，在不同的合金溫度處理下，當處理溫度由 400°C提高成 600°C時，此介面的主要傳導電流機制為熱場發射傳導傾向為熱離子發射傳導。

雖然銦錫氧化物無法形成較鎳金電極良好之甌姆接點於P型氮化鎵上，但在相當於元件正常工作條件 27 A-cm^{-2}的電流密度流過銦錫氧化物和P型氮化鎵的介面時，其接觸電阻係數約 2.6 x 10^{-2} ohm-cm^{2} ，雖然仍未盡理想，但是已經足夠應用在二極體上，而不至於產生過多的串接電阻，進而損耗過多的能量。使用銦錫氧化物為電極的氮化鎵發光二極體其整體特性表現如下，當 20 mA的電流注入時，順向電壓約為 3.43 V，雖然比傳統上使用鎳金金屬電極的發光二極體高了約 0.2 V， 但是外部量子效率和能量轉換效率卻分別提升了 46% 和 36%，這效率上的提升主要是減少了半透明金屬電極的吸收。 至於壽命試驗，經過 500°C退火處理的銦錫氧化物氮化鎵發光二極體，表現了類似傳統上使用鎳金金屬層的氮化鎵發光二極體的可靠度行為。因此，藉由中間層P型氮化鎵銦磊晶層的加入，使得銦錫氧化物能夠應用在高亮度、高可靠度的氮化鎵發光元件上。

在製作發光元件時，採用平台式的結構，正負電極位於絕緣基板的同一面，所以元件的操作電流為橫向傳導。然而在這個結構下，橫向傳導電流可能導致正

負電極附近電流過度擁擠，此效應將會影響元件的可靠度。因此，妥善的處理橫向傳導電流，避免元件在操作時產生局部過熱的現象是不可或免的。由於銦錫氧化物的導電特性遠不如金屬，所以當應用在氮化鎵發光元件時，必須考慮到透明電極厚度對元件特性的影響。當 20 mA 的電流注入時，60 奈米、180 奈米和 300 奈米厚銦錫氧化物薄膜電極的氮化鎵發光元件的順向電壓分別為 3.45、3.42 及 3.32 V，而輸出光功率則幾乎沒有太大的分別，但是所對應的光輸出轉換效率則和順向電壓及串接電阻成反向關係。除此之外，從元件操作電流密度分佈的模擬，60 奈米厚銦錫氧化物薄膜電極氮化鎵發光元件面臨嚴重電流散佈不均的問題，此問題將會導致電流擁擠效應且產生局部過熱的現象，在實驗中此元件在經過 1008 小時可靠度測試後，光輸出功率衰減了 48%且仍在持續劣化中，而非呈現一穩定的光輸出；相對之下，300 奈米厚銦錫氧化物薄膜電極氮化鎵發光元件在模擬中顯出均勻的電流散佈，且在經過 1008 小時可靠度測試後，光輸出功率呈現一穩定輸出且僅衰減 27%，因此妥善的處理氮化鎵發光元件橫向傳導電流是必需的，尤其對於以低導電係數氧化物導體為電極材料的發光元件，顯得更為重要。

在論文的第二部份，提出兩種表面結構的改良以增進發光元件的出光效率。首先，製作以銦錫氧化物為電極的微尺寸結構，提出一自我對準網狀發光二極體，此新元件的軸向光強度較傳統結構提昇了至少 10%，且並未對操作電壓及反向電流造成影響，同時輸出光有效地集中於正向，使得正向光強度在整個元件光輸出功率的比例遠高於傳統結構元件，此外經由改變網狀結構的尺寸及形狀，其外部量子效率的峰值也提升了 5%。由於軸向光的集中性和外部量子效率的提升，使得此結構有助於在表面黏著型封裝和低功率消耗發光元件上的應用。其次，提出一簡單而不必增加製程步驟的表面結構來增加氮化鎵發光二極體的出光效率，已知在乾蝕刻製程中，不同的蝕刻條件可以造成被蝕刻表面呈現平坦的、

六角狀孔洞、和奈米柱狀等等不同的型態，在此調整蝕刻條件造成被蝕刻面呈現六角孔洞型態，並應用在氮化鎵發光二極體的結構上。具有六角孔洞型態和平整型態的發光元件，不論是順向或者反向偏壓操作，皆呈現相似的電流電壓關係，表示蝕刻條件的變異並不會造成 N 型電極歐姆介面的破壞及被蝕刻側壁的損壞，導致順向偏壓及反向電流的增加，進而影響元件的電流電壓特性。在元件光輸出特性表現上，具有六角孔洞型態的氮化鎵發光二極體在直流電源 20 mA 操作下，正面亮度及整體光輸出功率分別較平整型態的氮化鎵發光二極體提高了 27%及 13%，這效率上的提升主要是六角孔洞型態的表面破壞了空氣-氮化鎵半導體-藍寶石的波導結構，使得部分原先因全反射現象而侷限在此波導結構的光子，透過六角孔洞而傳導入空氣中，因而增加了光強度和輸出功率。

Novel GaN-based Light-emitting Devices with Indium Tin Oxide Contacts and Surface Structure Modifications

Student: Jiunn-Yi Chu Advisor: Dr. Kow-Ming Chang

Department of Electronics Engineering &

Institute of Electronics

National Chiao-Tung University

Hsinchu, Taiwan, R.O.C.

ABSTRACT

GaN-based light-emitting devices have recently attracted much attention for their versatile applications and the rapid growth of market demand. Nowadays, the high-brightness GaN-based LEDs have already successfully applied in the handset keypad, LCD backlighting, camera flash light and full-color outdoor display since their commercial introduction in 1993. These devices are expected to change our life style and will save human beings from serious energy crisis. However, the light output efficiency is still insufficient as compared to that of a conventional light source. In order to fulfill the requirements of applications to solid-state lighting, there are remained many technologies limiting the performance of devices to be improved such as crystal quality, p-type ohmic contact, emission extraction, thermal management, etc.

In the dissertation, several approaches are utilized to improve light output efficiency of GaN-based LEDs including employing a lower absorptive current spreading layer and surface structure modifications. In Part 1, indium tin oxide (ITO) is employed to replace conventional Ni/Au contacts on p-GaN attributed to its high transparency characteristic. However, it is difficult to form an ohmic contact of ITO on p-GaN due to the large work function difference between ITO and p-GaN. Therefore, a thin p-type $In_{0.1}Ga_{0.9}N$ layer is inserted as an intermediate layer to reduce the Schottky barrier height between ITO and p-GaN, because p-$In_{0.1}Ga_{0.9}N$ is supposed to have a narrower band-gap than p-GaN. The transport mechanism of ITO ohmic contacts on p-GaN is characterized and investigated. Based on the variation of the contact resistivity with respect to the ambient temperature, the dominant transport mechanism of ITO/p-GaN interfaces varies with the post alloying temperature. The dominant transport mechanism has a tendency from thermionic-field emission to thermionic emission as rising alloyed temperature from $400^{o}C$ to $600^{o}C$. From the X-ray photoelectron spectroscopy (XPS), x-ray diffraction (XRD), and secondary ion mass spectroscopy (SIMS) results, the out-diffusion of gallium atoms and the formation of Ga-O bonds would introduce the gallium vacancies and increase the net concentration of carriers beneath the contact, which would make the ITO/p-GaN contact reveal ohmic characteristics.

Although ITO contacts does not reveal as good ohmic property as Ni/Au contacts, the contact resistivity is 2.6 x 10^{-2} ohm-cm^{2} at a current density of 27 A-cm^{-2} equivalent to that of 350 um-sized LEDs, and it is low enough for the application of LEDs. GaN-based LEDs with ITO contacts exhibit the forward voltage of 3.43 V at an injection current of 20 mA. The forward voltage is a little higher than the

conventional LEDs by 0.2 V, but the external quantum efficiency and power conversion efficiency are raised by 46% and 36%, respectively. As for the life test, LEDs with ITO contacts annealed at 500°C exhibit a similar reliability as the LEDs with conventional Ni/Au contacts. Therefore, ITO contacts with a thin p-$In_{0.1}Ga_{0.9}N$ intermediate can make GaN-based LED highly bright and reliable in practice.

GaN-based LEDs are fabricated on insulating sapphire substrates, and mesa structures with lateral current conduction are utilized in the devices. However, the lateral current conduction could result in a severe current crowding phenomenon near either n-type or p-type electrode and thus impacts on the reliability of devices. Hence, it is necessary to handle the lateral current conduction to alleviate local hot spots formation as device operated. GaN-based LEDs with various quarter wavelength thicknesses of ITO films are fabricated and characterized. Chips with various thick ITO films show nearly coincident output power-current curves and exhibit an enhancement of 30% as compared with Ni/Au contacts. At a current of 20 mA, the forward voltage is around 3.45, 3.42, and 3.32 V for devices with 60, 180, and 300-nm-thick ITO contacts, respectively. Thus, the power efficiency of LEDs with thicker ITO contacts is higher than with thinner ITO contacts due to the less power consumption. Moreover, from the simulation of current density distribution in devices, the LEDs with 60nm-thick ITO contacts present a worse distribution and it is considered to cause a severe current crowding issue and introduce local hot spots as device operated. Consequently, LEDs with 60nm-thick ITO contacts suffered an output power degradation of 48% after 1008-hour stress. On the other hand, LEDs with 300nm-thick ITO contacts exhibits a stable output after 1008-hour stress with merely 27% decay. Therefore, it is very important to handle the lateral current

conduction especially for devices with conductive oxide materials of low conductivity.

In Part 2, two surface structure modifications were proposed to increase the light extraction coefficient. First, a feasible method for fabricating micro-LEDs with ITO contact is demonstrated. In comparison with the conventional structured LEDs, the self-aligned micro-net ones are a least 10% brighter in the normal direction and 25% higher in the ratio of luminescence to total output power without sacrifice of operating voltage and leakage current. Moreover, the peak value of external quantum efficiency can be increased by 5% by varying the dimensions and the density of the holes at low current driving. With higher normal luminescence and external quantum efficiency, LEDs with such a structure are quite useful in surface-mounting and low-power-consuming devices.

Secondly, a simple way to increase extraction efficiency of GaN-based LEDs without taking any other extra processing step is presented. A mesa structure formed by dry etch is utilized in GaN-based LEDs, and the exposed n-GaN surface could reveal various morphologies, such as smooth surface, nano-rods or hexagonal cavities dependent on various etching conditions. LEDs with smooth morphology and hexagonal cavities on exposed n-GaN layers are fabricated and characterized. Both LEDs with various morphologies on n-GaN show very similar electrical properties. It means that the dry etching condition to reveal hexagonal cavities on n-GaN surface would neither do damage on the sidewalls of mesas nor deteriorate the n-type ohmic contacts. At 20-mA-current injection, the LEDs with hexagonal cavities on n-GaN exhibit higher normal luminescence and output power by 27% and 13% in comparison with LEDs with smooth surface. The enhancement is mainly attributed to

that photons guided laterally through the air–GaN–sapphire structure are partially interfered and extracted into the air through the hexagonal cavities.

誌謝(Acknowledgements)

首先誠摯的感謝指導教授張國明博士多年來的悉心指導與照顧，使我得以相繼完成碩士與博士學位，在這段攻讀博士學位的過程中，深刻的感受到老師淵博的學識、廣闊的學術視野、嚴謹認真的治學態度和勤奮工作的敬業精神，這些不僅令我在學術上有所精進，待人處世上更是受益匪淺。其次得感謝學長鄭兆禎博士的不吝指導與討論，提供了研究所需的資源，不厭其煩的指出我研究中的缺失，且總能在我迷惘時為我解惑，更是令我由衷的感激。另外得感謝過去在連勇科技一起工作打拼的同仁涂慶明、邱筱珮和黃政國，在那段日子裏，謝謝你們的協助與支持。

修業期間，特別感謝實驗室一同打拼的學長學弟以及同學們，尤其是學長楊知一、鄧一中、鄭兆禎、曾明豪、鍾元鴻、游凱翔、楊文誌與王敬業、同學趙高毅和林俊銘、學弟林建弘、郭俊銘、葉冠華、郭端祥與傅健銘等等，在這段相處的日子當中，受到各位的協助與幫忙，在此深表謝意。另外，對於國家奈米元件實驗室、交大奈米中心和貴重儀器中心的人員，謝謝您們的協助，使得此論文能夠順利完成。

最後，必須感謝我的家人，父母親、大哥、大嫂、姐姐、姊夫、妹妹與我的另一半雅玲在背後支持我，給我生活上的關心與照料，在我懈怠的時候，適時地予以鼓勵，讓我在無後顧之憂下完成學業。

Contents

Chinese Abstract i

English Abstract iv

Acknowledgements viii

Contents ix

Table Captions xii

Figure Captions xiii

Chapter 1 Introduction 1

Chapter 2 III-nitride Semiconductors, Process Technologies, and GaN-based LEDs

2.1 Physical Properties of GaN

2.1.1 Crystal and Band Structure 4

2.1.2 General Physical Properties 7

2.1.3 Internal Electrical Field 8

2.1.4 Polarity 9

2.2 Processing Techniques for III-V Nitride Semiconductors

2.2.1 Epitaxial Growth 12

2.2.2 Metal Contacts 14

2.2.3 High-density-plasma Dry Etch 16

2.3 GaN-based Light-emitting Diodes 17

References

Chapter 3 Highly Reliable GaN-Based Light-Emitting Diodes Formed by p-$In_{0.1}Ga_{0.9}N$/ITO Structure

3.1 Introduction 24

3.2 Experiment 25

3.3 Results and Discussion 29

3.4 Summary 35

References

Chapter 4 Investigation of ITO ohmic contact to p-type GaN

4.1 Introduction 38

4.2 Experiment 39

4.3 Results and Discussion 41

4.4 Summary 49

References

Chapter 5 Influence of ITO films Thickness on the Performance of GaN-based Light-emitting Diodes

5.1 Introduction 51

5.2 Experiment 52

5.3 Results and Discussion 53

5.4 Summary 61

References

Chapter 6 Brightness Enhancement of ITO/GaN LEDs by Self-aligned Micro-net Structures

6.1 Introduction 63

6.2 Experiment 64

6.3 Results and Discussion 67

6.4 Summary 74

References

Chapter 7 Improved Light Output Power of GaN-based Light-Emitting Diodes by Exposing N-type GaN with Hexagonal Cavities

7.1 Introduction 76

7.2 Experiment 78

7.3 Results and Discussion 79

7.4 Summary 84

References

Chapter 8 Conclusion and Future Work

8.1 Conclusion 87

8.2 Future Work 90

Table Captions

Table 2.1 Lattice constants of wurtzite nitrides at room temperature.

Table 2.2 Bandgap energy of wurtzite nitrides at 5 K and room temperature.

Table 2.3 Comparison of semiconductor material properties at 300 K.

Table 2.4 Calculated spontaneous polarization for III-V wurtzite nitrides.

Table 3.1 GaN-based LEDs of different ITO contacts are compared with that of Ni/Au contact.

Table 5.1 Summary of the contact characteristics of conductive layers on p-GaN with Ni/Au layer and with various thicknesses ITO layers

Table 6.1 Comparative data for LEDs with various structures.

Table 7.1 List of ICP dry etching conditions

Figure Captions

Fig. 2.1 (a) Wurtzite crystal structure. (b) Schematic band structure of wurtzite GaN along the k_z direction and in the k_x - k_y plane near Γ point.

Fig. 2.2 Schematic diagram of bandgap energies of wurtzite nitrides in a function of the lattice constant. The colorful area indicates the visible spectra region.

Fig. 2.3 (a) Spontaneous polarization induced by the nonideality of the tetrahedral structure of GaN; (b) Crystal structure of GaN with Ga-face polarity and spontaneous polarization.

Fig. 2.4 Schematic illustration of GaN wurtzite crystal structure exhibiting the polarity along the c-axis.

Fig. 2.5 Energy band diagrams for (a) Ga-face and (b) N-face GaN.

Fig. 2.6 Schematic diagram of GaN-based LEDs on sapphire substrate.

Fig. 3.1 The process flow diagrams of (a) GaN-based LEDs fabrication and (b) TLM structure formation.

Fig. 3.2 Transmittance spectra of the blank p-i-n GaN/sapphire, the ITO and Ni/Au films deposited on p-i-n GaN/sapphire under different annealing conditions.

Fig. 3.3 I-V characteristics of p-$In_{0.1}Ga_{0.9}N$/ITO contacts annealed at 500°C, 600°C and Ni/Au contact annealed at 540°C on p-GaN.

Fig. 3.4 Contact resistivities as functions of injection current density.

Fig. 3.5 The forward voltage and dynamic resistance as functions of injection current of GaN-based LEDs with p-$In_{0.1}Ga_{0.9}N$/ITO and Ni/Au contacts.

Fig. 3.6 The output power and power efficiency as functions of injection current of GaN-based LEDs with p-$In_{0.1}Ga_{0.9}N$/ITO and Ni/Au contacts.

Fig. 3.7 Room temperature life test of degradation of output power from GaN-based LEDs with p-$In_{0.1}Ga_{0.9}N$/ITO and Ni/Au contacts.

Fig. 4.1 The process flow diagrams TLM structure formation.

Fig. 4.2 Transmittance spectra of the blank p-i-n GaN/sapphire, the ITO and Ni/Au films deposited on p-i-n GaN/sapphire under different annealing conditions.

Fig. 4.3 I-V characteristics of ITO/p-GaN contacts annealed at 400°C, 500°C and 600°C and Ni/Au contact annealed at 540°C on p-GaN.

Fig. 4.4 Specific contact resistivities of different contacts on p-GaN as functions of the temperature.

Fig. 4.5 XPS depth profiling of 500°C-annealed ITO contact on p-GaN with different sputtering times.

Fig. 4.6 XRD of the native p-i-n GaN and ITO films deposited on p-GaN with different annealing temperatures.

Fig. 4.7 SIMS profiles of ITO films deposited on p-GaN with different annealing temperatures.

Fig. 4.8 Schematic drawings of the contact interface structures.

Fig. 5.1 The refractive index and extinction coefficient spectra of ITO films.

Fig. 5.2 Transmittance spectra of the double sides polished p-i-n GaN/sapphire samples with various thicknesses of ITO layers and with Ni/Au layers.

Fig. 5.3 SEM pictures of (a) 60 nm (b) 180 nm (c) 300 nm-thick ITO films.

Fig. 5.4 Specific contact resistivity and p-GaN sheet resistance of various contacts on p-GaN.

Fig. 5.5 Current-voltage characteristics of GaN-based LEDs with various thicknesses of ITO layers and Ni/Au layers.

Fig. 5.6 Output power-current characteristics of GaN-based LEDs with various thicknesses of ITO layers and Ni/Au layers.

Fig. 5.7 Room temperature reliability test of output power degradation of GaN-based LEDs with various thick ITO and Ni/Au layers contacts.

Fig. 5.8 Equivalent LED circuit with a *p* pad as a physical ground.

Fig. 5.9 Calculated current density distribution vs. the lateral length in a LED.

Fig. 6.1 Process flow diagrams of micro-net structure LEDs.

Fig. 6.2 Refractive index spectra of ITO and SiOxNy films.

Fig. 6.3 The SEM pictures of conventional LED and micro-net structure LEDs

Fig. 6.4 Measured forward voltages as a function of the injected currents of GaN-based LEDs with self-aligned micro-net and conventional structures.

Fig. 6.5 Normal luminescence and output power as functions of the injected currents of GaN-based LEDs with self-aligned micro-net and conventional structures.

Fig. 6.6 Ratios of normal luminescence to output power as functions of the injected currents of GaN-based LEDs with self-aligned micro-net and conventional structures.

Fig. 6.7 Emission images of LEDs with micro-net structures.

Fig. 6.8 External quantum efficiencies as functions of the injection currents of GaN-based LEDs with self-aligned micro-net and conventional structures.

Fig. 7.1 SEM and Microscopic emission images of the LEDs with smooth and hexagonal-pits n-GaN.

Fig. 7.2 (a) Forward and (b) reverse current-voltage characteristics of the LEDs with different n-GaN morphologies.

Fig. 7.3 Current-luminescence and current-power characteristics of the LEDs with

different exposed n-GaN morphologies.

Fig. 7.4 Ratios of normal luminescence to output power the LEDs with different n-GaN morphologies.

Fig. 7.5 Schematic diagram showing possible extraction paths of the photons laterally guided in the air-GaN-sapphire waveguide structure through hexagonal cavities.

Chapter 1

Introduction

GaN-based light emitting diodes (LEDs) have recently attracted much attention for their versatile applications and the rapid growth of market demand. Nowadays, the high-brightness GaN-based LEDs have already successfully applied in the handset keypad, LCD backlighting, camera flash light and full-color outdoor display since their commercial introduction in 1993. These devices are expected to change our life style and will save human beings from serious energy crisis. However, the light output efficiency is still insufficient as compared to that of a conventional light source. In order to fulfill the requirements of solid-state lighting, there are remained many technologies limiting the applications of devices to be improved such as crystal quality, p-type ohmic contact, emission extraction, thermal management, etc. In this thesis, the works will concentrate on the light output efficiency enhancement of GaN-based LEDs by several approaches including employing a lower absorptive current spreading layer and structure modifications to increase the extract coefficient.

The dissertation is consisted of 8 chapters. After the short introduction in this chapter, some basic properties regarding to the GaN-based LEDs are briefly introduced in chapter 2. Some of the most important properties of III-nitride materials are surveyed in the first section. Then, the process technologies specially developed for the materials including epitaxy, metallization of ohmic contacts, and dry etching are introduced, and finally the common structure of GaN-based LEDs is shown in the last section.

Chapter 3 presents GaN-based LEDs with lower absorptive indium tin oxide (ITO)

films as current spreading layers in comparison with the conventional LEDs with higher absorptive Ni/Au layers. However, it is difficult to form an ohmic contact of ITO on p-GaN due to the large work function difference between ITO and p-GaN. Therefore, a thin p-type $In_{0.1}Ga_{0.9}N$ layer is inserted as an intermediate layer to reduce the Schottky barrier height between ITO and p-GaN, because it is supposed to have a narrower band-gap than p-GaN. The ITO contacts on p-GaN reveal ohmic property with a thin intermediate layer of p-$In_{0.1}Ga_{0.9}N$. The electrical and optical characteristics of the ITO-contact LEDs are demonstrated and in comparison with that of the conventional Ni/Au-contact LEDs. The reliability results of the GaN-based LEDs with ITO and Ni/Au contacts are also discussed in this chapter.

Chapter 4 investigates the ohmic contact formation of indium tin oxide (ITO) contacts on p-type GaN. The ITO contacts reveal ohmic characteristics but not as good as the conventional Ni/Au contacts. The variation of the contact resistivity with respect to temperature measurement is utilized to justify the transport mechanism of this contact. The XPS, XRD and SIMS analyses are also introduced to understand the formation mechanism of the ohmic contacts.

Chapter 5 discusses the influence of the various thicknesses of ITO films on the performance of GaN-based LEDs. GaN-based LEDs are fabricated on insulating sapphire substrates and mesa structures with lateral current conduction are utilized in the devices. The lateral current conduction could result in a severe current crowding phenomenon near either n-type or p-type electrode and thus impacts on the reliability of devices. It is necessary to handle the lateral current conduction to alleviate this effect. Here LEDs with quarter wavelength thicknesses of ITO films are fabricated and characterized.

Chapter 6 presents a feasible method for fabricating micro-LEDs with ITO contact. The sidewalls in micro-LEDs are important in the extraction of light from the mesa

structure. A higher ratio of the total surface-area, including the top and sidewall areas, to the light-emission-area is desired, because then more pathways are available by which the generated photons can escape. In this chapter, a simplified method of fabricating micro-LEDs with ITO contacts on p-GaN and SiO_xN_y protection layers is demonstrated to increase the light extraction area and shorten the optical paths. The micro-net LEDs are also characterized and compared with the conventional structures.

Chapter 7 presents a simple way to increase extraction efficiency of GaN-based LEDs without taking any other extra processing step. Proper dry etching condition would result in smooth, hexagonal pits or nano-rods morphology. GaN-based LEDs with exposed hexagonal-pits n-GaN were fabricated and characterized in this work. The photons guided laterally through the air–GaN–sapphire structure are partially interfered and extracted through the hexagonal cavities into the air. Therefore, optical performance of LED is improved by utilizing this approach in comparison with the conventional structure.

Finally, the summaries of this thesis and a suggestion for the future work are addressed in chapter 8.

Chapter 2

III-nitride Semiconductors, Process Technologies, and GaN-based LEDs

In this chapter, some basic properties regarding to GaN-based light emitting diodes (LEDs) are briefly introduced. Some of the most important properties of III-nitride materials are surveyed in the first part. Then, the process technologies specially developed for the materials including epitaxy, metallization of ohmic contacts, and dry etching are introduced, and finally the common structure of GaN-based LEDs is presented.

2.1 Physical Properties of III-Nitride Semiconductors

2.1.1 Crystal and band structure

The III-nitride semiconductors (AlN, GaN and InN) crystallize preferentially in hexagonal wurtzite structure. The cubic zinc-blende phase of GaN is metastable and is observed only for heteroepitaxial layers on a cubic substrate like GaAs. Though cubic nitrides are expected to have possible technical advantages in electrical properties, high crystal quality cannot be easily achieved due to the metastability of the cubic form. The wurtzite nitrides have provided the best results to date for optoelectronic application, and this study is mainly concerned with the material.

The wurtzite crystal structure is shown in Figure 2.1(a). There are two interpenetrating hexagonal close-packed structures, displaced from each other along the c-axis by u. The lattice constants appropriate to this structure are given in Table 2.1 for nitrides. The lattice constants vary strongly with the chemical compositions, leading to a large lattice mismatch for heterojunctions; e.g. 2.5% for GaN/AlN, 11% for InN/GaN.

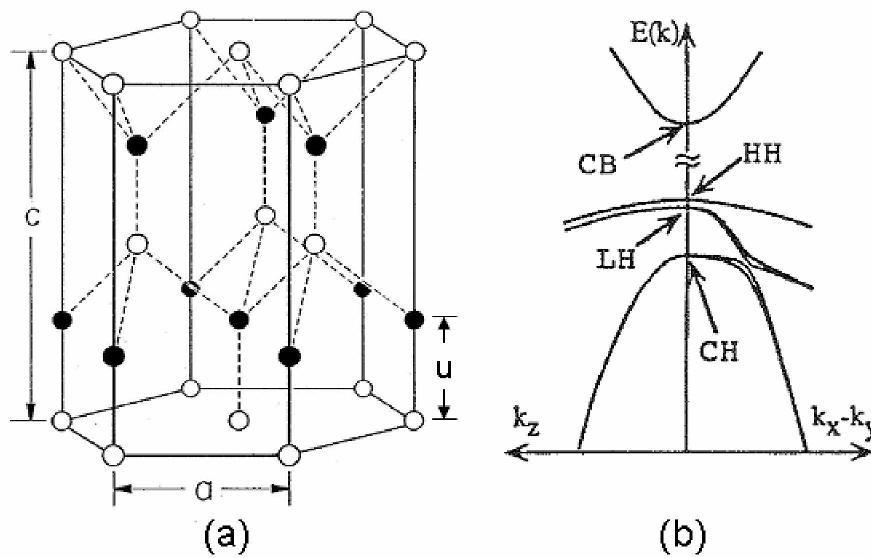

Fig. 2.1 (a) Wurtzite crystal structure [1]. (b) Schematic band structure of wurtzite GaN along the k_z direction and in the k_x - k_y plane near Γ point [2].

Table 2.1 Lattice constants of wurtzite nitrides at room temperature [3]. For an ideal closed packed hexagonal structure *c*/*a*=1.633 and *u*=0.375.

Lattice Parameters	AlN	GaN	InN
a (Å)	3.110±0.002	3.1892±0.0009	3.540±0.008
c (Å)	4.978±0.002	5.1850±0.0005	5.8±0.10
c/a	1.601	1.626	1.611
u/c	0.38	0.376	0.377

The band structures of the group-III nitrides have direct band gaps at the center of the Brillouin zone (Γ point). The band gap energies of wurtzite nitrides at 5 K and room temperature are given in Table 2.2. Therefore, these materials including their ternary alloys could in principle cover almost all the visible and near-ultraviolet regions of the spectrum as schematically depicted in Fig. 2.2. The bandgap of ternary alloys $Al_xGa_{1-x}N$ and $In_xGa_{1-x}N$ is given by [4]:

$$E_g(Al_xGa_{1-x}N) = xE_g(AlN) + (1-x)E_g(GaN) - b_1x(1-x) \quad (1.1)$$

$$E_g(In_xGa_{1-x}N) = xE_g(InN) + (1-x)E_g(GaN) - b_2x(1-x) \quad (1.2)$$

Where E_g is the bandgap energy and b_1, b_2 are the so-called bowing parameters.

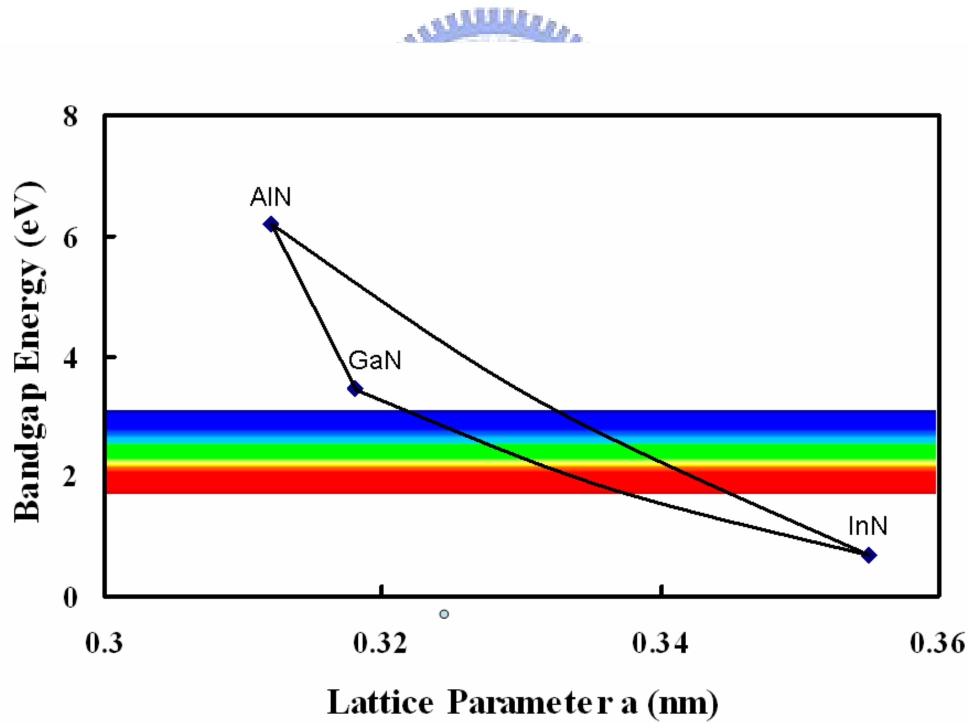

Fig. 2.2 Schematic diagram of bandgap energies of wurtzite nitrides in a function of the lattice constant. The colorful area indicates the visible spectra region.

Table 2.2 Bandgap energy of wurtzite nitrides at 5 K and room temperature [5]-[8]

		AlN	GaN	InN
E_g (5K)	eV	6.28	3.50	1.91
E_g (300K)	eV	6.20	3.44	0.7 (1.89)

The band structure over a small k range around band extreme is concentrated on because the electric and optical properties are generally governed by this local E(k) relationship. Figure 2.1(b) shows the schematic band structure near Γ point of wurtzite GaN. The low symmetry of the wurtzite structure affects the band structure, in particular, the valence band. The valence bands in hexagonal semiconductors are split into three separate sub-bands, heavy hole (HH), light hole (LH), and crystal-field split-off hole (CH) bands. The relative energies of the valence band maxima are determined by a combination of spin-orbit splitting and axial crystal field strength.

2.1.2 General physical properties

Compared with other semiconductor materials, III-Nitrides are also characterized by other superior properties, such as high breakdown field, high peak velocity of electron carriers, high thermal conductivity [9]-[13]. Table 2.3 shows the comparison of some important characteristics between GaN and other semiconductors. These unique properties make this material suitable for high-power and high-frequency devices particularly operating at elevated temperature.

Table 2.3 Comparison of semiconductor material properties at 300 K

Property		Si	GaAs	GaN
Bandgap E_g	eV	1.12	1.42	3.40
Breakdown field E_B	MV/cm	0.25	0.4	4.0
Hole mobility μ_h	cm^2/V s	450	400	30
Electron mobility μ_e	cm^2/V s	1500	8500	1300
Peak velocity v_s	10^7 cm/s	1.0	2.0	3.0
Thermal conductivity χ_T	W/cm K	1.5	0.5	4.3
Relative dielectric constant ε_r		11.8	12.8	9.0

2.1.3 Internal electrical field

An important characteristic of the nitrides that influences the device properties is the presence of strong internal electrical fields inside the epitaxial structures. Wurtzite nitrides have a non-centrosymmetric crystal structure with a polar axis along the c-axis. Therefore, the misfit strain in heterostructures grown along the c-axis can generate an electric moment due to the piezoelectric effect [14]-[16]. In addition to the strain-induced polarization, theory predicts that the spontaneous polarization is very large in the nitrides even if the material is at zero strain [15]. Indeed, the wurtzite structure has the highest symmetry compatible with the existence of spontaneous polarization (or pyroelectric field with reference to its change with temperature) as shown in Fig. 2.3 [17], [18]. The calculated spontaneous polarization for AlN, GaN, and InN is summarized in Table 2.4. According to the calculation, the field resulting from the spontaneous polarization has a fixed orientation which is parallel to the [0001]-direction.

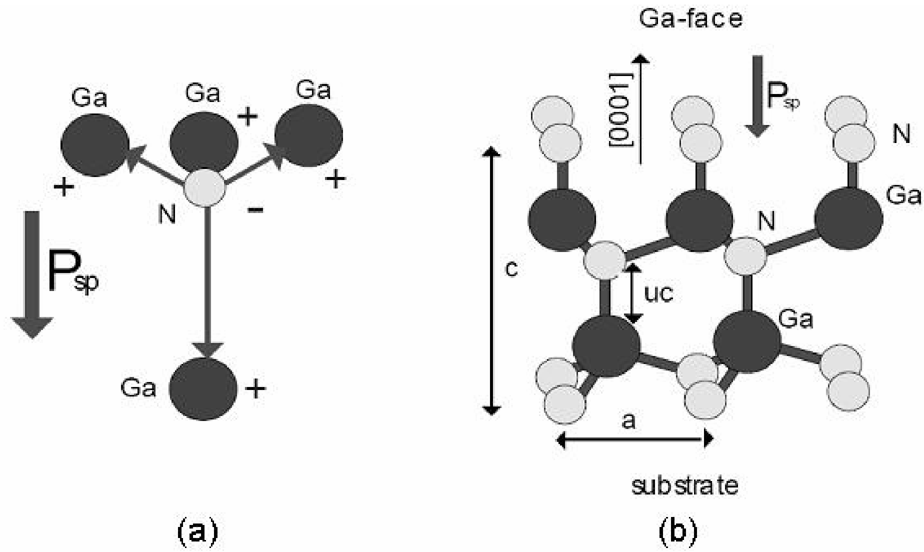

Fig. 2.3 (a) Spontaneous polarization induced by the nonideality of the tetrahedral structure of GaN; (b) Crystal structure of GaN with Ga-face polarity and spontaneous polarization

Table 2.4 Calculated spontaneous polarization for III-V wurtzite nitrides [15]

		AlN	GaN	InN
P_{sp}	C/m^2	-0.081	-0.029	-0.032

2.1.4 Polarity

When three of the bonds on a Ga atom with tetrahedral coordination face towards the substrate, the polarity is typically called Ga-face. In contrast, when three bonds face in the growth direction, the material is termed N-face, as shown in Fig. 2.4. There are four possible surface structures in wurtzite III-nitrides, considering both the termination atom and the crystallographic polarity, e.g. Ga-terminated N-face polarity. Although the terms Ga- and N-face, Ga- and N-termination have been used as a sign

of polarity, it is very complicated to distinguish the polarity from the termination atoms, though Seelmann-Eggebert et al. do use 'termination' to represent the polarity [19]. Furthermore, since AlN, InN and their alloys also need to be considered, the polar structure with the three bonds of III-atom facing toward the substrate is defined as +c polarity and the opposite as –c polarity.

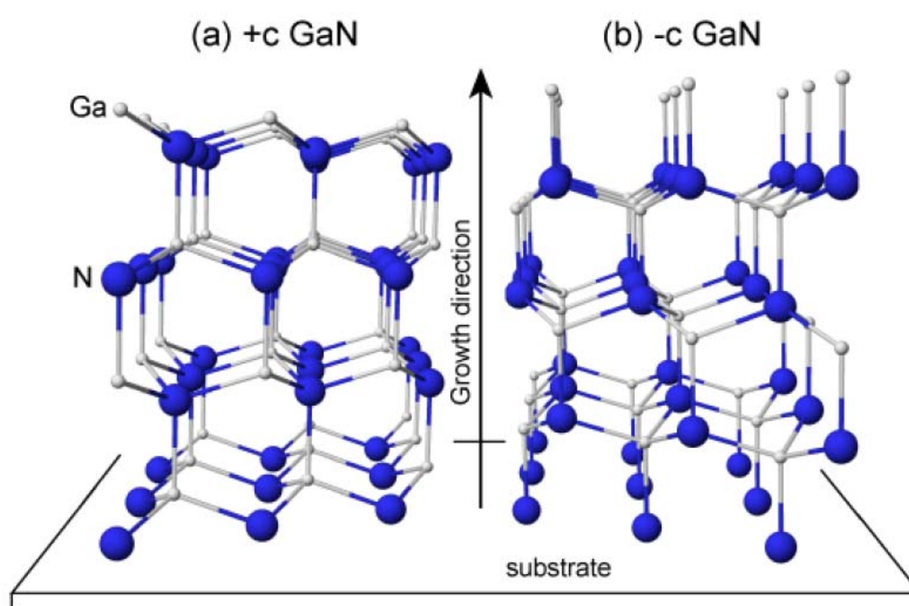

Fig. 2.4 Schematic illustration of GaN wurtzite crystal structure exhibiting the polarity along the c-axis. GaN with Ga-face (+c) polarity on left side and GaN with N-face (-c) polarity on right side. When the direction of the three bonds of the III-element is towards the substrate, the polar structure is defended as +c polarity. On the other hand, when that of these bonds are upward against substrate, it is defined as having –c polarity.

Yang et al. exhibited the difference between Ga- and N-face by using UV-photoelectron emission microscopy (PEEM) [20]. It was indicated that the

emission threshold of the N-face region is lower than that of the Ga-face region, and the phenomenon can be explained by the model of the surface band bending induced by the polarization bound surface charges as shown in Fig. 2.5. The much higher threshold energy at Ga-face than N-face surface would make Ga-face more chemical inert than N-face GaN.

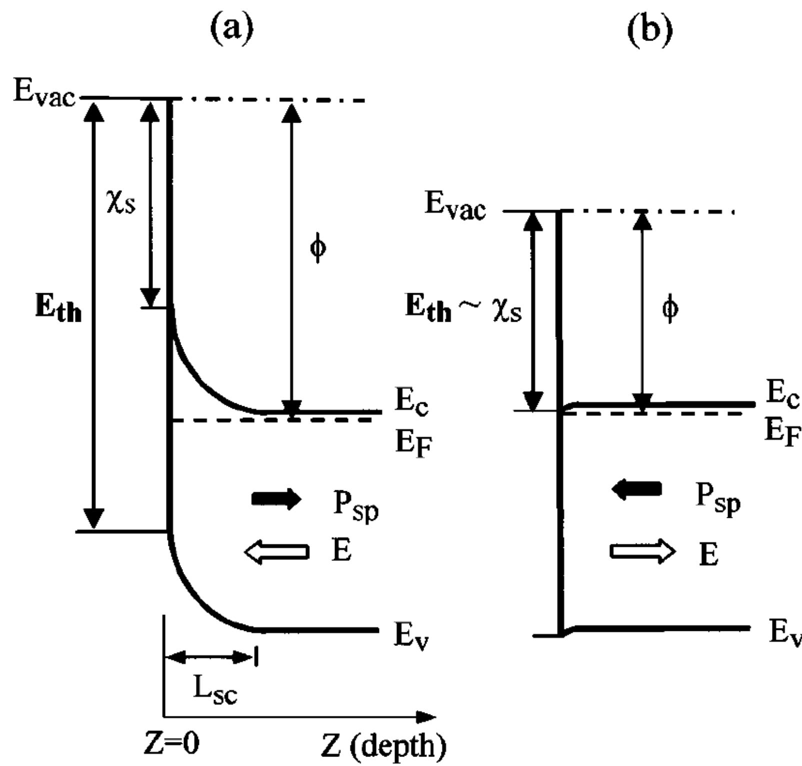

Fig. 2.5 Energy band diagrams for (a) Ga-face and (b) N-face GaN. The quantities ϕ, χ_s, E_{th}, and L_{sc} are the surface electron affinity, work function, photo-threshold energy, and space charge layer, respectively. The arrows represent the directions of spontaneous polarization, P_{sp}, and the internal electric field, E [20].

2.2 Processing Techniques for III-V Nitride Semiconductors

In order to utilize the excellent properties of III-V nitride semiconductors and fulfill the devices, various processing techniques have been developed specifically for these materials. In this section, these techniques including epitaxy, ohmic contacts formation, and high-density-plasma etching will be introduced.

2.2.1 Epitaxial Growth

III-nitrides decompose into the group-III element and nitrogen before they start to melt because of the extremely high melting temperature. This would make it difficult to grow crystals from the nitrides in the melt. The growth of GaN crystals from gallium solution requires again, high temperature (1400 – 1500°C) and elevated nitrogen vapor pressure (10 kbar). The lateral size of bulk single crystals of GaN is therefore limited to up to several millimeters. The difficulty in the growth of bulk substrate material results in epitaxial growth on foreign substrates like sapphire (α-Al_2O_3) and silicon carbide (6H-SiC).

The nitride semiconductors grown on sapphire or SiC substrates by metal-organic chemical vapor deposition (MOCVD) are commercially available [21]-[23]. The major precursors include tri-methyl or tri-ethyl forms of Ga, Al, and In. Silane (SiH_4) and Cp_2Mg are used as n-type and p-type dopant sources, respectively. The growth condition is set at the temperature of around 1000°C and under the pressure of about 100 torr. Owing to the lattice mismatch between sapphire substrates and GaN semiconductors, a thin buffer layer is usually grown directly on the substrate at a low temperature of 500°C to serve as a template of nucleation [24]. However, the densities

of the threading dislocations in these materials are still in the range of $10^9 \sim 10^{10}$ cm^{-2}, which is on the order of million times higher than that of other semiconductors, like Si or GaAs. The lateral epitaxial overgrowth (LEO) can be employed to further reduce the dislocation density by about 5 orders [25]-[27]. In addition, a few of bulk GaN substrates with low defects are successfully produced by metal organic hydrogen chloride vapor phase epitaxy [28]-[31].

The growth of the ternary nitrides is more complex than that of GaN. In particular, the growth of InGaN is complicated by numerous problems. Due to the thermal instability of InN, In incorporation is expected to be elevated by the reduction of the growth temperature, which can be achieved at the expense of a diminished crystalline quality. Further more, the large lattice mismatch between InN and GaN produces considerable internal strain in the InGaN alloy due to a crystalline lattice distortion, which leads to phase separation and immiscibility [32]-[35]. The existence of large compositional fluctuation may be encouraged by the miscibility cap in this system [32].

The as-grown p-type GaN layer has very few carriers because the Mg-dopants are trapped by hydrogen atoms which come from the reactive sources and carrier gases. To obtain the real p-type GaN layers, these Mg-H bonds must be broken after an activation process, which is performed by a post thermal annealing at 500 ~ 700°C under a pure nitrogen atmosphere [36]. However, there is only about 1% of the Mg atoms ionized at room temperature owing to the deep acceptor level of around 170 meV above the valence band edge [37]. The typical mobility of holes is as low as 20 cm^2/Vs, just allowing the realization of p-n junctions. A record value of 150 cm^2/Vs was ever obtained by compensating the scattering atoms [38].

2.2.2 Metal Contacts

Metal-Semiconductor (MS) junctions are of great importance since they are present in every semiconductor device. They can behave either as a Schottky barrier or as an ohmic contact dependent on the characteristics of the interface. Low-resistance, thermally stable ohmic contacts to GaN are crucial for obtaining good performance of light emitting diodes. This section will primarily focus on the formation of ohmic contact on GaN.

Unlike the cases of Si and GaAs, the Fermi level at the interface between the GaN semiconductor and the metal would be unpinned due to the substantial ionic component of the bonds in GaN [39]. Therefore, the Schottky barrier height ($e\Phi_b$), which is the difference between the semiconductor band edge and the Fermi level at the junction, can be evaluated as follows.

$e\Phi_b = e\Phi_m - e\chi_s$, for n-type GaN, (1.3)

$e\Phi_b = E_g - (e\Phi_m - e\chi_s)$, for p-type GaN (1.4)

Where $e\Phi_m$ represents the work function of the contact metal, and $e\chi_s$ (= 4.1eV) is the electron affinity of GaN.

A metal-semiconductor junction results in an ohmic contact (i.e. a contact with voltage independent resistance) if the Schottky barrier height, Φ_b, is zero or negative. In such case, the carriers are free to flow in or out of the semiconductor so that there is a minimal resistance across the contact. For n-type GaN, this means that the work function of the metal must be close to or smaller than the electron affinity of GaN (~ 4.1 eV). For p-type GaN, it requires that the work function of the metal must be close to or larger than the sum of the electron affinity and the bandgap energy. However, the work function of most metals is less than 6 eV, and the sum of the electron affinity and the bandgap energy (~ 3.4 eV) is about 7.5 eV. It can be problematic to find a

metal that provides a good ohmic contact to p-type GaN.

For n-type GaN, choosing the metals of low work functions and increasing the doping concentration of n-type GaN can provide a good ohmic contact. At first, Al and Au ohmic contacts to GaN were used. These contacts yielded specific contact resistances of 10^{-4} and 10^{-3} Ωcm^2, respectively. [40] The use of Ti in ohmic contacts to GaN resulted in much smaller contact resistance. Lin et al. [41] described an Al/Ti ohmic contact to n-GaN with a specific contact resistance of $8x10^{-6}$ Ωcm^2. Later, Fan et al. [42] reported on the Al/Ni/Al/Ti contact to n-GaN and obtained the specific ohmic resistance as low as $9x10^{-8}$ Ωcm^2 after alloy at a proper temperature. The mechanism of obtaining such a low contact resistance was shown to be the formation of TiN, which leads to a large concentration of N vacancies (that behave as donors in GaN) near the surface [43]. The dependence of the specific contact resistance on doping was studied by Khan et al. [44]. Wolter et al. [45] studied ZrN/Zr ohmic contact to GaN that showed a promising thermal stability with a reasonable specific contact resistance of $2x10^{-5}$ Ωcm^2 for n-GaN with the electron concentration of $7x10^{17}$ cm^{-3}. These contacts exhibited excellent thermal stability in evacuated quartz tubes at 600^oC for 1000 hours. Holloway et al. [46] reviewed the results obtained for ohmic contacts to GaN. A low contact metallization for ohmic contacts was reported in [47].

As for p-type GaN, it is a great challenge to form low-resistivity ohmic contacts due to the following reasons.

(a) According to the equation of (1.4), the work function of the metal should be close to 7.5 eV. However, most metal exhibits a work function being lower than 6 eV.

(b) The carrier concentration in p-type GaN is low due to the deep ionization level of the Mg acceptor. There are only 1% of dopants ionized in p-GaN and this low hole concentration can not lead to a tunneling junction at the metal/p-GaN

interface.

(c) There is a tendency for the preferential loss of nitrogen from the GaN surface during processing, which may produce surface conversion to n-type conductivity.

A bilayer metal film of Ni/Au on p-type GaN is most common structure adopted for GaN-based optoelectronic devices. Ni/Au layer is deposited on p-GaN by an e-beam evaporator and subsequently annealed at 500-700°C. The typical contact resistance is around 10^{-3}-10^{-2} Ωcm^2 [48], [49]. Although the contact resistivity is not low enough, it is allowable for application in LEDs. It was also found that the specific contact resistance of Ni/Au could be reduced to $4x10^{-6}\Omega cm^2$ after annealing in an oxygen ambience [50]-[52], but both the reliability and the reproducibility were disputable [53], [54]. Furthermore, $Al_{0.15}Ga_{0.85}N$/GaN strained superlattices were fabricated to enhance the surface carrier concentration, so the contact resistance was reduced effectively with the traditional Ni/Au-contact method [55], [56]

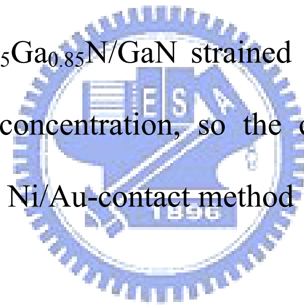

2.2.3 High-density-plasma Dry Etch

Due to the inert properties of III-Nitrides, it is difficult to etch GaN with wet chemicals. It was only found that GaN could be etched at practical rate with molten salts such as KOH or NaOH at temperatures above 250°C. Although the technique of photochemical etching has been developed for nitrides [57], the difficult procedure of adding electrodes to spread current and selectivity over polarity of GaN restricts its application. It is much easier to etch N-polarity than Ga-polarity GaN owing to the much lower photo threshold energy of N-polarity GaN as mentioned in section 1.1.4. However, the epitaxial quality of N-polarity material is always poorer than

Ga-polarity one, and it is necessary to utilize Ga-polarity materials to fabricate devices with high performance.

Dry etching is the most practical and feasible method. Especially, the high-density plasma (HDP) etchers, which use inductively coupled plasma (ICP) or electron cyclotron resonance (ECR) techniques to generate the plasma sources with 10^{11}~$10^{12}$$cm^{-3}$ densities, can provide higher etching rates than the typical reactive ion etcher (RIE) without serious damages on the GaN surface [58], [59]. A variety of reactive gases have been investigated for GaN etching. Some special recipes can improve the etching selectivity among different epi-layers [60]. The chlorine-based gas mixtures are usually adopted owing to fair volatilities of gallium chlorides. Methane (CH_4) is also added in the mixture in order to etch the epi-layer containing indium content.

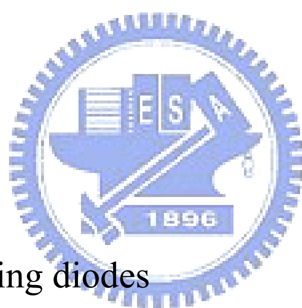

2.3 GaN-based light emitting diodes

In general, one excites electron-hole (e-h) pairs by an external source of energy in a semiconductor, and they are in non-equilibrium state. In most cases, the electrons and holes will relax to quasi-thermal equilibrium distribution through a thermalization process such as carrier-carrier and carrier-phonon interaction. In the final step, the e-h pairs recombine, and their energy is released. Radiative recombination produces emission of photons and the non-radiative recombination release the energy to crystal lattice in the form of heat.

As shown in Fig. 1.6, the GaN-based LED is schematically illustrated. N-type, multi-quantum wells and p-type GaN is epitaxially grown on sapphire substrates in sequence by MOCVD, and processed by dry etching to expose the n-GaN layer

followed by metallization to form the transparent ohmic contacts on p-type GaN as a current spreading layer. P- and n-electrode are both formed on etch type of GaN. Finally, the sapphire substrates were thinned to about 90um by polishing and were scribed and sliced into chips.

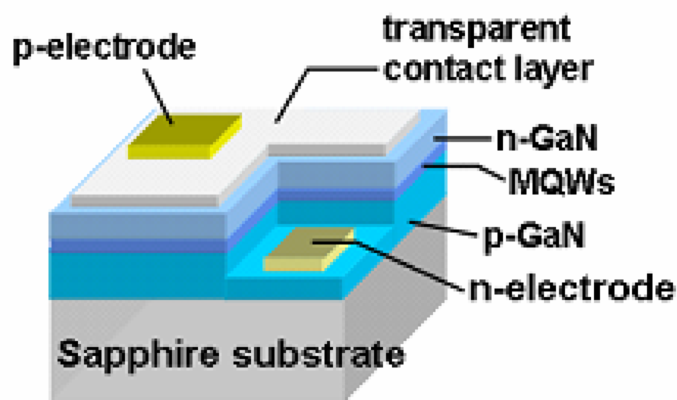

Fig. 2.6 Schematic diagram of GaN-based LEDs on sapphire substrate

References

[1] J. H. Edgar, Properties of group III nitrides (INSPEC, IEE, London, 1994).

[2] M. Suzuki and T. Uenoyama, J. Appl. Phys., vol. 80, pp. 6868-6874, Dec. 1996.

[3] J. W. Orton and C. T. Foxon, Semicond. Sci. Technol., vol. 13, pp. 310-313, 1998.

[4] Z. Dridi, B. Bouhafs, and P. Ruterana, Semicond. Sci. Technol., vol. 18, pp. 850-856, 2003.

[5] S. Strite and H. Morkoc, J. Vac. Sci. Technol. B, vol. 10, pp.1237-1266, Jul/Aug. 1992.

[6] T. L. Tansley and C. P. Foley, J. Appl. Phys., vol. 59, pp. 3241-3244, May 1986.

[7] Q. Guo and A. Yoshida, Jpn. J. Appl. Phys., vol. 33, pp. 2453-2456, May 1994.

[8] V. Y. Davydov, A. A. Klochikhin, V. V. Emtsev, S. V. Ivanov, V. V. Vekshin, F. Bechstedt, J. Furthmuller, H. Harima, A. V. Mudryi, A. Hashimoto, A. Yamamoto, J. Aderhold, J. Graul, and E. E. Haller, Phys. Stat. Sol. (b), vol. 230, pp. R4-R6, 2002.

[9] V. W. L. Chin, T. L. Tansley, and T. Osotchan, J. Appl. Phys., vol. 75, pp. 7365-7372, Feb. 1994.

[10] M. Shur, B. Gelmont, and M. A. Khan, J. Electronic Materials, vol. 25, pp. 777-785, May 1996.

[11] K. S. Kim, C. S. Oh, W. -H. Lee, K. J. Lee, G. M. Yang, C. -H. Hong, E. -K. Suh, K. Y. Lim, H. J. Lee, and D. J. Byun, J. Crystal Growth, vol. 210, pp. 505-510, 2000.

[12] B. E. Foutz, S. K. O'Leary, M. S. Shur, and L. F. Eastman, J. Appl. Phys., vol. 85, pp.7727-7734, Jun. 1999.

[13] W. J. Fan, M. F. Li, T. C. Chong, and J. B. Xia, Solid State Communications, vol. 97, pp. 381-384, 1996.

[14] A. Bykhovski, B. Gelmont, and M. Shur, J. Appl. Phys., vol. 74, pp. 6734-6739, Dec. 1993.

[15] F. Bernardini, V. Fiorentini, and D. Vanderbilt, Phys. Rev. B, vol. 56, pp. R10024-R10027, Oct. 1997.

[16] C. Kisielowski, J. Kruger, S. Ruvimov, T. Suski, J. W. Ager III, E. Jones, Z. Liliental-Weber, M. Rubin, E. R. Weber, M. D. Bremser, and R. F. Davis, Phys. Rev. B, vol. 54, pp. 17745-17753, Dec. 1996.

[17] J. F. Nye, Physical properties of crystals (Clarendon Press, Oxford, 1995).

[18] O. Gfrorer, C. Gemmer, J. Off, J. S. Im, F. Scholz, and A. Hangleiter, Phys. Stat. Sol. (b), vol. 216, pp. 405-408, 1999.

[19] M. Seelmann-Eggebert, J. L. Weyher, H. Obloh, H. Zimmermann, A. Rar, and S. Porowski, Appl. Phys. Lett., vol. 71, pp. 2635-2637, Nov. 1997.

[20] W.-C. Yang, B. J. Rodriguez, M. Park, R. J. Nemanich, O. Ambacher and V. Cimalla, J. Appl. Phys., vol. 94, pp. 5720-5725, Nov. 2003.

[21] S. Nakamura, Jpn. J. Appl. Phys., vol. 30, pp. L1705-L1707, Oct. 1991.

[22] Q. Guo, O. Kato, and A. Yoshida, J. Appl. Phys., vol. 73, pp. 7969-7971, Jun. 1993.

[23] O. Ambacher, M. S. Brandt, R. Dimitrov, T. Metzger, M. Stutzmann, R. A. Fischer, A. Miehr, A. Bergmaier, and G. Dollinger, J. Vac. Sci. Technol. B, vol. 14, pp. 3532-3542, Nov/Dec. 1996.

[24] H. Amano, N. Sawaki, I. Akasaki, and Y. Toyada, Appl. Phys. Lett., vol. 48, pp. 353-355, Feb. 1986.

[25] D. Kapolnek, S. Keller, R. Vetury, R. D. Underwood, P. Kozodoy, S. P. Den Baars, and U. K. Mishra, Appl. Phys. Lett., vol. 71, pp. 1204-1206, Sep. 1997.

[26] X. Li, A. M. Jones, S. D. Roh, D. A. Turnbull, S. G. Bishop, and J. J. Coleman, J. Electronic Materials, vol. 26, pp. 306-309, 1996.

[27] G. Nataf, B. Beaumont, A. Bouille, P. Vennegues, S. Haffouz, M. Vaille, P. Gibart, Materials Science and Engineering: B, vol. 59, pp. 112-116, 1999.

[28] S. Kurai, Y. Naoi, T. Abe, S. Ohmi, and S. Sakai, Jpn. J. Appl. Phys., vol. 35, pp. L77-L79, Jan. 1996.

[29] S. Porowski, J. Crystal Growth, vol. 166, pp. 583-589, 1996.

[30] M. K. Kelly, R. P. Vaudo, V. M. Phanse, L. Gorgens, O. Ambacher, and M. Stutzmann, Jpn. J. Appl. Phys., vol. 38, pp. L217-L219, Mar. 1999.

[31] Y. Kumagai, H. Murakami, A. Koukitu, K. Takemoto, and H. Seki, Jpn. J. Appl. Phys., vol. 39, pp. L703-L706, Jul. 2000.

[32] I. Ho and G. B. Stringfellow, Appl. Phys. Lett., vol. 69, pp. 2701-2703, Oct.

1996.

[33] N. A. El-Masry, E. L. Piner, S. X. Liu, and S. M. Bedair, Appl. Phys. Lett., vol. 72, pp. 40-42, Jan. 1998.

[34] R. Singh, R. J. Molnar, M. S.Unlu, and T. D. Moustakas, Appl. Phys. Lett., vol. 64, pp. 336-338, Jan. 1994.

[35] S. Y. Karpov, MRS Internet J. Nitride Semicond. Res., vol. 3, pp. 1-5, 1998.

[36] S. Nakamura, T. Mukai, M. Senoh, N. Iwasa, Jpn. J. Appl. Phys., vol. 31, pp. L139-L142, Feb.1992.

[37] D. J. Kim, D. Y. Ryu, N. A. Bojarczuk, J. Karasinski, S. Guha, S. H. Lee, and J. H. Lee, J. Appl. Phys., vol. 88, pp. 2564-2569, Sep. 2000.

[38] O. Brandt, H. Yang, H. Kostial, and K. Ploog, Appl. Phys. Lett. vol. 69, pp. 2707-2709, Oct. 1996.

[39] S. Kurtin, T. C. McGill, and C. A. Mead, Physical Review Letters, vol. 22, pp. 1433-1436, Jun. 1969.

[40] J. S. Foresi and T. D. Moustakas, Appl. Phys. Lett., vol. 62, pp. 2859-2861, May 1993.

[41] M E. Lin, Z. Ma, F. Y. Huang, Z. F. Fan, L. H. Allen, and H. Morkoc, Appl. Phys. Lett., vol. 64, pp. 1003-1005, Feb. 1994.

[42] Z. F. Fan, S. N. Mohammad, W. Kim, O. Aktas, A. E. Botchkarev, and H. Morkoc, Appl. Phys. Lett., vol. 68, pp. 1672-1674, Mar. 1996.

[43] S. Ruvimov, Z. Liliental-Weber, J. Washburn, K. J. Duxstad, E. E. Haller, Z. -F. Fan, S. N. Mohammad, W. Kim, A. E. Botchkarev, and H. Morkoc, Appl. Phys. Lett., vol. 69, pp. 1556-1558, Sep. 1996.

[44] M. A. Khan, M. S. Shur, and Q. Chen, Appl. Phys. Lett., vol. 68, pp. 3022-3024, May 1996.

[45] S. D. Wolter, B. P. Luther, S. E. Mohney, R. F. Karlicek, Jr., and R. S. Kern,

Electrochemical and Solid-State Letters, vol. 2, pp. 151-153, 1999.

[46] P. H. Holloway, T. -J. Kim, J. T. Trexler, S. Milla, J. J. Fijol, W. V. Lampert, and T. W. Haas, Appl. Surface Science, vol. 117/118, pp. 362-372, 1997.

[47] D. Qiao, Z. F. Guan, J Carlton, S. S. Lau, G. J. Sullivan, Appl. Phys. Lett., vol. 74, pp. 2652-2654, May 1999.

[48] J. -L. Lee, J. K. Kim, J. W. Lee, Y. J. Park, and T. Kim, Solid-State Electronics, vol. 43, pp. 435-438, Feb. 1999.

[49] J. K. Sheu, Y. K. Su, G. C. Chi, W. C. Chen, C. Y. Chen, C. N. Huang, J. M. Hong, Y. C. Yu, C. W. Wang, and E. K. Lin, J. Appl. Phys., vol. 83, pp. 3172-3175, Mar. 1998.

[50] J. -K. Ho, C. -S. Jong, C. C. Chiu, C. -N. Huang, C. -Y. Chen, and K. -K. Shih, Appl. Phys. Lett., vol. 74, pp. 1275-1277, Mar. 1999.

[51] L. -C. Chen, J. -K. Ho, C. -S. Jong, C. C. Chiu, K. -K. Shih, F. -R. Chen, J. -J. Kai, L. Chang, Appl. Phys. Lett., vol. 76, pp. 3703-3705, Jun. 2000.

[52] L. -C. Chen, F. -R. Chen, J. -J. Kai, L. Chang, J. -K. Ho, C. -S. Jong, C. C. Chiu, C. -N. Huang, C. -Y. Chen, and K. -K. Shih, J. Appl. Phys., vol. 86, pp. 3826-3832, Oct. 1999.

[53] T. Maeda, Y. Koide, and M. Murakami, Appl. Phys. Lett., vol. 75, pp. 4145-4147, Dec. 1999.

[54] H. Kim, D. -J. Kim, S. -J. Park, and H. Hwang, J. Appl. Phys., vol. 89, pp. 1506-1508, Jan. 2001.

[55] C. H. Kuo, J. K. Sheu, G. C. Chi, Y. L. Huang, T. W. Yeh, Solid-State Electronics, vol. 45, pp. 717-720, May 2001.

[56] J. K. Sheu, G. C. Chi, and M. J. Jou, IEEE Electron Device Letters, vol. 22, pp. 160-162, Apr. 2001.

[57] C. Youtsey, I. Adesida, and G. Bulman, Appl. Phys. Lett., vol. 71, pp. 2151-2153,

Oct. 1997.

[58] S. J. Pearton, Materials Science and Engineering: B, vol. 40, pp. 101-118, 1996.

[59] R. J. Shul, G. A. Vawter, C. G. Willison, M. M. Bridges, J. W. Lee, S. J. Pearton, and C. R. Abernathy, Solid-State Electronics, vol. 42, pp. 2259-2267, Dec. 1998.

[60] R. J. Shul, C. G. Willison, M. M. Bridges, J. Han, J. W. Lee, S. J. Pearton, C. R. Abernathy, J. D. Mackenzie, and S. M. Donovan, Solid-State Electronics, vol. 42, pp. 2269-2276, Dec. 1998.

Chapter 3

Highly Reliable GaN-Based Light-Emitting Diodes Formed by p-$In_{0.1}Ga_{0.9}N$/ITO Structure

3.1 Introduction

Group III-Nitride semiconductors have attracted much attention for their versatile applications recently [1], [2]. A high-brightness GaN-based light emitting diode is an interesting issue because of its important role in full-color display and lighting applications [3], [4]. Following the successful demonstration of p-type conductivity on Mg-doped GaN by post-growth thermal annealing in nitrogen ambience, blue and green LEDs become real and commercially available [5]. However, poor conductivity of p-GaN layer still limits the current spreading, and it is necessary to deposit a conductive layer for current spreading. This layer should not only form good ohmic contacts to p-GaN but also be transparent to the emitted light from the active layer. In the past, much work focused on materials and methods to form good contacts to p-GaN [6]-[8]. Among these studies, Ni/Au is usually used as a semi-transparent current spreading layer due to its good contact characteristics. However, Sheu et al. [9] showed that the transmittance of semi-transparent Ni/Au films for blue LEDs is only about 60% to 85% in the 450-550 nm wavelengths. To improve the transmittance, it is feasible to replace the conventional Ni/Au contact by a better transparent conductive contact. Nowadays transparent conductive oxide materials (TCO), such as indium-tin-oxide (ITO), aluminum-doped-zinc-oxide (AZO)

and cadmium-tin-oxide (CTO), are widely applied to optical electrical devices [10], [11]. There are also several studies [12]-[15] discussing the applications of ITO to GaN-based LEDs. Margalith et al. [12] obtained the Schottky but not Ohmic characteristics of the ITO/p-GaN interface after thermal annealing. This result could be attributed to a large work function difference between ITO and p-GaN. In order to improve the contact characteristics, some authors added an interfacial layer such as Ni or NiO before ITO deposition by a little sacrifice of transparency [13]-[15]. In this chapter, we demonstrate a thin p-$In_{0.1}Ga_{0.9}N$ layer as an intermediate between ITO and p-GaN to form a nearly ohmic contact. The LEDs with this structure exhibit excellent reliability under a 50-mA current stress.

3.2 Experimental

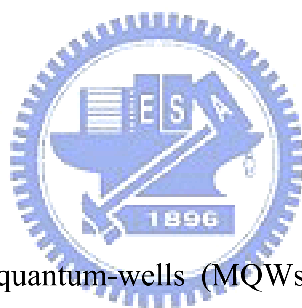

The InGaN–GaN multi-quantum-wells (MQWs) LED wafers were grown on c-face sapphire substrates by a metal-organic chemical vapor deposition (MOCVD) system. The epitaxial structure comprised 4-μm-thick n-GaN, 0.1-μm-thick InGaN–GaN (MQWs) active layer, and 0.1-μm-thick p-GaN, as shown in Fig. 3.1 (1). Moreover, the carrier concentrations of the p-GaN and n-GaN were 5×10^{17} cm^{-3} and 3×10^{18} cm^{-3}, respectively. A wafer with a peak wavelength at 465 nm was chosen and cut into 4 pieces. One piece was prepared for the conventional LEDs with Ni/Au contact, and the other three were re-loaded into the same MOCVD chamber to grow a 10-nm-thick p-$In_{0.1}Ga_{0.9}N$ layer for LEDs with ITO contacts.

GaN-based LEDs (300 μm x 300 μm) and the corresponding transmission line model (TLM) structures for p-type ohmic contact characterization with different conducting layers were fabricated as shown in Fig. 3.1. First, inductance coupled

plasma (ICP) etcher was used to form mesa structures and then these samples were immersed in H_2SO_4:H_2O_2 and NH_4OH:H_2O solutions to remove resist and native oxides. Next, ITO (280 nm) was deposited on the p-$In_{0.1}Ga_{0.9}N$/p-GaN samples by E-beam evaporator at 300°C in oxygen ambience with a partial pressure of 5 x 10^{-4} Torr, and the Ni/Au (4 nm/4 nm) was deposited on the p-GaN sample by E-beam evaporator with a base pressure of 2 x 10^{-6} Torr. The p-$In_{0.1}Ga_{0.9}N$/ITO contact samples were subsequently annealed at 500°C and 600°C in nitrogen ambience. As for the Ni/Au contact sample, it was annealed at 540°C in nitrogen ambience to achieve the optimal ohmic contact to p-GaN. Cr/Au (0.08 μm/0.8 μm) metallization was employed for the n-type contact layer, p- and n- bonding pads. TLM structures were used to measure the contact resistivity of the conducting layers on p-GaN. The pad size is 300 μm x 80 μm and the spacings were 2, 3, 4, 6, 8, 15 and 20 μm. The current-voltage characteristics were measured at room temperature by an HP-4156 analyzer with a current source.

After measuring, these samples were subsequently polished, scribed and sliced into chips. We chose 10 chips per sample to package into TO-Can forms. A Keithley 2430 source meter was connected with an integrating sphere to measure the current-voltage and current-power characteristics of these LEDs. During the reliability testing, these chips with TO-Can form were stressed by a 50-mA current injection at room temperature and relative humidity of 40%.

In order to truly exhibit the effects of absorption, internal reflection and interference of the conducting films on GaN-based LEDs, the p-i-n GaN with a double-side-polished sapphire substrate was used in the transmittance measurement. The transmittance spectra of these samples were measured by Hitachi U3010 spectrophotometer.

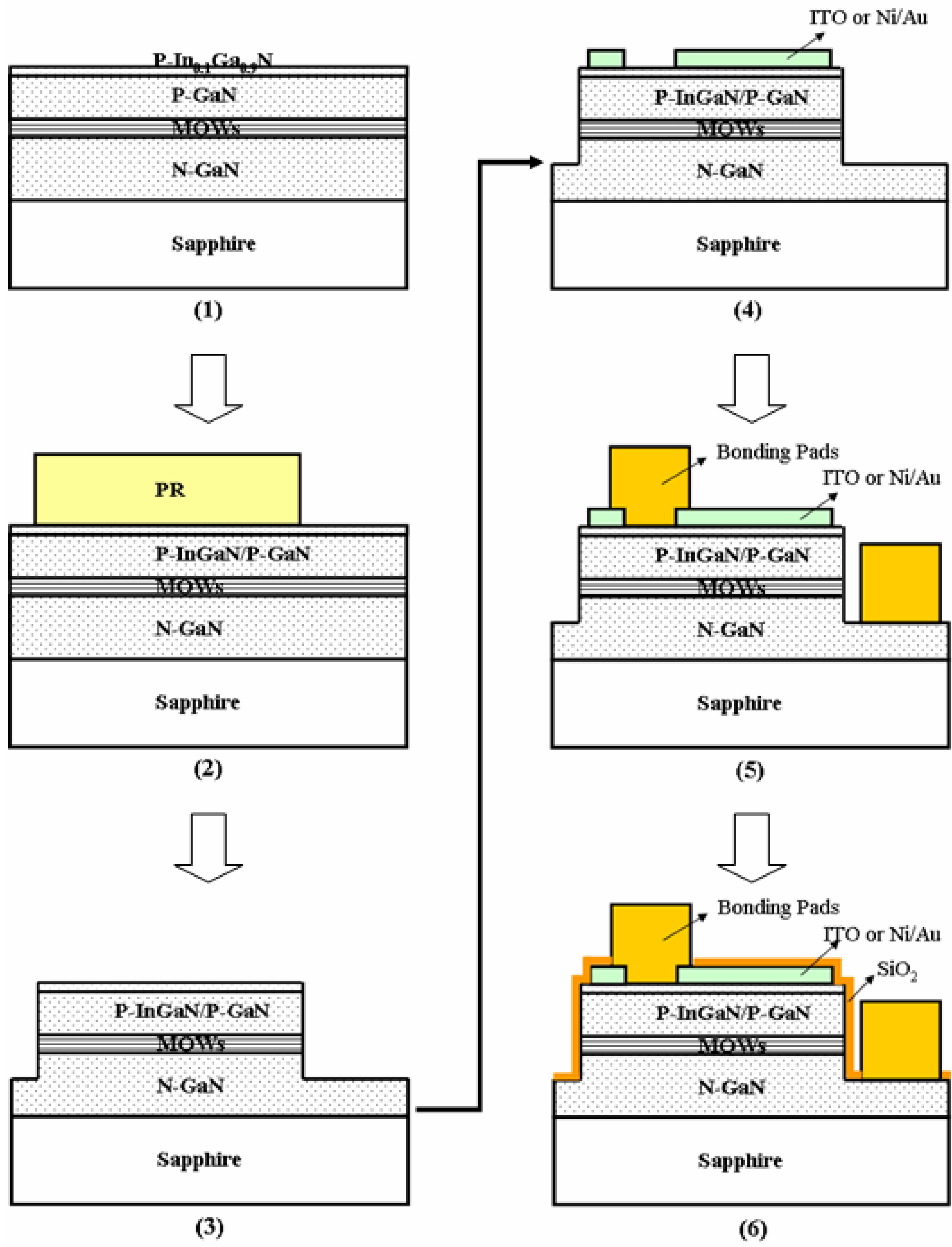

(a)

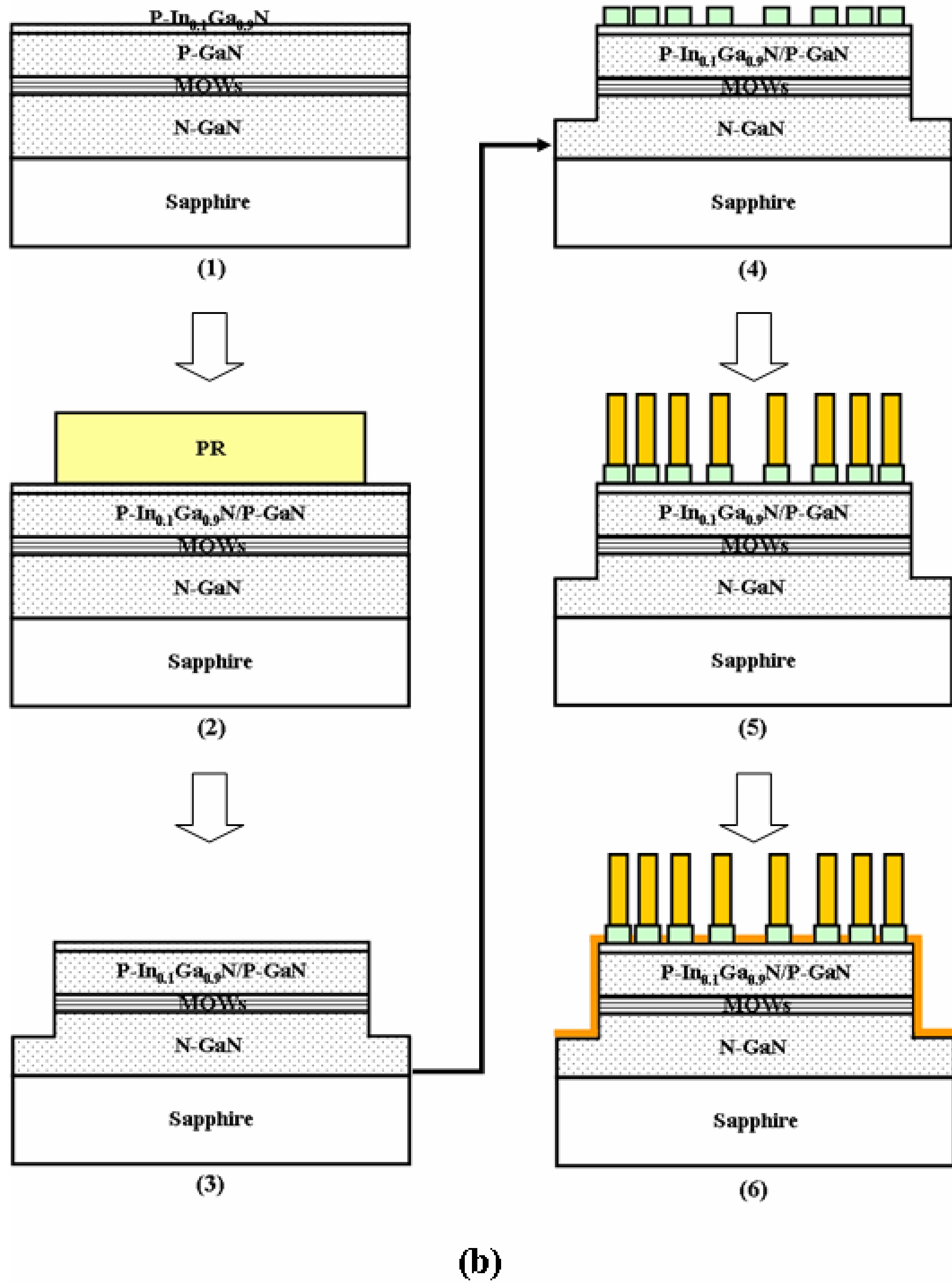

Fig. 3.1 The process flow diagrams of (a) GaN-based LEDs fabrication and (b) TLM structure formation: (1) epitaxial structure (2) lithographic patterning (3) ICP etching to expose n-GaN layer (4) ITO deposition and patterning, (5) bonding pads metallization (6) SiO_2 protection layer.

3.3 Results and Discussion

Figure 3.2 shows the transmittance of the p-i-n GaN/sapphire, ITO and Ni/Au layers deposited on p-i-n GaN/sapphire samples with different annealing temperatures. Due to the great difference of optical index between GaN and air, the blank sample with p-i-n GaN/sapphire structure exhibits relatively poor transmittance. The curves of ITO samples annealed at 500°C and 600°C are nearly coincident, and the light transmittance at 465 nm is 83% while Ni/Au sample shows only 61% due to the high extinction coefficient of Ni and Au. It is supposed that ITO can extract more light than the conventional Ni/Au layer does.

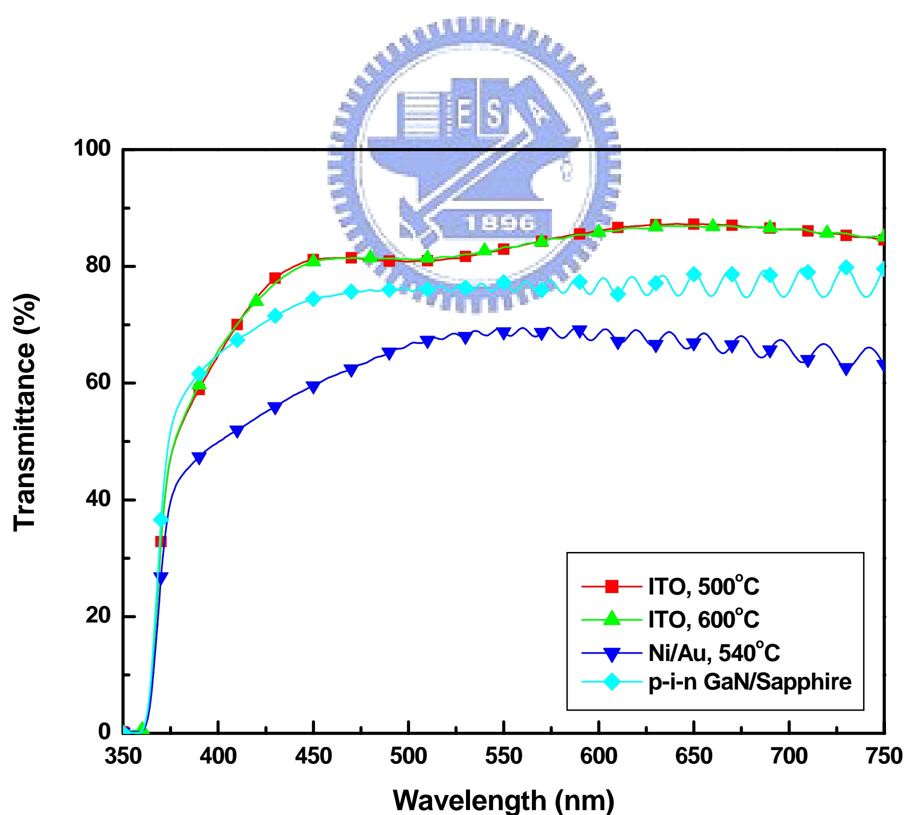

Fig. 3.2 Transmittance spectra of the blank p-i-n GaN/sapphire, the ITO and Ni/Au films deposited on p-i-n GaN/sapphire under different annealing conditions. (n_{ITO} @ 470 nm = 1.8, n_{GaN} @ 470 nm = 2.5)

Figure 3.3 presents the current-voltage characteristics of different contacts on p-GaN. The Ni/Au sample exhibits a linear ohmic property, while the sample of p-$In_{0.1}Ga_{0.9}N$/ITO shows a nearly linear ohmic characteristic after annealed at the temperature of 500°C, which is the optimal condition.

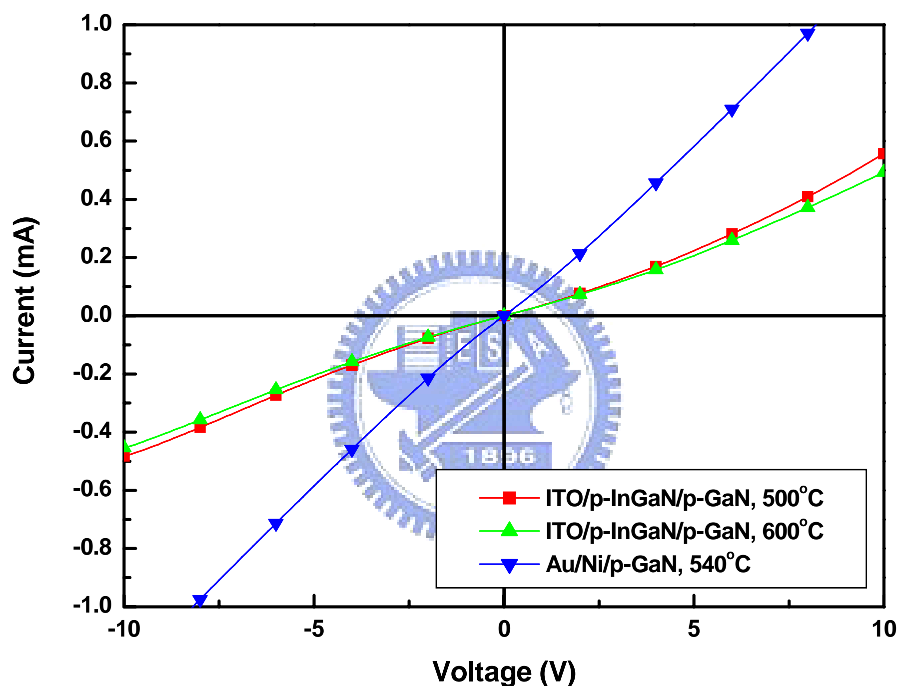

Fig. 3.3 I-V characteristics of p-$In_{0.1}Ga_{0.9}N$/ITO contacts annealed at 500°C, 600°C and Ni/Au contact annealed at 540°C on p-GaN. (The spacing between two electrodes is 2 um)

As shown in Fig. 3.4, the contact resistivity of Ni/Au contact decreases from 8 x 10^{-3} ohm-cm^2 to 3 x 10^{-3} ohm-cm^2 with increasing the current density from 0 to 50 A-cm^{-2}. As for the p- $In_{0.1}Ga_{0.9}N$/ITO contact samples, the contact resistivity reduces

from 2 x 10^{-1} ohm-cm^2 to 2.5 x 10^{-2} ohm-cm^2 with raising the current density from 0 to 50 A-cm^{-2}. The results imply that both the interfaces of p-GaN with Ni/Au and p-$In_{0.1}Ga_{0.9}N$/ITO contacts are not ideal ohmic contacts, but the former exhibits better contact property than the latter. Moreover, this figure also indicates that the contact resistivity is 2.6 x 10^{-2} ohm-cm^2 under a current density of 27 A-cm^{-2}, which is equivalent to a current of 20 mA applied during the normal LED operation. This result shows that the p-$In_{0.1}Ga_{0.9}N$/ITO contact is good enough to be used in LED application.

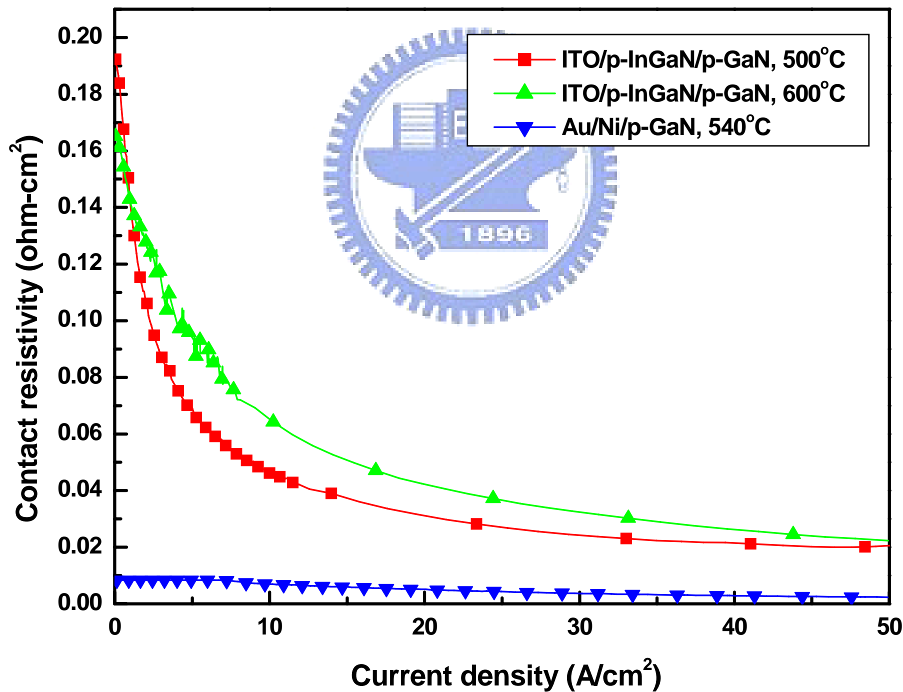

Fig. 3.4 Contact resistivities as functions of injection current density.

The electrical characteristic is shown in Fig. 3.5. The forward voltage increases

and the dynamic resistance decreases with elevating the injected current. At the current of 20 mA, the forward voltage and the dynamic resistance are 3.43 V and 17.1 ohm chips with p-$In_{0.1}Ga_{0.9}N$/ITO contacts annealed at 500°C, respectively. On the other hand, the conventional chips with Ni/Au contacts show 3.21 V and 14.8 ohm. The ITO contact LEDs exhibit a little bit higher but acceptable forward voltage and dynamic resistance by 0.2 V and 2.3 ohm in comparison with the conventional Ni/Au contact LEDs.

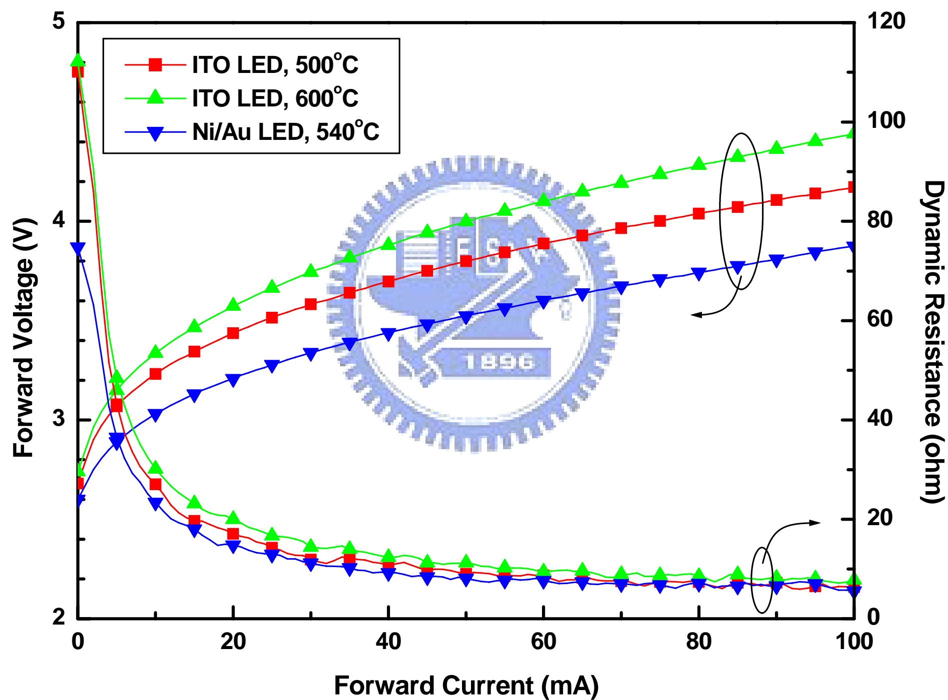

Fig. 3.5 The forward voltage and dynamic resistance as functions of injection current of GaN-based LEDs with p-$In_{0.1}Ga_{0.9}N$/ITO and Ni/Au contacts.

Figure 3.6 shows the optical properties of LEDs with different contacts. The output power increases with raising the injected current. But the power efficiency of

ITO contacts and Ni/Au contacts LEDs has a maximum value of 8.12% and 5.83% at 3-mA-current injection, respectively, and then decreases with elevating the injected current. At the current of 20 mA, the output power and power efficiency are 4.30 mW and 6.26% for chips with 500°C-annealed p-$In_{0.1}Ga_{0.9}N$/ITO contacts in comparison with that of 2.95 mW and 4.60% for the conventional Ni/Au contacts LEDs. It is estimated that LEDs with p-$In_{0.1}Ga_{0.9}N$/ITO contacts can enhance the external quantum efficiency and power efficiency by about 46% and 36% at 20 mA, respectively. This improvement is definitely attributed to the high transparent contacts and relatively low contact resistance. The electrical and optical characteristics of LEDs with ITO contacts are summarized in table 3.1 compared with the previous works.

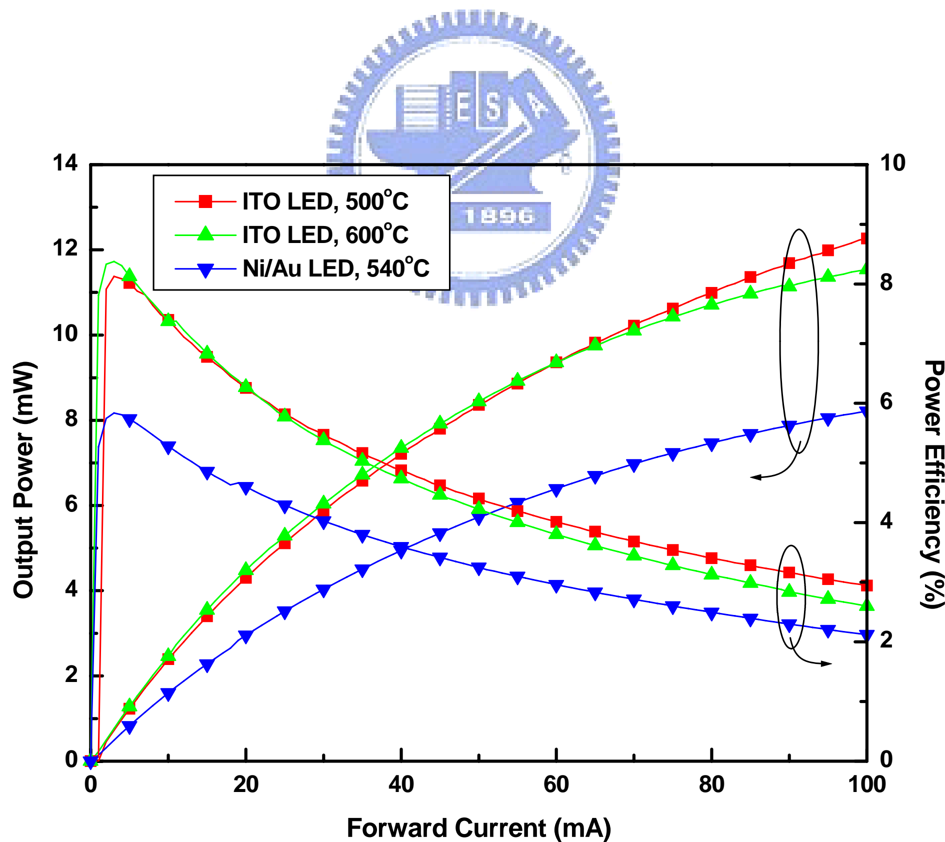

Fig. 3.6 The output power and power efficiency as functions of injection current of GaN-based LEDs with p-$In_{0.1}Ga_{0.9}N$/ITO and Ni/Au contacts.

Table 3.1 GaN-based LEDs of different ITO contacts are compared with that of Ni/Au contact.

Group	**Margalith *et al.*** [12]	**Lin *et al.*** [14]		***Pan *et al.*** [15]	**This study**
Structure	ITO	ITO	ITO/Ni	ITO/NiOx	ITO/p-InGaN
Contact Property	Schottky	a little Schottky	ohmic	ohmic	nearly ohmic
ΔV_F	+2V	+0.39V	+0.02V	+0.04V	+0.2V
Enhance of external quantum efficiency	**N. A.	42%	25%	38%	46%
Enhance of power efficiency	**N. A.	27%	25%	36%	36%

* Data from Pan et al. is compared with Ni/Au oxides contacts.

** N. A. means "Not Available".

From the results of life test shown in Fig. 3.7, the conventional Ni/Au samples would suffer the output power decay of 27% after 1008-hour stress and the 500°C-annealed ITO samples showed a similar decay of 25%. However, the light power was deteriorated by 36% for the p-$In_{0.1}Ga_{0.9}N$/ITO samples annealed at 600°C. This result is probably due to the poor contact property which will induce a severe heating effect under high current injection. Besides, the surface morphology of 600°C ITO films seemed to contain a lot of pits and defects.

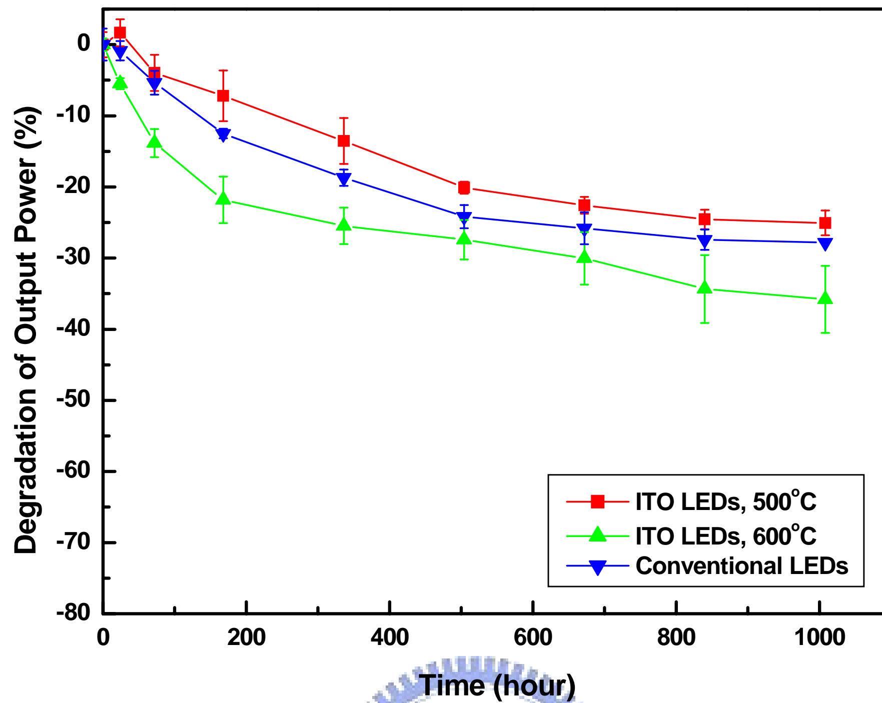

Fig. 3.7 Room temperature life test of degradation of output power from GaN-based LEDs with p-$In_{0.1}Ga_{0.9}N$/ITO and Ni/Au contacts.

3.4 Summary

This chapter presented highly transparent and nearly ohmic contacts of p-$In_{0.1}Ga_{0.9}N$/ITO on p-GaN and exhibited the excellent reliability of the p-$In_{0.1}Ga_{0.9}N$/ITO contact LEDs. The contact resistivity is 2.6 x 10^{-2} ohm-cm^2 at a current density of 27 A-cm^{-2}, and this value is low enough for the application of LEDs. GaN-based LEDs with p-$In_{0.1}Ga_{0.9}N$/ITO contacts were also fabricated and the forward voltage was 3.43 V at a current injection of 20 mA. Although the forward voltage was a little higher than the conventional LEDs by 0.2 V, the external quantum

efficiency and power efficiency were raised by 46% and 36%, respectively. As for the life test, LEDs with p-$In_{0.1}Ga_{0.9}N$/ITO contacts annealed at 500^oC exhibits a similar reliability as the conventional Ni/Au LEDs do. Therefore, p-$In_{0.1}Ga_{0.9}N$/ITO contacts can make GaN-based LED highly bright and reliable in practice.

References

[1] S. Nakamura, M. Senoh, N. Iwasa, and S. Nagahama, Appl. Phys. Lett., vol. 67, pp. 1868-1870, Sep. 1995.

[2] S. Nakamura, M. Senoh, S. Nagahama, N. Iwasa, T. Yamada, T. Matsushita, H. Kiyoku, Y. Sugimoto, T. Kozaki, H. Umemoto, M. Sano, and K. Chocho, Appl. Phys. Lett., vol. 72, pp. 2014-2016, Apr. 1998.

[3] W. S. Wong, T. Sands, N. W. Cheung, M. Kneissl, D. P. Bour, P. Mei, L. T. Romano, and N. M. Johnson, Appl. Phys. Lett., vol. 77, pp. 2822-2824, Oct. 2000.

[4] C. M. Lee, C. C. Chuo, I. L. Chen, J. C. Chang, and J. I. Chyi, IEEE Electron Device Lett., vol. 24, pp. 156-158, Mar. 2003.

[5] S. Nakamura, T. Mukai, M. Senoh, and N. Iwasa, Jpn. J. Appl. Phys., vol. 31, pp. L139-L142, Feb. 1992.

[6] J. K. Kim, J. L. Lee, J. W. Lee, H. E. Shin, Y. J. Park, and T. Kim, Appl. Phys. Lett., vol. 73, pp. 2953-2955, Nov. 1998.

[7] J. K. Ho, C. S. Jong, C. C. Chiu, C. N. Huang, K. K. Shih, L. C. Chen, F. R. Chen, and J. J. Kai, J. Appl. Phys., vol. 86, pp. 4491-4497, Oct. 1999.

[8] J. K. Sheu, G. C. Chi, and M. J. Jou, IEEE Electron Device Lett., vol. 22, pp.160-162, Apr. 2001.

[9] J. K. Sheu, Y. K. Su, G. C. Chi, P. L. Koh, M. J. Jou, C. M. Chang, C. C. Liu, and

W. C. Hung, Appl. Phys. Lett. vol. 74, pp. 2340-2342, Apr. 1999.

[10] J. F. Lin, M. C. Wu, M. J. Jou, C. M. Chang, B. J. Lee, and Y. T. Tsai, Electron. Lett., vol. 30, pp. 1793-1794, Oct. 1994.

[11] D. R. Kammler, T. O. Mason, D. L. Young, and T. J. Coutts, J. Appl. Phys., vol. 90, pp.3263-3268, Oct. 2001.

[12] T. Margalith, O. Buchinsky, D. A. Cohen, A. C. Abare, M. Hansen, S. P. DenBaars, and L. A. Coldren, Appl. Phys. Lett., vol. 74, pp. 3930-3932, Jun. 1999.

[13] R. H. Horng, D. S. Wuu, Y. C. Lien, and W. H. Lan, Appl. Phys. Lett., vol. 79, pp. 2925-2927, Oct. 2001.

[14] Y. C. Lin, S. J. Chang, Y. K. Su, T. K. Tsai, C. S. Chang, S. C. Shei, C. W. Kuo, and S. C. Chen, Solid-State Electronics, vol. 47, pp. 849-853, May 2003.

[15] S. M. Pan, R. C. Tu, Y. M. Fan, R. C. Yeh, and J. T. Hsu, IEEE Photon. Technol. Lett., vol. 15, pp. 646-648, May, 2003.

Chapter 4

Investigation of ITO ohmic contact to p-type GaN

4.1 Introduction

GaN-based LEDs have become commercially available since Nakamura et al. [1] successfully demonstrated the activation of Mg-doped GaN by post-growth thermal annealing in nitrogen ambience. However, the poor conductivity of p-GaN still limits the current spreading due to the low concentration of carriers. It is necessary to deposit a conductive layer on p-GaN to spread current uniformly, and this conductive film should not only form ohmic contacts to p-GaN but also be transparent to the emitted light from the active layer. There were many works focusing on materials and methods to form good ohmic contacts to p-GaN in the past [2]-[6]. Among the studies, Ni/Au films were commonly used as the semi-transparent current spreading layers due to their good contact characteristics to p-GaN. Kim *et al*. [5] presented the micro formation mechanism of Ni/Au contacts on p-GaN. Ga atoms diffused out from the GaN substrate and dissolved into Ni-Au solid solution would lead to the generation of Ga vacancies below the contact. The net concentration of holes below the contact increased, and therefore the contact resistivity was reduced. However, it was also shown that the transmittance of semi-transparent Ni/Au films for blue LEDs is only about 60% to 85% in the 450-550 nm wavelengths by Sheu *et al*. [7]. In order to reduce the absorption of the semi-transparent film, it is feasible to replace the conventional Ni/Au contact by a more transparent conductive material. There are also several researches [8]-[12] discussing the applications of ITO to GaN-based LEDs.

Margalith *et al*. [10] showed Schottky characteristics of the ITO/p-GaN interface after thermal annealing. This result could be attributed to a large work function difference between ITO and p-GaN. In order to improve the contact properties, some authors added an interfacial layer such as Ni or NiO prior to ITO deposition by a little sacrifice of transparency [9]-[11], and the interfacial material could provide ohmic contact between ITO and p-GaN. LEDs with that kind of contact structure would have a moderately higher forward voltage but a large enhancement in external quantum efficiency and power efficiency. However, very little information is available about the mechanism of forming ITO ohmic contacts on p-GaN.

In this chapter, the contact structure of ITO/p-$In_{0.1}Ga_{0.9}N$/p-GaN is utilized for investigation. X-ray photoelectron spectroscopy (XPS), x-ray diffraction (XRD), and secondary ion mass spectroscopy (SIMS) measurements are employed to characterize the chemical and physical properties of the interface. The mechanism of ohmic contact between ITO and p-GaN is clarified by these results.

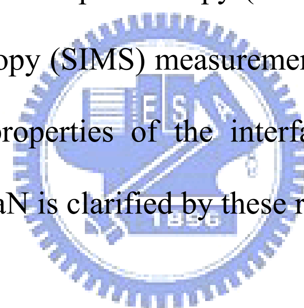

4.2 Experimental

The contact structure of ITO/p-$In_{0.1}Ga_{0.9}N$/p-GaN was utilized for investigation. The InGaN–GaN multi-quantum-wells (MQWs) LED wafers were grown on c-face sapphire substrates by a metal-organic chemical vapor deposition (MOCVD) system. The epitaxial structure comprised 4-μm-thick n-GaN, 0.1-μm-thick InGaN–GaN (MQWs) active layer, 0.2-μm-thick p-GaN, and a 10-nm-thick p-$In_{0.1}Ga_{0.9}N$ top layer.

Transmission line model (TLM) structure was employed to electrically characterize p-type contacts. The pad size was 280 μm x 75 μm and the spacings between the pads were 10, 20, 30, 40 and 65 μm. The TLM structures with ITO and

Ni/Au contacts were formed as shown in Fig. 4.1. First, an inductively coupled (ICP) plasma etcher was used to form a mesa structure with n-GaN layer revealed. Thus, p-GaN layer is isolated and the current crowding effect of TLM patterns is prohibited. Then the sample was immersed in H_2SO_4 and NH_4OH solutions to remove resists, organic contaminants and native oxides. Next, ITO or Ni/Au films was deposited and patterned on p-GaN layer as contacting materials by E-beam evaporation, respectively. For the deposition conditions, ITO (300 nm) film was prepared at 300°C in oxygen ambience with a partial pressure of 2 x 10^{-4} Torr, and Ni/Au (4 nm/4 nm) films were evaporated with a base pressure of 3 x 10^{-6} Torr. The ITO contact samples were subsequently annealed at 400°C, 500°C and 600°C in nitrogen ambience, and the Ni/Au contact sample was annealed at 540°C in the nitrogen ambience to achieve the optimal ohmic contact to p-GaN. Cr/Au (0.08 μm/0.8 μm) metallization films were employed for the probing pads on contacting materials. A semiconductor parameter analyzer HP-4156 was used to measure the current-voltage characteristics. In order to identify the current transport mechanism of ITO/p-GaN contact, the dependence of the specific contact resistivity on temperature was also evaluated from 25°C to 277°C.

There are also samples with ITO/p-$In_{0.1}Ga_{0.9}N$/p-GaN contacts prepared for SIMS, XPS and XRD measurements to investigate the formation mechanism. XPS depth profiling was used to monitor the binding energy of depth from the ITO film surface to p-GaN. This analysis was performed by a Thermo VG ESCALAB250 electron spectroscopy system with an energy resolution better than 25 meV, and the Ar^+ beam sputtering with 3KeV and 3uA was utilized in situ etching to p-GaN. SIMS measurement was carried out by a Cameca IMS-4f mass spectrometer system with Cs^+ beam. XRD was examined by a Rigaku RU-H3R diffractometer system with Cu K_α radiation.

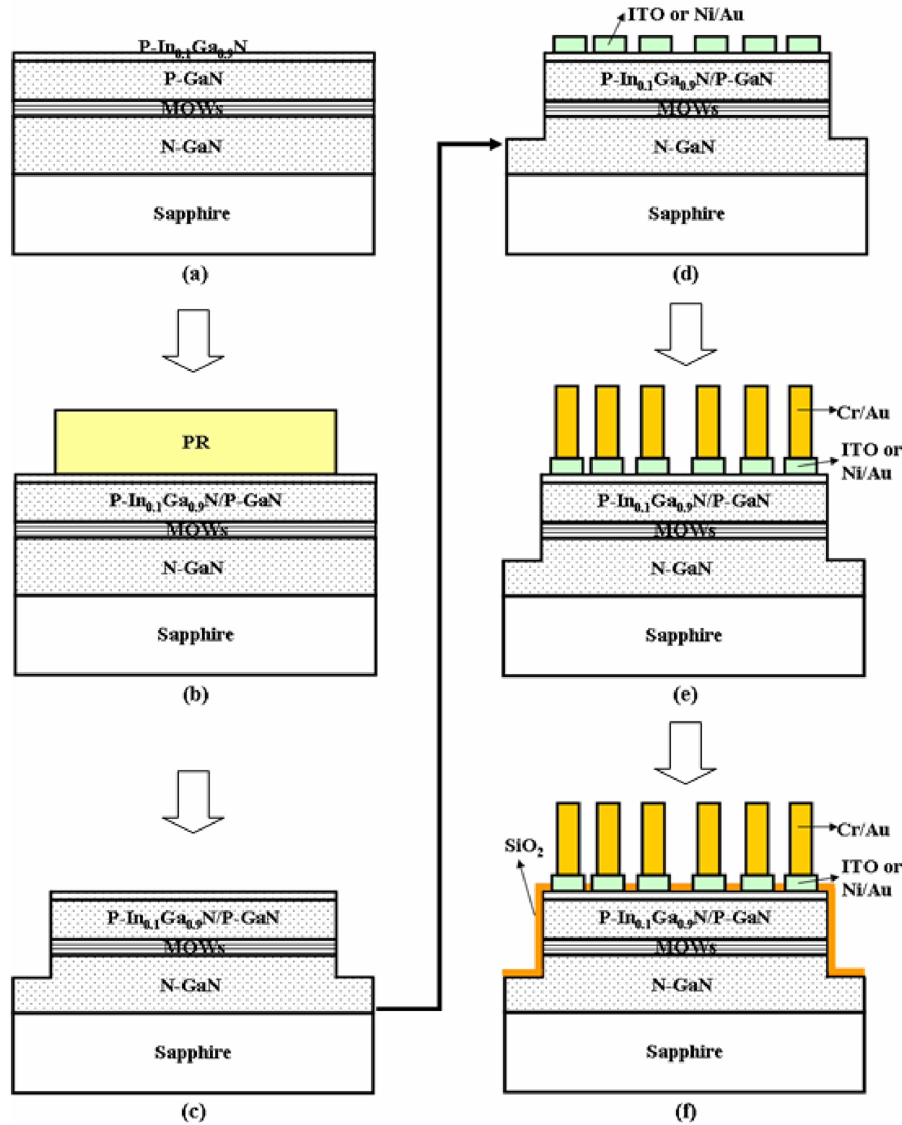

Fig. 4.1 The process flow diagrams TLM structure formation: (a) epitaxial structure (b) lithographic patterning (c) ICP etching to expose n-GaN layer (d) ITO deposition and patterning, (e) bonding pads metallization (f) SiO_2 protection layer

4.3 Results and Discussion

Figure 4.2 shows the transmittance spectra of the blank p-i-n GaN/sapphire, ITO and Ni/Au films deposited on p-i-n GaN/sapphire under different annealing conditions. The transmittance of the blank sample shows only around 75% in the visible spectrum region due to the great reflection at the interface resulted from the large difference of

indices between GaN (n_r = 2.4) and the air. The spectra of ITO samples annealed at 400°C, 500°C and 600°C are nearly coincident, and the transparency is all above 85%, which is higher than that of Ni/Au sample. Thus, the ITO film is considered more transparent than Ni/Au film and is suitable to be an optical medium between GaN and the air. Besides, the refractive index (n_r = 1.9) ranges between GaN and the air. Therefore, LEDs with ITO contact are supposed to be able to extract more light than the conventional LEDs with Ni/Au contact.

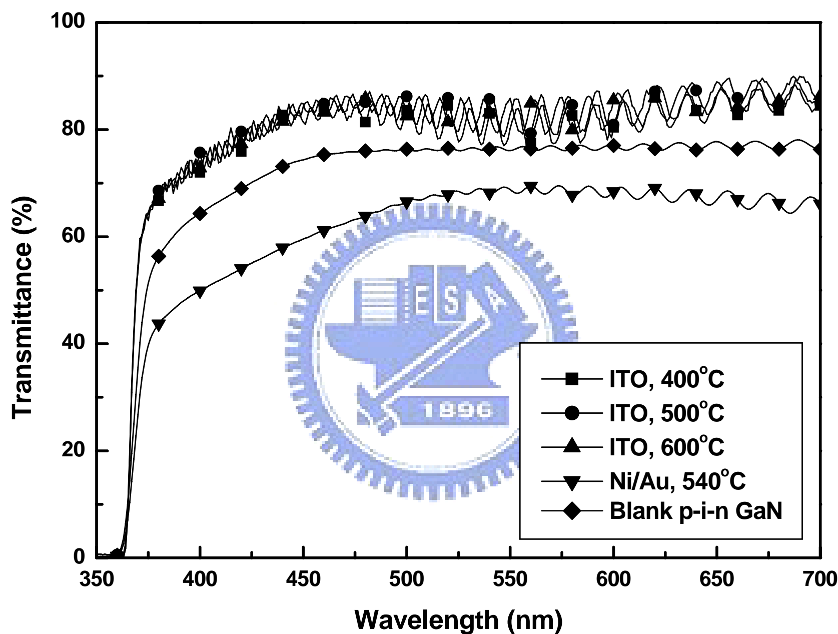

Fig. 4.2 Transmittance spectra of the blank p-i-n GaN/sapphire, the ITO and Ni/Au films deposited on p-i-n GaN/sapphire under different annealing conditions.

Figure 4.3 demonstrates the current-voltage relationship of TLM pads with a 10-μm-spacing, and the curves are measured with a voltage source from –5 V to 5 V at room temperature. The ITO contact samples annealed at different temperatures reveal ohmic characteristics, and the resistance between pads increases while arising annealing temperature from 400°C to 600°C for a fixed duration time. Although the

Ni/Au contact still shows better performance than ITO contact, the linear current-voltage characteristic makes it possible to apply ITO to the GaN-based LEDs with a quite low voltage drop at the interface.

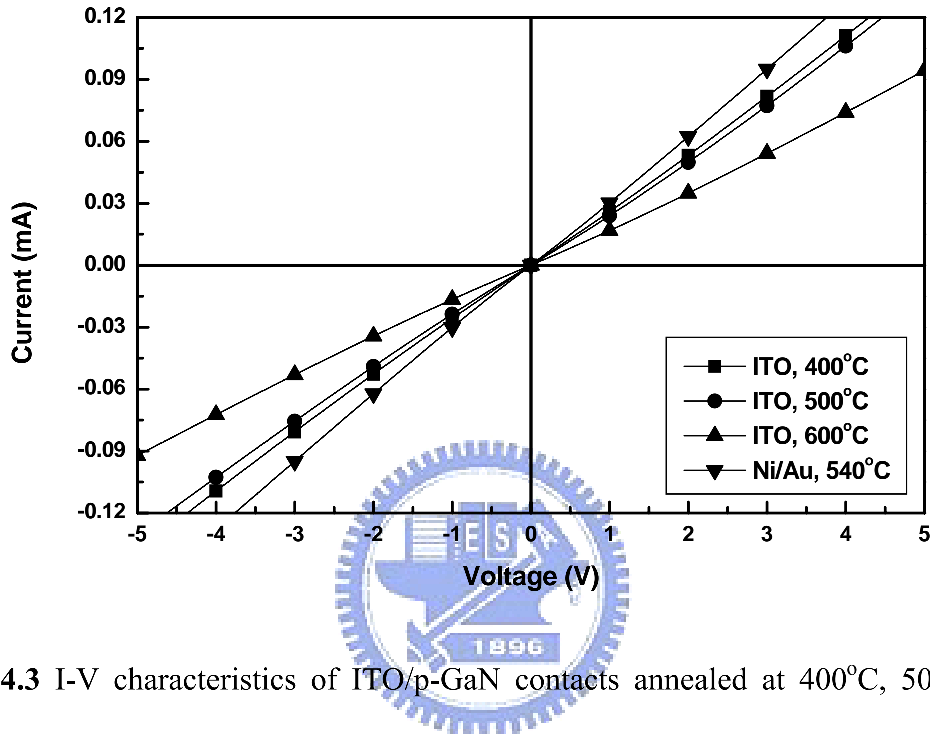

Fig. 4.3 I-V characteristics of ITO/p-GaN contacts annealed at 400°C, 500°C and 600°C and Ni/Au contact annealed at 540°C on p-GaN.

From the transport theory of metal-semiconductor junction, the specific contact resistivity of a metal-semiconductor contact dominated by thermionic emission, thermionic field emission or field emission is given by the following simple formulas,

$$\rho_c = \frac{k}{qA^*T}\exp(\frac{q\phi_B}{kT}) \qquad \text{(Thermionic Emission)}$$

$$\rho_c \approx \exp(\frac{q\phi_B}{E_0}) \qquad \text{(Thermionic Field Emission)}$$

$$\rho_c \approx \exp(\frac{q\phi_B}{\sqrt{N_A}}) \qquad \text{(Field Emission)}$$

where k is the Boltzmann constant, A^* is the Richardson constant, T is the

temperature and ϕ_B is the Schottky barrier height. The specific resistivity of metal-semiconductor contact dominated by thermionic emission is exponentially in inverse proportion to the temperature, while the specific resistivity of metal-semiconductor dominated by field emission is less dependent on the temperature. So the variation of the specific contact resistivity related to the inverse temperature represents the tendency of the electrical transport mechanism to thermionic emission or to field emission.

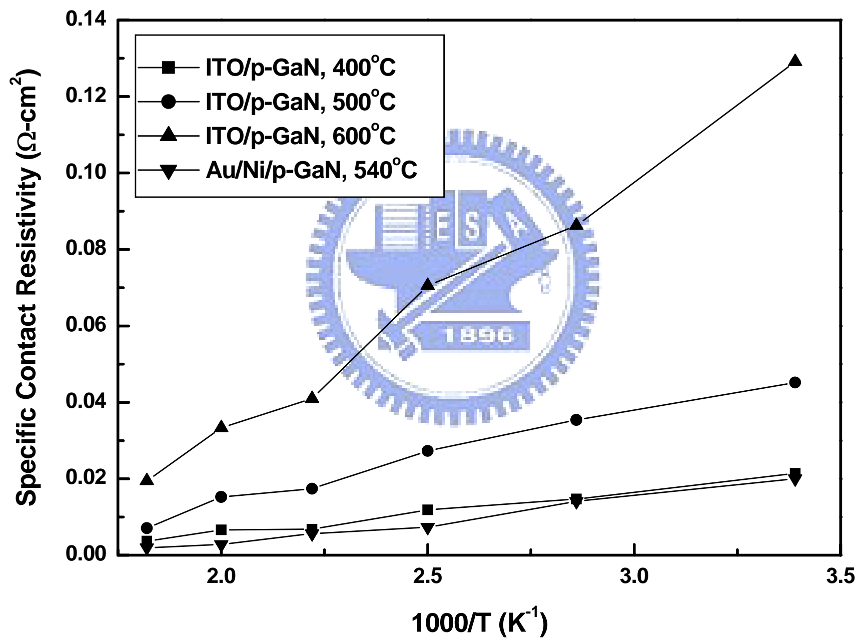

Fig. 4.4 Specific contact resistivities of different contacts on p-GaN as functions of the temperature.

Figure 4.4 shows the temperature dependent specific contact resistivity of the different temperature annealed ITO/p-GaN contacts. The specific resistivities of 400°C, 500°C, and 600°C-annealed samples decrease from 2.1 x 10^{-2}, 4.5 x 10^{-2}, and 1.3 x 10^{-1} ohm-cm^2 at room temperature to 3.7 x 10^{-3}, 7.1 x 10^{-3}, and 1.9 x 10^{-2}

ohm-cm^2 at 277°C, respectively. The variation of 600°C-annealed sample is larger than the other temperature annealed samples. It is supposed that the dominant transport mechanism of ITO/p-GaN structure tends from thermionic field emission to thermionic emission while varying the annealed temperature from 400°C to 600°C. As for the conventional Ni/Au contact, the transport mechanism is also dominated by thermionic field emission.

In order to investigate the chemical properties of constituents in depth, the 500°C-annealed ITO/p-GaN ohmic contact is analyzed by XPS with different sputtering times. Figure 4.5 demonstrates the binding energies of Ga 2$p_{3/2}$ and O 1s as functions of sputtering times. The peak of Ga 2$p_{3/2}$ varies from 1117.1 eV in the bulk p-GaN to 1117.9 eV around the ITO/p-GaN interface region. The chemical shift is due to the different partial-ionicities with O and N, which are bound with GaN in the bulk and the interface region, respectively. For the O 1s peak, the binding energy shifts from 530.1 eV in the ITO film to 530.3 eV at the interface of ITO/p-GaN. Similarly, the peak shift is also resulted from the different partial-ionicities with In and Ga, which are bound with ITO in the ITO film and the interface region, respectively. The Ga-O bonding is speculated to form at the interface and supposed to be helpful to form ohmic contacts by the previous study [9]. The formation of gallium oxide would result in gallium vacancies and increase the net concentration of holes below the contact, which can enhance the probability of carrier tunneling. Thus, the contact property could be improved by the formation of gallium oxide.

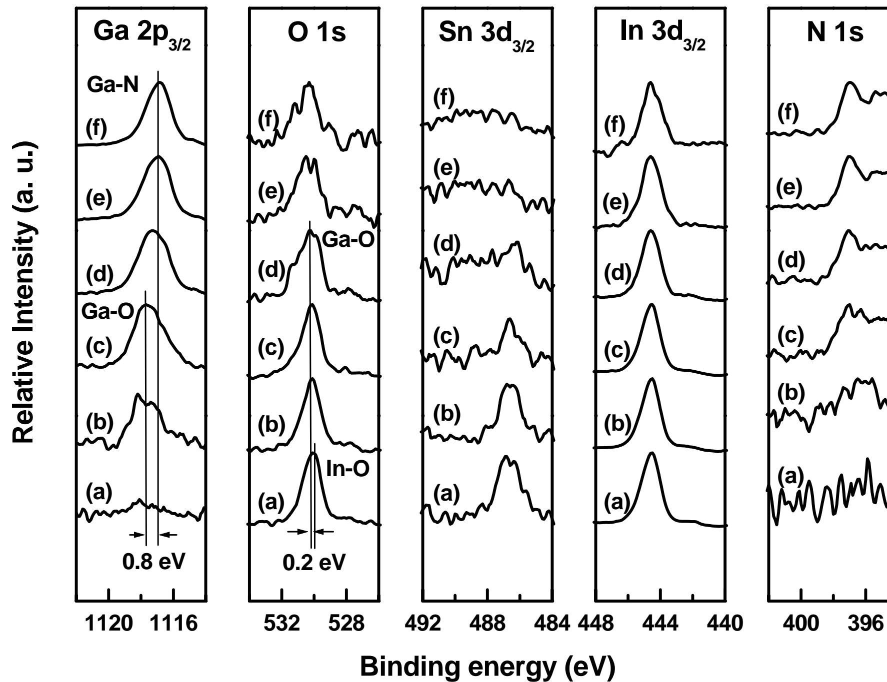

Fig. 4.5 XPS depth profiling of 500°C-annealed ITO contact on p-GaN with different sputtering times: (a) 0 (b) 120 (c) 210 (d) 300 (e) 390 (f) 480 seconds.

Figure 4.6 shows the X-ray diffraction results of the bare GaN and the GaN samples with ITO contact by thermal treatments. The peaks are all positioned with respect to the fixed Al_2O_3 (006) peak and the intensities are normalized by the GaN (002) peak intensities in the θ/2θ scans. The as-deposited ITO film on p-GaN is preferentially oriented along (222) and (400) crystallographic directions. As the annealing temperature is raised, the ITO (222) peak intensity increases but the ITO (400) peak diminishes after annealing. Therefore, the polycrystalline ITO film exhibits a preferential facet of (222) on GaN after annealing. The interfacial Ga-O bonding, which is observed by XPS, does not form a crystalline phase that can be detected by x-ray scan.

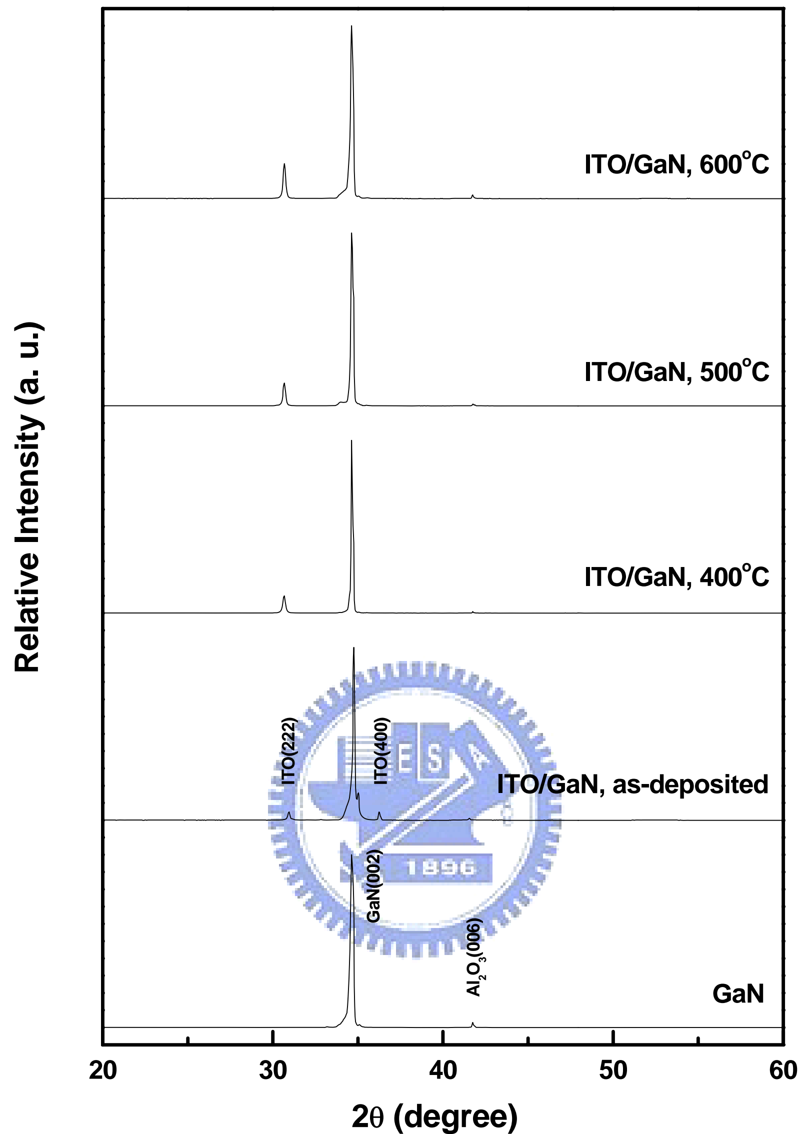

Fig. 4.6 XRD of the native p-i-n GaN and ITO films deposited on p-GaN with different annealing temperatures.

Figure 4.7 presents the SIMS profiles of the ITO/p-GaN samples. In comparison with the as deposition ITO sample, there is no significant diffusion observed when the samples are annealed at the temperature below 500°C. However, the interdiffusion of gallium and indium atoms becomes apparent as the ITO sample is annealed at 600°C. This serious interdiffusion phenomenon could be the main cause that leads the contact

to poor ohmic characteristics when the contact is annealed at the same temperature.

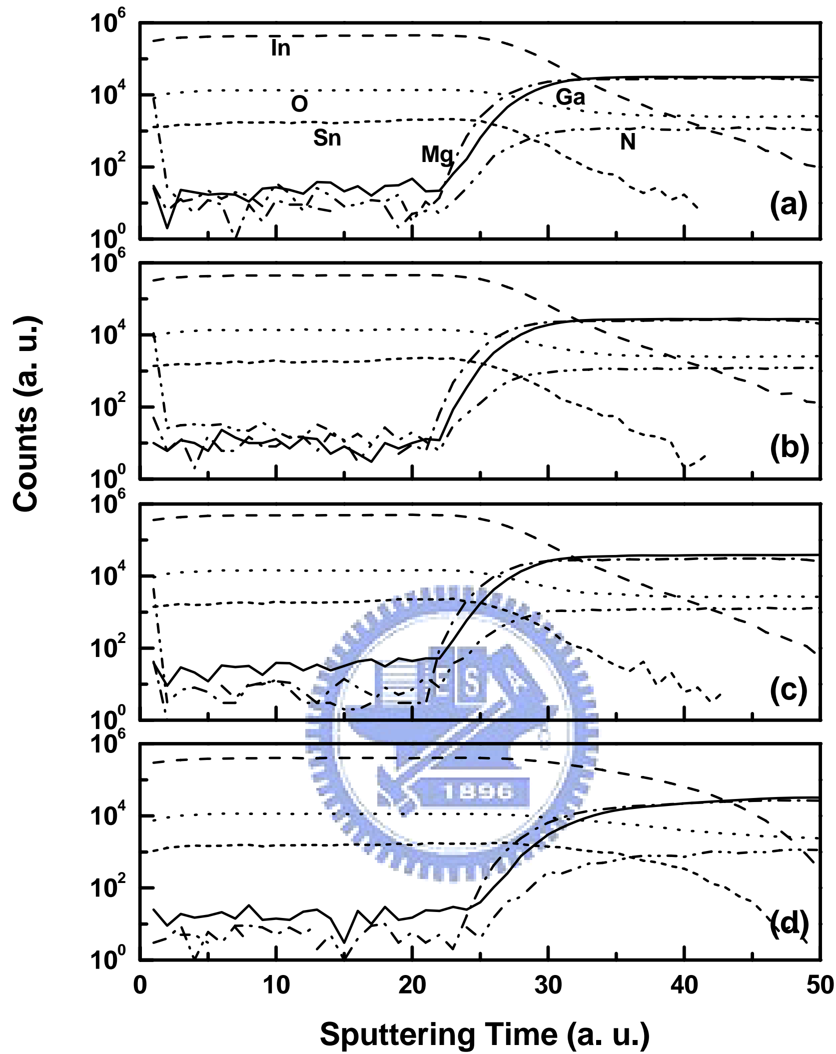

Fig. 4.7 SIMS profiles of ITO films deposited on p-GaN with different annealing temperatures: (a) as-deposited (b) 400°C (c) 500°C (d) 600°C.

From the results of XPS and SIMS, gallium oxides and gallium vacancies are formed in the interfacial region and the schematic drawings are shown in Fig. 4.8 to illustrate the contact interface structures before and after annealing.

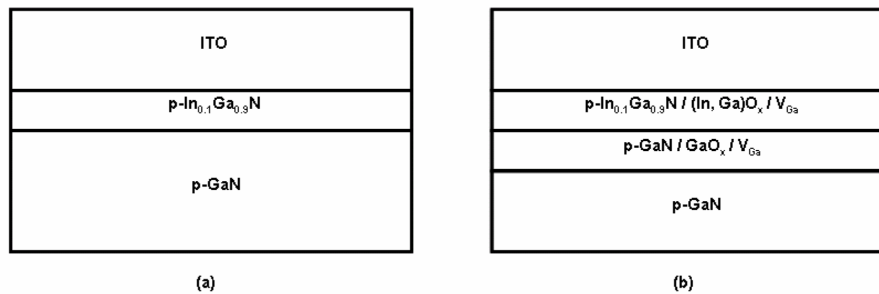

Fig. 4.8 Schematic drawings of the contact interface structures (a) before annealing and (b) after annealing.

4.4 Summary

In this chapter, the formation of ohmic contacts at the interface of ITO/p-GaN is investigated. The specific contact resistivity 4.5 x 10^{-2} ohm-cm^2 was obtained while annealing ITO/p-GaN contacts at 500°C. Based on the variation of the contact resistivity with respect to temperature, the dominant transport mechanism of ITO/p-GaN structure tended from thermionic field emission to thermionic emission as increasing annealing temperature from 400°C to 600°C. From the XPS, XRD and SIMS results, the outdiffusion of gallium atoms and the formation of Ga-O bonds would introduce the gallium vacancies and increase the net concentration of carriers beneath the contact, which would make the ITO/p-GaN contact reveal ohmic characteristic. However, the excess interfacial reaction and interdiffusion would result in the contact deterioration when the annealing temperature increased to 600°C. Therefore, ITO contacts can make GaN-based LED highly bright and reliable in practice as presented in chapter 3.

References

[1] S. Nakamura, T. Mukai, M. Senoh, and N. Iwasa, Jpn. J. Appl. Phys., vol. 31, pp. L139-L142, Feb. 1992.

[2] J. K. Kim, J. L. Lee, J. W. Lee, H. E. Shin, Y. J. Park, and T. Kim, Appl. Phys. Lett., vol. 73, pp. 2953-2955, Nov. 1998.

[3] J. K. Ho, C. S. Jong, C. C. Chiu, C. N. Huang, K. K. Shih, L. C. Chen, F. R. Chen, and J. J. Kai, J. Appl. Phys., vol. 86, pp. 4491-4497, Oct. 1999.

[4] J. K. Sheu, G. C. Chi, and M. J. Jou, IEEE Electron Device Lett., vol. 22, pp.160-162, Apr. 2001.

[5] J. K. Kim, J. H. Je, J. –L. Lee, Y. J. Park, B.-T. Lee. J. Electrochemical Society, vol. 147, pp. 4645-4651, Dec. 2000.

[6] L. –C. Chen, F.-R. Chen, J. –J. Kai, L. Chang, J. –K. Ho, C. –S. Jong, J. Appl. Phys., vol. 86, pp. 3826-3832, Oct. 1999.

[7] J. K. Sheu, Y. K. Su, G. C. Chi, P. L. Koh, M. J. Jou, C. M. Chang, C. C. Liu, and W. C. Hung, Appl. Phys. Lett., vol. 74, pp. 2340-2342, Apr. 1999.

[8] T. Margalith, O. Buchinsky, D. A. Cohen, A. C. Abare, M. Hansen, S. P. DenBaars, and L. A. Coldren, Appl. Phys. Lett., vol. 74, pp. 3930-3932, Jun. 1999.

[9] R. H. Horng, D. S. Wuu, Y. C. Lien, and W. H. Lan, Appl. Phys. Lett., vol. 79, pp. 2925-2927, Oct. 2001.

[10] Y. C. Lin, S. J. Chang, Y. K. Su, T. K. Tsai, C. S. Chang, S. C. Shei, C. W. Kuo, and S. C. Chen, Solid-State Electronics, vol. 47, pp. 849-853, 2003.

[11] S. M. Pan, R. C. Tu, Y. M. Fan, R. C. Yeh, and J. T. Hsu, IEEE Photon. Technol. Lett., vol. 15, pp. 646-648, May, 2003.

[12] K. -M. Chang, J. –Y. Chu, C. –C. Cheng. IEEE Photon. Technol. Lett., vol. 16, pp. 1807-1809, Aug. 2004.

Chapter 5

Influence of ITO films thickness on the performance of GaN-based light-emitting diodes

5.1 Introduction

GaN-based LEDs are fabricated on insulating sapphire substrates and mesa structures with lateral current conduction are utilized in the devices [1], [2]. However, the lateral current conduction could result in a severe current crowding phenomenon near either n-type or p-type electrode and thus impacts on the reliability of devices. Therefore, it is necessary to handle the lateral current conduction to alleviate this effect. There are many studies discussing the modeling of lateral current transport in GaN-based LEDs [3]-[6]. Kim et al. demonstrated that the finite resistance on both sides of the p-n junction should be taken into consider [6]. The total series resistance is categorized into the lateral resistance components of the n-GaN layer and the current spreading layer, and the vertical component of p-GaN layer and the p-type contact. Based on the model, the current density across the active layer can distribute uniformly by proper design of LED structure and contact geometry and thus the reliability of devices can be improved.

Indium tin oxide (ITO) film is utilized as a current spreading layer to replace the conventional Ni/Au contacts owing to its excellent optical characteristics [7], [8]. However, the resistivity of ITO films is much higher than that of Ni/Au films by at least 3 orders and that would limit the current spreading uniformly. Therefore, it is

necessary to reduce the sheet resistance of ITO film by increasing it thickness to have a uniform current injection. Here we will discuss the influence of varying thickness of ITO films on the performance of GaN-based LEDs.

5.2 Experimental

GaN-based LEDs (350 μm x 350 μm) and the corresponding transmission line model (TLM) structures for p-type ohmic contact characterization with different conducting layers were fabricated. The epitaxial structure was shown in the previous chapters. The samples were processed by dry etching to expose n-GaN layers and followed by metallization to form the ohmic contacts on each type of GaN respectively. ITO and Ni/Au films are deposited and alloyed on p-GaN layers as transparent p-type electrodes. Figure 5.1 shows the optical refractive index and extinction coefficient spectra of ITO films. It exhibits refractive index of 1.85 at 465 nm and optical bandgap energy of 3.35 eV. In order to reduce the reflection at the interface of ITO/p-GaN, the quarter-wavelength thick ITO films were utilized and the thickness is shown below,

$$t_{ITO} = \frac{\lambda}{4 \times n} \times \text{ (Odd Number)} \quad \text{(nm)}$$

Therefore, the thickness of ITO films for the emission wavelength at 465 nm is estimated to be around 60, 180, 300 nm, etc. TLM structures were used to measure the contact resistivity of the conducting layers on p-GaN. The chips are packaged into TO-Can forms, and an IS system is connected with Keithley 2430 source meter to measure the current-voltage and current-power characteristics of these LEDs. During the reliability testing, these chips with TO-Can form are stressed by a 50-mA current

injection at room temperature and relative humidity of 40%.

Various thick ITO films were also deposited on the p-i-n GaN with double-side-polished sapphire substrates to measure the transmittance, and the measurement was performed by Hitachi U3010 spectrophotometer. The sheet resistance of these conducting films was also measured by a four-point measurement after alloying.

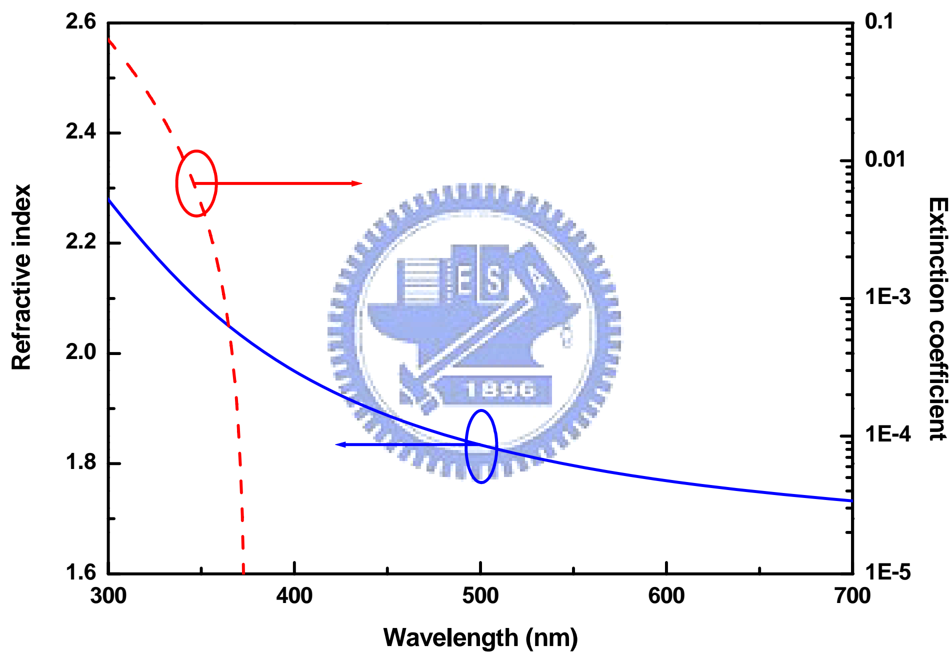

Fig. 5.1 The refractive index and extinction coefficient spectra of ITO films.

5.3 Results and Discussion

Figure 5.2 presents the transmittance of the various thick ITO and Ni/Au layers on p-i-n GaN/sapphire samples with a following alloying process. The curves of samples

with various thicknesses of ITO films annealed at 500°C all show around 80% at 465 nm, while Ni/Au sample shows only 60% due to the high absorption of Ni and Au metal layers. It is supposed that devices with various thicknesses of ITO films can have higher light extraction than with conventional Ni/Au contacts.

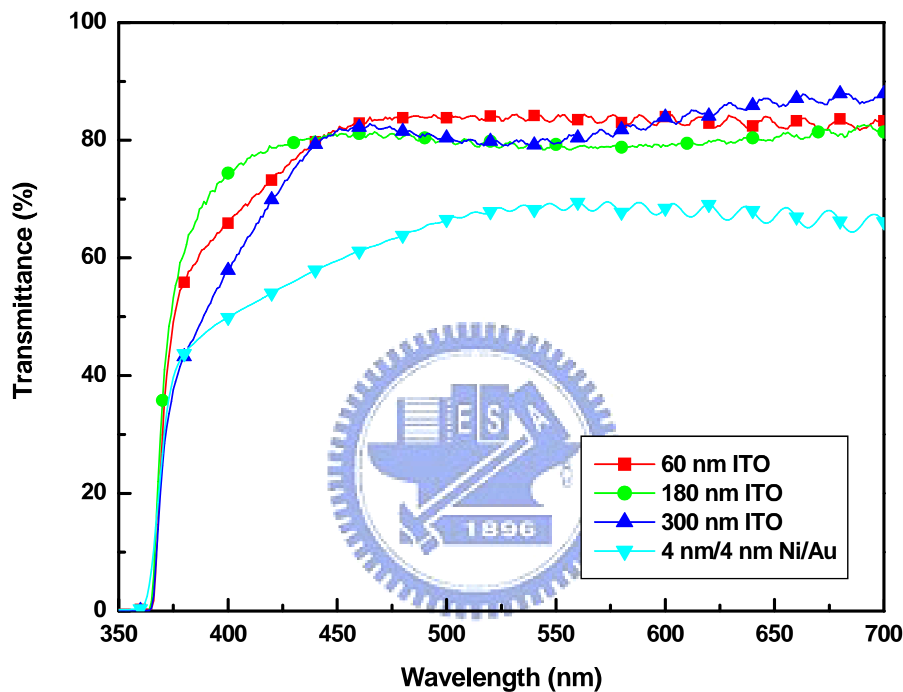

Fig. 5.2 The transmittance of the double sides polished p-i-n GaN/sapphire samples with various thicknesses of ITO layers and with Ni/Au layers.

Figure 5.3 shows the scanning electron microscope (SEM) pictures of ITO films after 500°C alloyed. The grain size of 180 nm- and 300 nm-thick ITO films are very close but much larger than that of 60 nm-thick ITO film. It is considered that ITO grains grow to a saturated size during evaporation. The grain size and boundary density might influence the resistivity of materials, and thus the sheet resistance of films does not linearly proportional to the inverse of films' thickness.

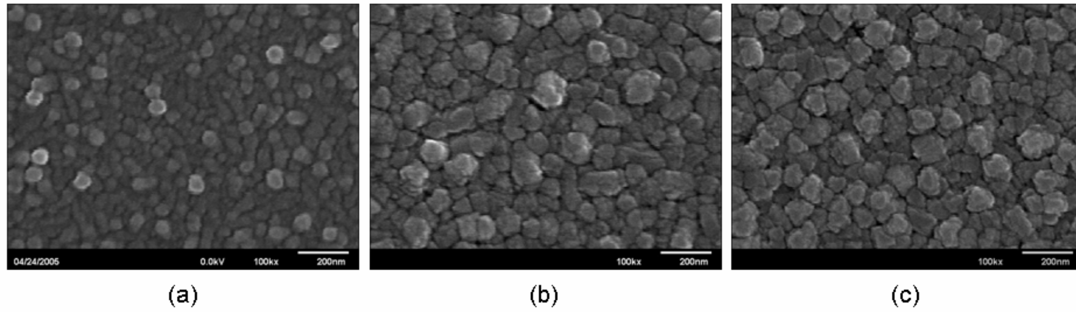

Fig. 5.3 SEM pictures of (a) 60 nm (b) 180 nm (c) 300 nm-thick ITO films.

Figure 5.4 shows the specific contact resistivity of different layers on p-GaN and the sheet resistance of p-GaN measured by TLM structures. From the results, the contact resistivity of ITO/p-GaN with various thicknesses of ITO films does not have a great difference from each other and it shows a value of around 0.1 ohm-cm2. Although the value is an order higher than that of Ni/Au layers contact on p-GaN, the ohmic contact of ITO/p-GaN is acceptable for the application of LEDs. The contact properties of conductive layers on p-GaN with Ni/Au layer and with various thicknesses ITO layers are summarized in Table 5.1.

Table 5.1 Summary of the contact characteristics of conductive layers on p-GaN with Ni/Au layer and with various thicknesses ITO layers. (t_p is about 200nm)

	60 nm ITO	180nm ITO	300nm ITO	Ni/Au
r_t (ohm/sq)	117.0	31.5	20.1	25.9
r_c (ohm-cm2)	0.103	0.131	0.121	0.009
$r_{s,p\text{-}GaN}$ (ohm/sq)	690513	895349	691878	983412
r_p (ohm-cm)	13.81	17.91	13.84	19.67
$r_p{*}t_p$	0.00028	0.00036	0.00028	0.00039

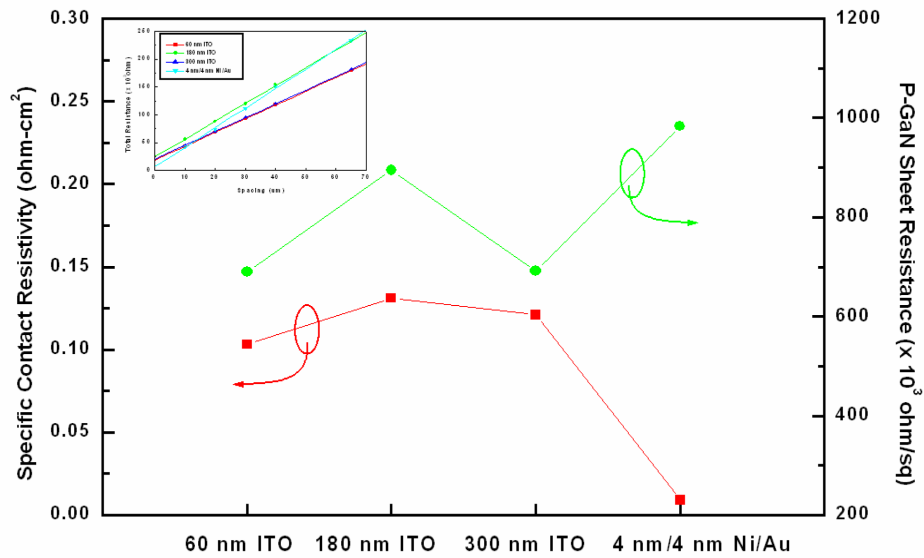

Fig. 5.4 Specific contact resistivity and p-GaN sheet resistance of various contacts on p-GaN.

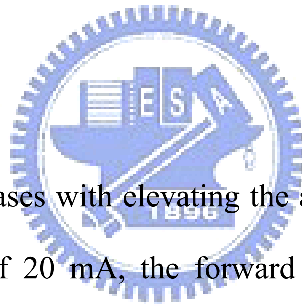

The forward current increases with elevating the applied voltage as demonstrated in Fig. 5.5. At the current of 20 mA, the forward voltage and the corresponding dynamic resistance are around 3.45, 3.42, 3.32, 3.20 V and 21.7, 18.8, 17.2, 16.6 ohm for chips with 60-, 180-, 300-nm-thick ITO and Ni/Au contacts, respectively. All the LEDs with ITO contacts present a forward voltage by at least 0.12 V higher than that with Ni/Au contacts due to the poorer contact properties. The chips with 300nm-thick ITO contacts exhibit the lower forward voltage and dynamic resistance as compared with chips with ITO contacts of other thickness. Therefore, the extra spreading resistance coming from the transparent conductive layers would result in higher series resistance and operation voltage.

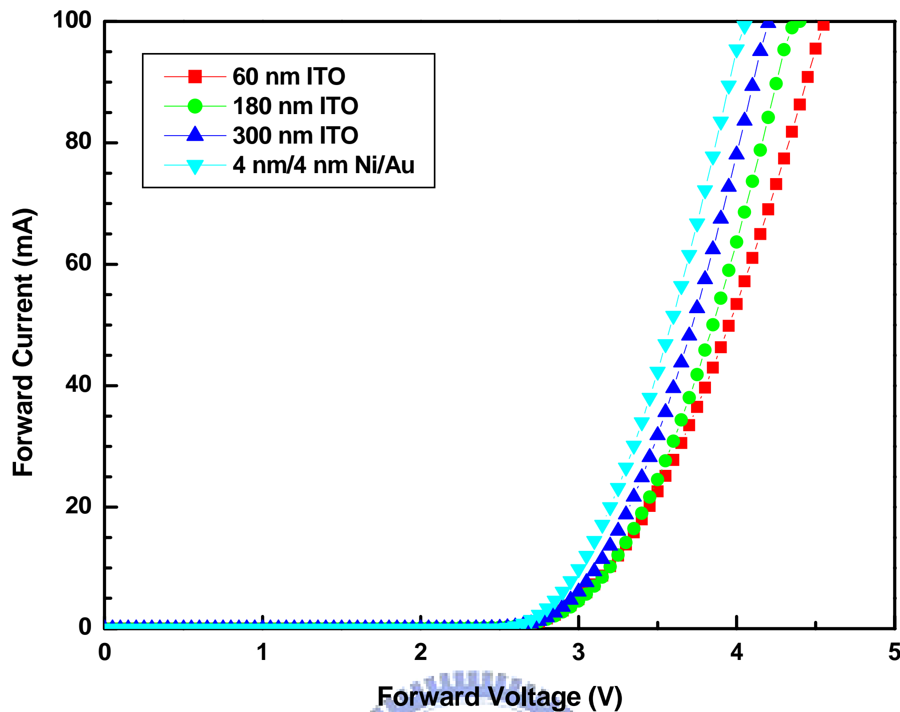

Fig. 5.5 The current-voltage characteristics of GaN-based LEDs with various thicknesses of ITO layers and Ni/Au layers.

Figure 5.6 shows the output power-current characteristics of LEDs with different contacts. The curves of LEDs with various thicknesses of ITO films are nearly coincident and exhibit an increase of around 30% in comparison with the curve of Ni/Au contacts LEDs. The great enhancement is mainly attributed to the higher transparency of ITO films than Ni/Au films. The chips with various thicknesses of ITO films show similar output power characteristics; hence the output power is independent of uniformity of current distribution but dependent on the transparency of conductive layers.

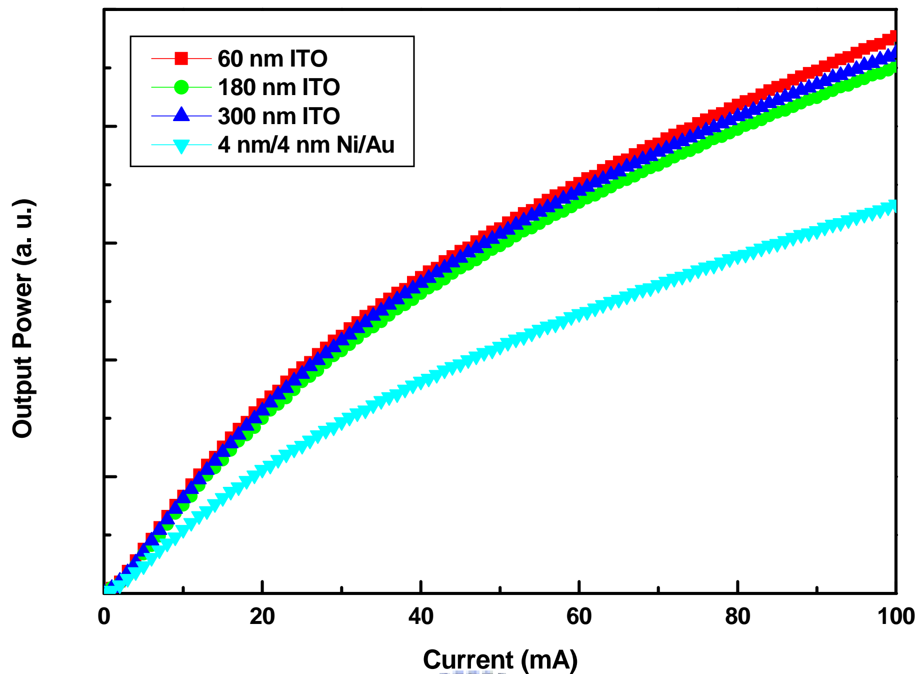

Fig. 5.6 The output power-current characteristics of GaN-based LEDs with various thicknesses of ITO layers and Ni/Au layers.

From the results of reliability test shown in Fig. 5.7, the conventional Ni/Au samples would suffer the output power decay of 22% after 1008-hour stress and the 300nm-thick ITO samples underwent a similar decay of 27%. However, the 60 nm-thick ITO contacts chips did not reveal a stable output power even though the samples had already suffered a degradation of 48% after 1008-hour stress. This phenomenon is probably due to the non-uniform current distribution which would induce local hot spots under high current injection. Besides, the dynamic resistance of the 60nm-thick ITO sample is higher than the others, and thus there is more heat generated while the devices are stressed at high current driving.

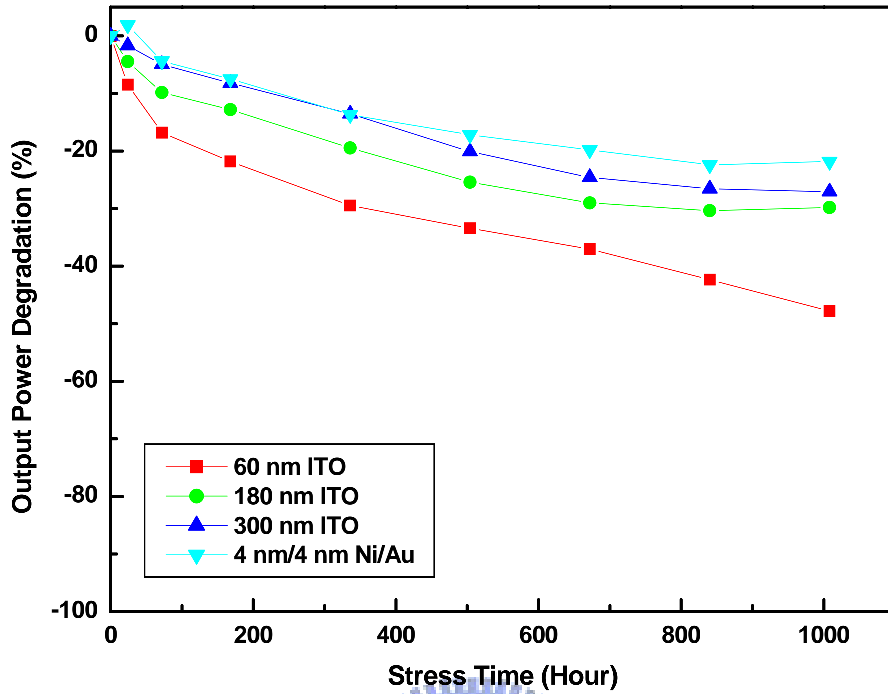

Fig. 5.7 Room temperature reliability test of output power degradation of GaN-based LEDs with various thick ITO and Ni/Au layers contacts.

Figure 5.8 shows the schematic LED structure with lateral transport geometry. In this structure, important distributed components of the total series resistance can be categorized into the lateral resistance components of the n layer (rs) and the transparent electrode (rt), and the vertical component of the p layer (rp) and the p contact (rc). As a result of derivation, the distribution of current density across the p-n junction is as following,

$$J(x) = J(0)\exp\left(\mp \frac{x}{\sqrt{(\rho_c + \rho_p t_p)\left|\frac{\rho_n}{t_n} - \frac{\rho_t}{t_t}\right|^{-1}}} \right) \quad , \qquad \begin{aligned} - &: \frac{\rho_t}{t_t} \leq \frac{\rho_n}{t_n} \\ + &: \frac{\rho_t}{t_t} > \frac{\rho_n}{t_n} \end{aligned}$$

Where J(0) is the reverse saturation current density at the mesa edge.

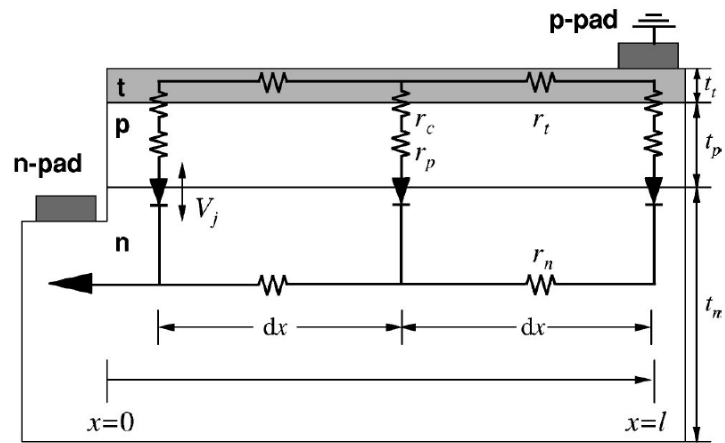

Fig. 5.8 Equivalent LED circuit with a *p* pad as a physical ground [6].

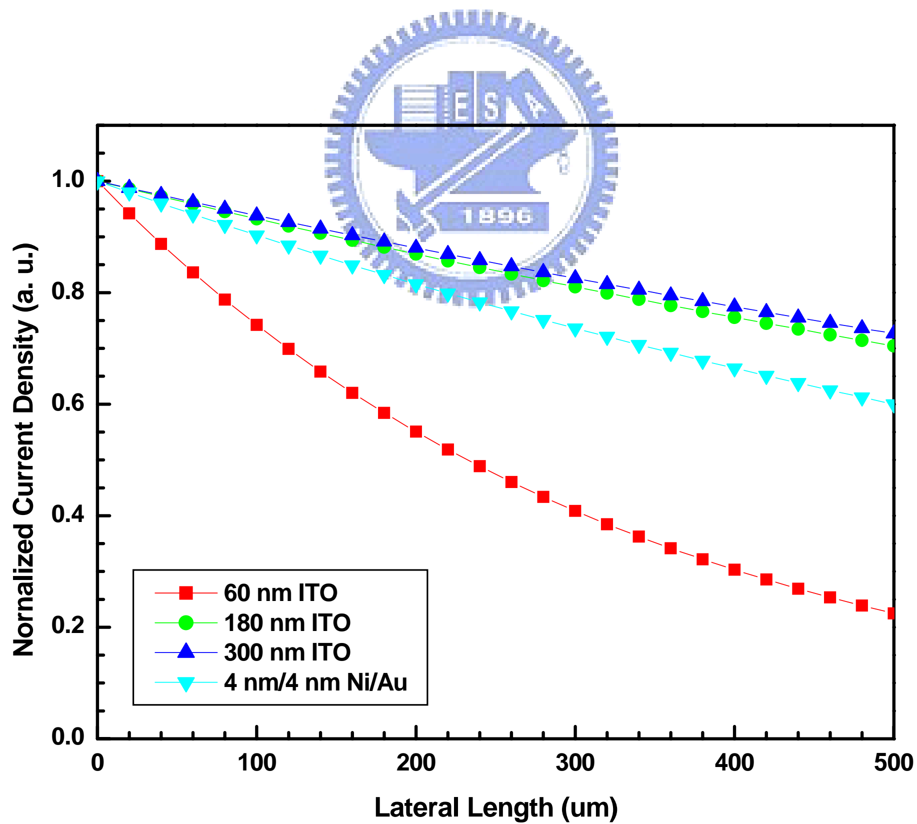

Fig. 5.9 Calculated current density distribution vs. the lateral length in a LED.

The calculated current density distribution of the GaN-based LED is shown in Fig. 5.9. Parameters used in the calculation are given by ρ_n/t_n = 25 ohm/sq, tp = 200 nm, and other parameters are shown in table 5.1. The LED with 60nm-thick ITO contact exhibit a worse current distribution and it would cause a serious current crowding problem introducing local hot spots as devices operated. Therefore, the performance of devices would be degraded under high current stress once the local hot spots are formed.

5.4 Summary

This chapter investigates the influence of various thicknesses of ITO films on the performance of GaN-based LEDs. LEDs with quarter wavelength thicknesses of ITO films are fabricated and characterized. LEDs with various thicknesses of ITO films show nearly coincident output power-current curves and exhibit an increase of 30% as compared with Ni/Au contacts devices. At a current of 20 mA, the forward voltage are around 3.45, 3.42, and 3.32 V for chips with 60 nm, 180 nm, 300nm-thickness ITO contacts, respectively. Although LEDs with various thicknesses of ITO films exhibit similar external quantum efficiencies, the power efficiencies are raised with increasing the thickness of ITO layer due to the difference in series resistance. From the current distribution simulation in devices, the LEDs with 60 nm ITO contacts present a worse result and it would cause a serious current crowding problem introducing local hot spots as devices operated. As a result, the LEDs with 60 nm ITO contacts suffered an output power degradation of 48% rafter 1008-hour stress but still did not reach a stable status.

References

[1] S. Nakamura, T. Mukai, and M. Senoh, Appl. Phys. Lett., vol. 64, pp. 1687-1689, Mar. 1994.

[2] S. Nakamura, M. Senoh, N. Iwasa, and S. Nagahama, Appl. Phys. Lett., vol. 67, pp. 1868-1870, Sep. 1995.

[3] H. Kim, J. Lee, C. Huh, S. Kim, D. Kim, S. Park, and H. Hwan, Appl. Phys. Lett., vol. 77, pp.1903-1904, Sep. 2000.

[4] H. Kim, S. Park, and H. Hwang, IEEE Transaction on Electron Devices, vol. 48, pp. 1065-1068, Jun. 2001.

[5] X. Guo and E. F. Schubert, J. Appl. Phys., vol. 90, pp. 4191-4195, Oct. 2001.

[6] H. Kim, S. Park, H. Hwang, and N. Park, Appl. Phys. Lett., vol. 81, pp. 1326-1328, Aug. 2002.

[7] T. Margalith, O. Buchinsky, D. A. Cohen, A. C. Abare, M. Hansen, S. P. DenBaars, and L. A. Coldren, Appl. Phys. Lett., vol. 74, pp.3930 – 3932, Jun. 1999.

[8] K. -M. Chang, J. –Y. Chu, C. –C. Cheng. IEEE Photon. Technol. Lett., vol. 16, pp. 1807-1809, Aug. 2004.

Chapter 6

Brightness enhancement of ITO/GaN LEDs by self-aligned micro-net structures

6.1 Introduction

Group III-nitride semiconductors have recently attracted much attention for solid-state lighting applications [1], [2]. Increasing the external quantum efficiency is very important in fabricating high-brightness GaN-based light-emitting diodes (LEDs). In contrast to p-type GaAs or InP semiconductors, the low concentration of holes limits the conductivity of p-type GaN semiconductor. Top-emitting LEDs depend on a conductive film deposited on the p-GaN layer to spread the current uniformly. This conductive layer should not only form an ohmic contact with p-GaN but also be transparent to light emitted from the active layer. Ni/Au films are often used as semi-transparent current spreading layers because they exhibit good contact characteristics with p-GaN. However, Sheu *et al.* [3] showed that the transmittance of Ni/Au films is only 60% to 80% at wavelengths of 450-550 nm. The conventional Ni/Au contacts can be replaced with more transparent conductive materials to reduce the absorption of the current spreading layers and thus increase the external quantum efficiency of LEDs. Numerous studies [4]-[7] have addressed the application of indium-tin-oxide (ITO) to GaN-based LEDs. The transmittance of ITO films exceeds 85% in the visible spectrum region, and LEDs with ITO contacts are now commercially available. Several works [8]-[10] have discussed improving the light

extracted from LEDs using micron-scale structures. Choi *et al.* [9], [10] demonstrated that the sidewalls in micro-LEDs were important in the extraction of light from the mesa structure. A higher ratio of the total surface-area, including the top and sidewall areas, to the light-emission-area is desired, because then more pathways are available by which the generated photons can escape. However, LEDs with ITO contacts are normally encapsulated by epoxy materials after packaging and the refractive index of ITO (n_r = 1.9 @ 460 nm) differs from that of epoxy material (n_r = 1.5 @ 460 nm). SiO_xN_y (n_r = 1.67 @ 460 nm) passivation can be introduced to act as an optical medium to reduce the reflection at the interface because its refractive index is just between that of ITO and epoxy materials. In this article, ITO is applied to the micro-LEDs with SiO_xN_y passivation and the process is simplified by self-aligned method to increase the light extraction area and shorten the optical paths.

6.2 Experimental

The InGaN–GaN multi-quantum-wells (MQWs) LED wafers were grown on c-face sapphire substrates by a metal-organic chemical vapor deposition (MOCVD) system. The epitaxial structure comprised 4-μm-thick n-GaN, a 0.1-μm-thick InGaN–GaN (MQWs) active layer, and 0.1-μm-thick p-GaN as shown in Fig. 6.1 (a). Additionally, the carrier concentrations of the p-GaN and n-GaN were 5 x 10^{17} cm^{-3} and 3 x 10^{18} cm^{-3}, respectively. A wafer with a peak wavelength at 465 nm was cleaned in H_2SO_4 and NH_4OH solutions to remove organic contaminants and native oxides. The simplified self-alignment process was performed as depicted schematically in Fig. 6.1. The ITO (280 nm) and SiO_2 (400 nm) films were initially deposited on p-GaN by e-beam evaporation and plasma enhanced chemical vapor

deposition (PECVD) systems. Arrays of square- and hexagonal-hole of various dimensions were patterned on the SiO_2/ITO/GaN structure. After SiO_2 was reactively etched with CHF_3/O_2 plasma, the photoresist was removed by O_2 plasma and ITO/GaN was subsequently reactively etched using inductively coupled Cl_2/Ar plasma. After a micro-net structure was formed, the samples were immersed in buffered oxide etch (BOE) solution to remove the SiO_2 mask and then annealed at 500°C in the nitrogen ambient to produce ohmic contacts. Cr/Au (0.08 μm/0.8 μm) metallization was employed for the n-type contact layer, and the p- and n- bonding pads. The samples were passivated with SiO_xN_y (210 nm) film by PECVD. Reactive gases, SiH_4, N_2O, NH_3 and N_2, were supplied inside the reactor chamber and their flow rates were 5, 20, 20 and 355 sccm. The temperature, pressure and RF power during deposition were 250 ^{o}C, 500 mTorr and 100 W. Figure 6.2 shows the refractive index spectra of SiO_xN_y and ITO films measured by N&K Analyzer. The refractive indices of SiO_xN_y and ITO films are 1.67 and 1.87 at the wavelength of 470 nm, respectively. After the front-end process had been completed, the samples were polished, scribed and diced into chips. Finally, each kind of chip with its own micro-net structure was packaged into TO-Can forms. The scanning electron microscopy (SEM) pictures of diced devices are taken by the model of JEOL JSM-6380. An IS CAS-140B system integrated with a Keithley 2430 source meter was used to measure the current-voltage and current-power characteristics of these LEDs. The luminescence was obtained in conformity with CIE (International Commission on Illumination) specifications, and the total power was measured by collecting all directional light inside an integrated sphere.

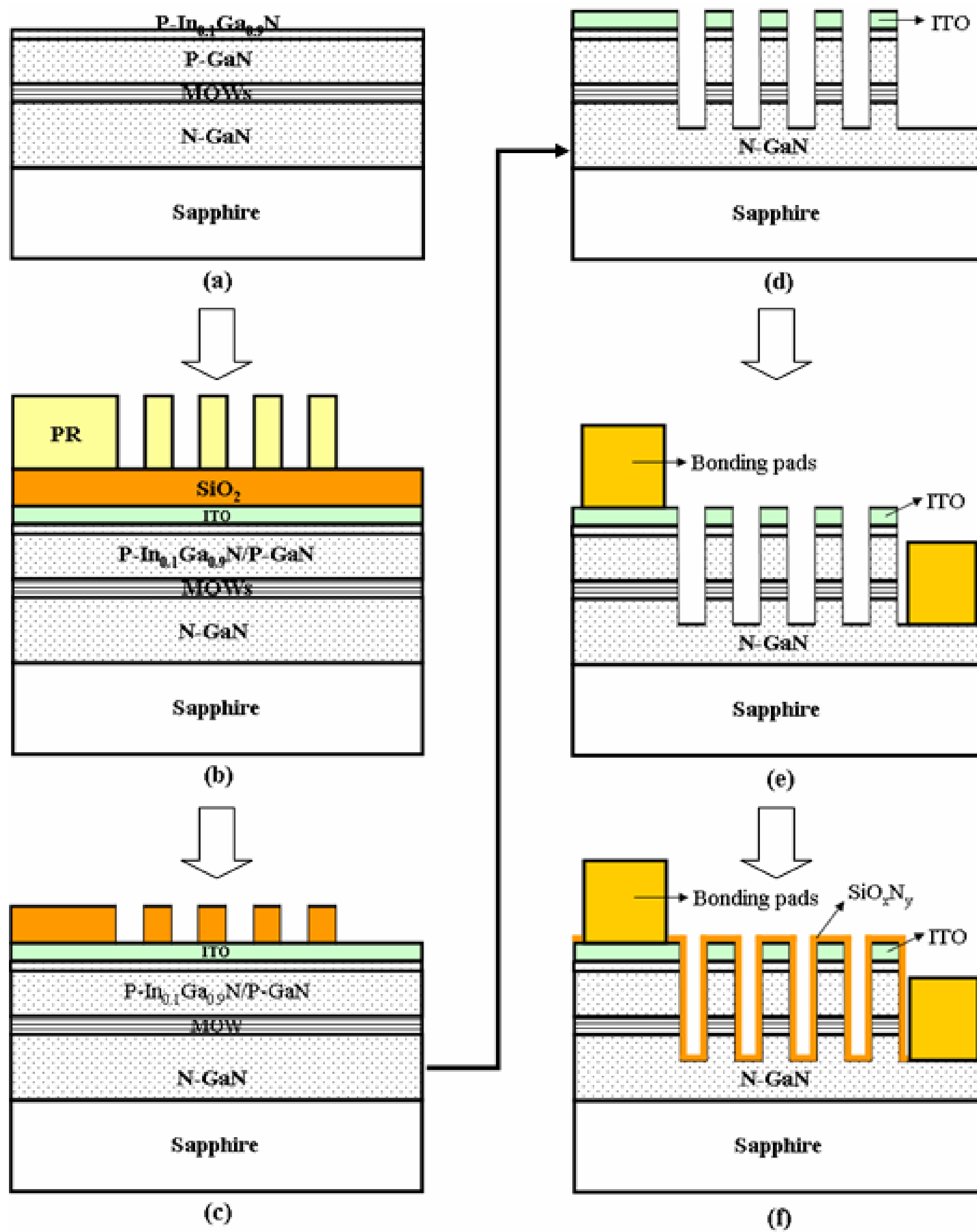

Fig. 6.1 The process flow diagram: (a) epitaxially structure, (b) ITO/SiO_2 deposition and lithographic patterning, (c) etching SiO_2 and removing the photoresist, (d) etching ITO/GaN, removing SiO_2 and annealing, (e) Cr/Au metallization, (f) SiO_xN_y passivation.

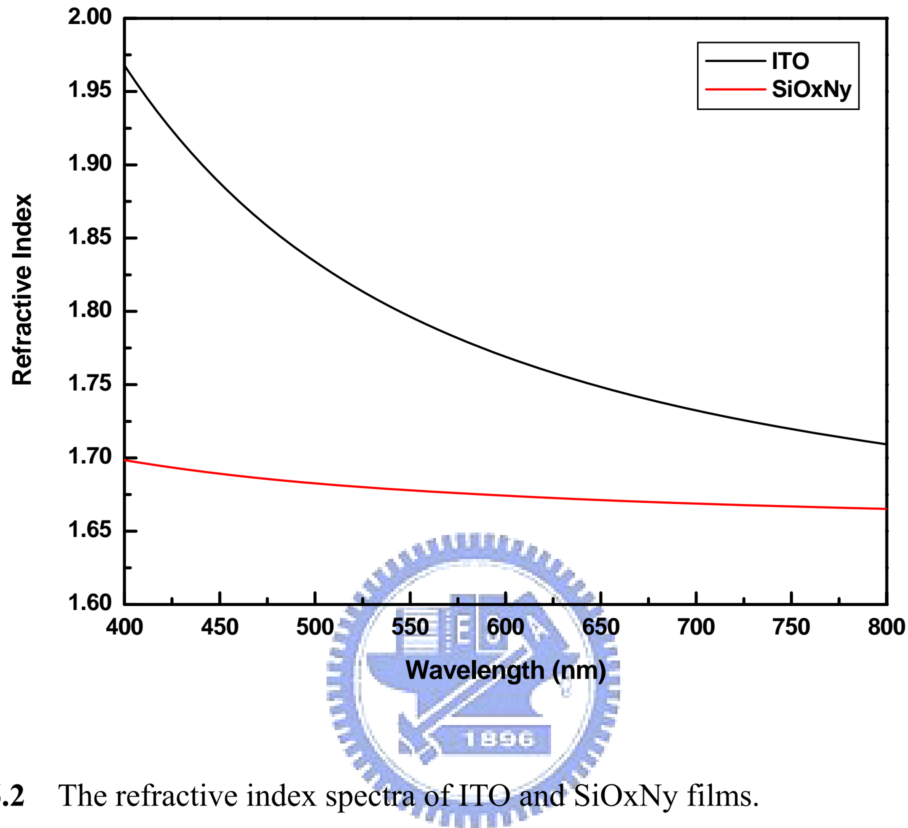

Fig. 6.2 The refractive index spectra of ITO and SiOxNy films.

6.3 Results and Discussion

Figure 6.3 shows the SEM pictures of the fabricated devices. It can be seen clearly micro-net structures with holes arrays on the active regions of the devices. It should be noted that although the original mask pattern was square and hexagonal holes arrays, the observed micro-net structures have some erosion at the sidewalls of holes. Such a discrepancy could be attributed to the side etching of oxide mask and ITO films during pattern transfer.

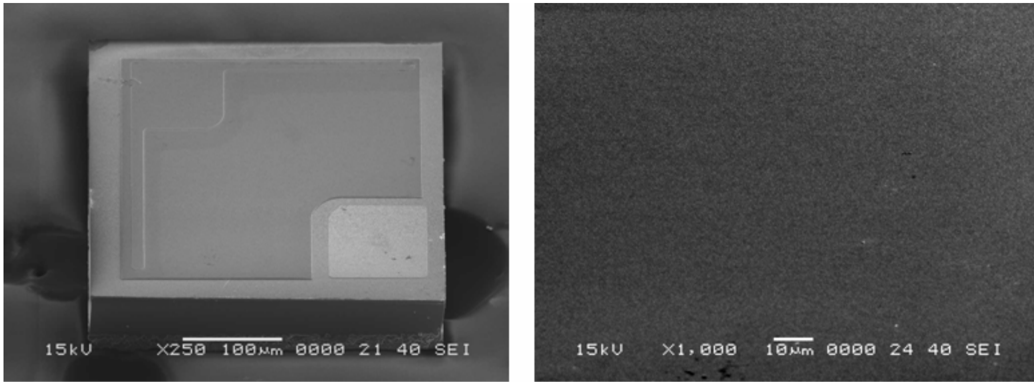

(a)

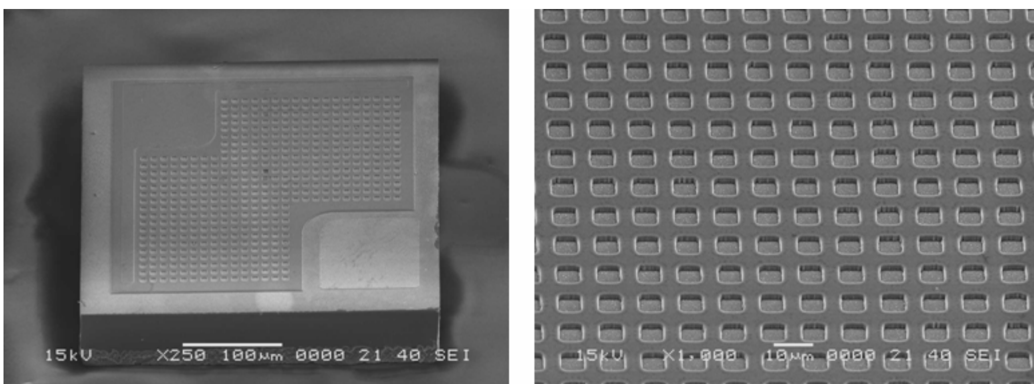

(b)

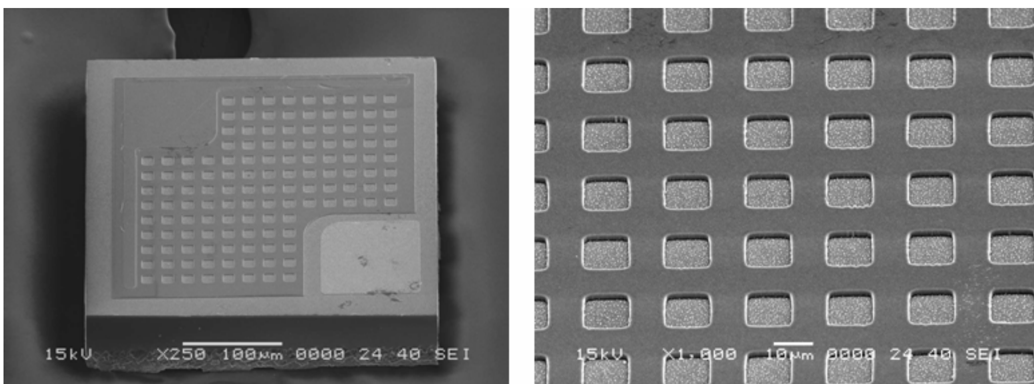

(c)

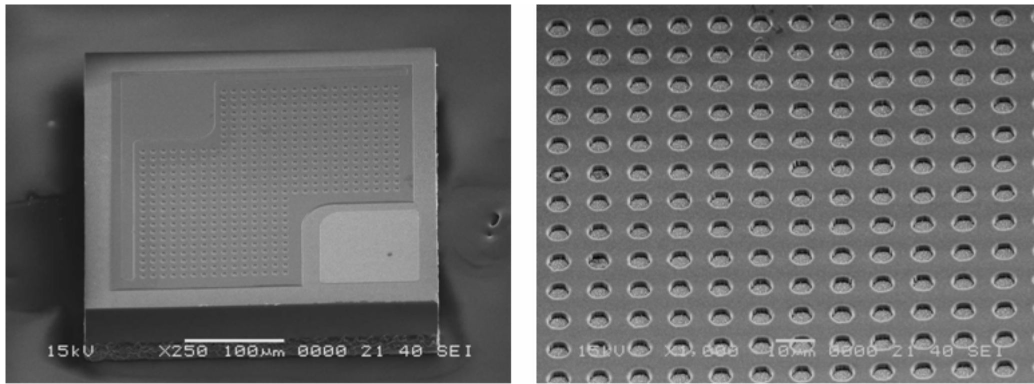

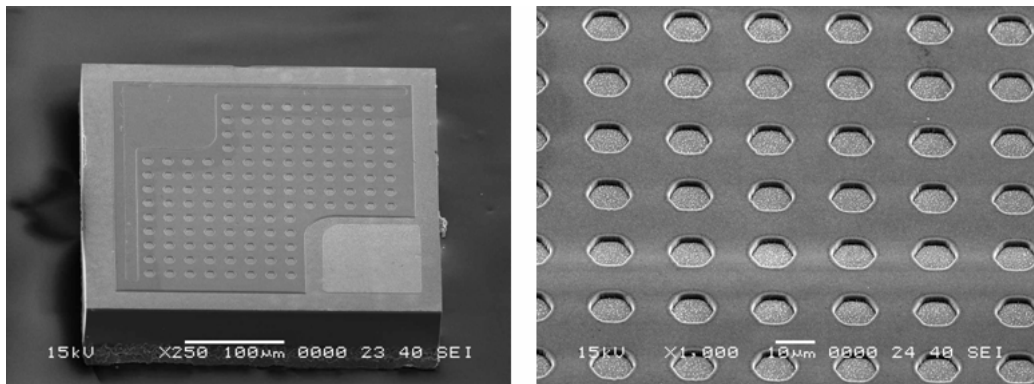

Fig. 6.3 The SEM pictures of (a) conventional LED and micro-net structure LEDs with (b) 5-um square (c) 10-um square (d) 5-um hexagonal (e) 10-um hexagonal holes arrays.

Figure 6.4 plots the forward current-voltage characteristics of the micro-net LEDs with arrays of square and hexagonal holes with 5 and 10-μm-dimensions. The LED with the conventional structure exhibits a forward voltage of 3.2 V and a micro-net structure of 3.3 V when a 20-mA-current is injected. The forward voltage of the micro-net LEDs may have been slightly higher because of the additional contact resistance resulted from the reduction in effective ohmic contact area of ITO with p-GaN.

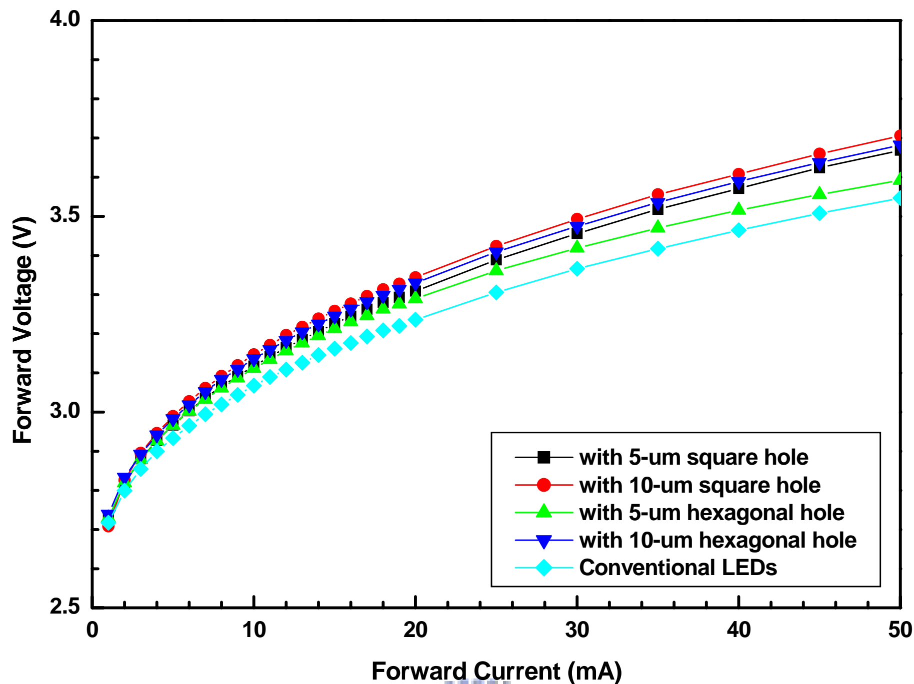

Fig. 6.4 Measured forward voltages as a function of the injected currents of GaN-based LEDs with self-aligned micro-net and conventional structures.

Figure 6.5 plots the current-luminescence and current-power relationships of LEDs. When a 20mA-current is injected, the LEDs with the micro-net structures have a similar output power but a 10% better normal luminescence than the conventional LEDs. Figure 5.6 also plots the ratio of normal luminescence to output power of the LEDs with different structures versus the injected currents. The ratio represents the concentration of the extracted light in the axial direction. Notably, the LEDs with arrays of 5-μm hexagonal holes structure reveal a 25% higher ratio at a 50-mA current, which is equivalent to a current density of 100 A/cm^2, than the conventional ones. It might be attributed to the larger sidewall area provided by the micro-net structure and thus increase the scattering probability of the photons extracted through the sidewalls in the axial direction.

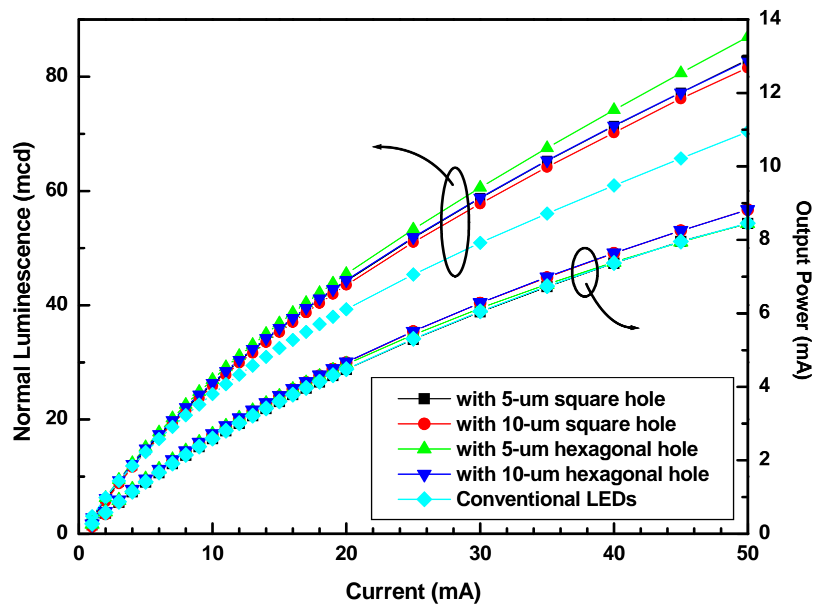

Fig. 6.5 Normal luminescence and output power as functions of the injected currents of GaN-based LEDs with self-aligned micro-net and conventional structures.

ES 1896

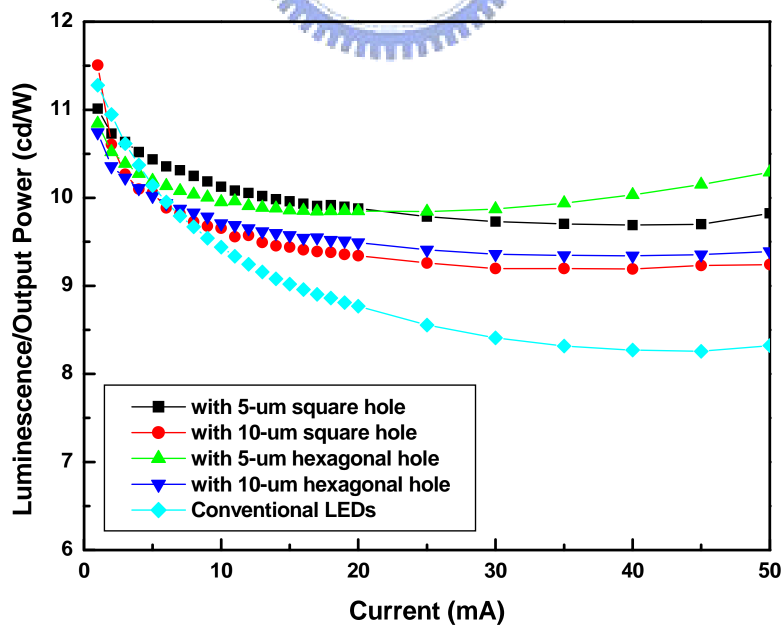

Fig. 6.6 Ratios of normal luminescence to output power as functions of the injected currents of GaN-based LEDs with self-aligned micro-net and conventional structures.

As shown in Fig. 6.7, the emission image reveals the higher intensity of light extracted from the sidewall than the top-surface of the micro-net structure. Therefore, more extracted light from micro-net LEDs would normally propagate than that from conventional LEDs. Table 6.1 summarizes the electrical and optical characteristics of the micro-net and the conventional LEDs. When the LEDs with various structures were negatively biased at 5 V, the devices exhibited almost the same leakage level.

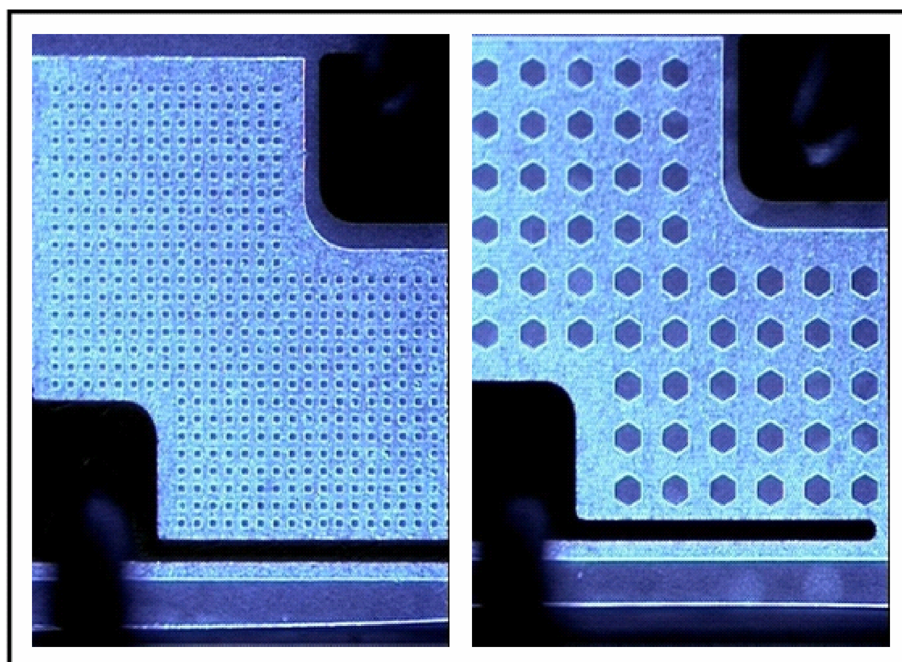

Fig. 6.7 Emission images of LEDs with micro-net structures.

Figure 6.8 plots the relationship between the external quantum efficiency and the driving current. The external quantum efficiency of LEDs with micro-net structures exceeds that of the conventional LEDs by approximately 5%. The dimensions and the density of the holes can be varied to maximize external quantum efficiency of the LEDs at an operating current of 3 mA. This structure is quite useful for increasing the output power at low current.

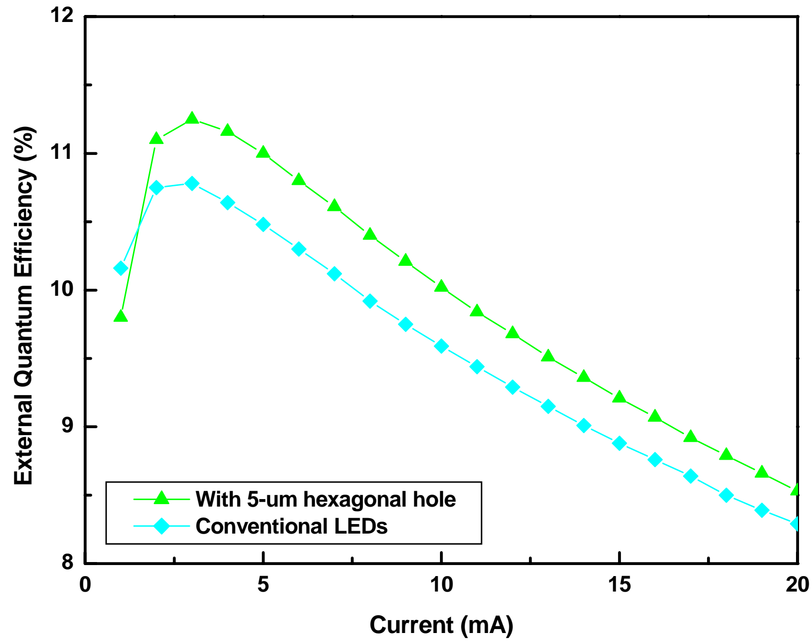

Fig. 6.8 External quantum efficiencies as functions of the injection currents of GaN-based LEDs with self-aligned micro-net and conventional structures.

Table 6.1 Comparative data for LEDs with various structures (Forward and reverse characteristics of LEDs obtained with a 20-mA injection current and a –5 V bias).

Shape of Holes	Dimension (μm)	Forward Voltage (V)	Luminescence (mcd)	Output Power (mW)	L/PO (cd/W)	Reverse Current (μA)
Square	5	3.31	44.2	4.48	9.9	0.56
Square	10	3.34	43.5	4.66	9.3	0.46
Hexagon	5	3.29	45.5	4.62	9.8	0.49
Hexagon	10	3.33	44.4	4.67	9.5	0.54
Conventional	None	3.24	39.3	4.48	8.8	0.54

6.4 Summary

This chapter proposes a feasible method for fabricating micro-LEDs with ITO contact. The self-aligned micro-net LEDs are a least 10% brighter than the conventional structure in the normal direction without loss of operating voltage and leakage current. The ratio of luminescence to total output power is increased by 25% at a current density of 100 A/cm^2. Additionally, the peak value of external quantum efficiency can be increased by 5% by varying the dimensions and the density of the holes at a low current of 3 mA. With higher normal luminescence and external quantum efficiency, LEDs with such a structure are quite useful in surface-mounting and low-power-consuming devices.

References

[1] S. Nakamura, M. Senoh, N. Iwasa, and S. Nagahama, Appl. Phys. Lett., vol. 67, pp. 1868-1870, Sep. 1995.

[2] C. M. Lee, C. C. Chuo, I. L. Chen, J. C. Chang, and J. I. Chyi, IEEE Electron Device Lett., vol. 24, pp. 156-158, Mar. 2003.

[3] J. K. Sheu, Y. K. Su, G. C. Chi, P. L. Koh, M. J. Jou, C. M. Chang, C. C. Liu, and W. C. Hung, Appl. Phys. Lett., vol. 74, pp. 2340-2342, Apr. 1999.

[4] T. Margalith, O. Buchinsky, D. A. Cohen, A. C. Abare, M. Hansen, S. P. DenBaars, and L. A. Coldren, Appl. Phys. Lett., vol. 74, pp. 3930-3932, Jun. 1999.

[5] R. H. Horng, D. S. Wuu, Y. C. Lien, and W. H. Lan, Appl. Phys. Lett., vol. 79, pp. 2925-2927, Oct. 2001.

[6] Y. C. Lin, S. J. Chang, Y. K. Su, T. K. Tsai, C. S. Chang, S. C. Shei, C. W. Kuo, and S. C. Chen, Solid-State Electronics, vol. 47, pp. 849-853, May 2003.

[7] K. -M. Chang, J. -Y. Chu, and C. –C. Cheng, IEEE Photon. Technol. Lett., vol. 16, pp. 1807-1809, Aug. 2004.

[8] L. Dai, B. Zhang, J. Y. Lin, and H. X. Jiang, J. Appl. Phys., vol. 89, pp. 4951-4954, May 2001.

[9] H. W. Choi, C. W. Jeon, M. D. Dawson, P. R. Edwards, R. W. Martin, and S. Tripathy, J. Appl. Phys., vol. 93, pp.5978-5982, May 2003.

[10] H. W. Choi, M. D. Dawson, P. R. Edwards, and R. W. Martin, Appl. Phys. Lett., vol., 83, pp. 4483-4485, Dec. 2003.

Chapter 7

Improved Light Output Power of GaN-based Light-Emitting Diodes by Exposing N-type GaN with Hexagonal Cavities

7.1 Introduction

GaN-based light emitting diodes (LEDs) have recently attracted much attention for their versatile applications and the rapid growth of market demand. Nowadays, the high-brightness GaN-based LEDs have already successfully applied in the handset keypad, LCD backlighting, camera flash light and full-color outdoor display since their commercial introduction in 1993 [1], [2]. However, even though the brightness of LEDs continues increasing, the light output efficiency is still quite low as compared to that of a conventional light source. Therefore, a better way of extracting more light from the devices or chips must be taken into consider immediately. It is well known that the external quantum efficiency is much smaller than the internal quantum efficiency for the current GaN-based LEDs. The large discrepancy between the two quantum efficiencies is due to the low light extraction efficiency, and the total internal reflection phenomenon must be mainly responsible for that. There is a large difference in refractive index at the interfaces of GaN-Air (2.5-1) and of GaN-Sapphire (2.5-1.8), and that would lead the critical angles [$\theta_c = \sin^{-1}(n_2/n_1)$] to 23° and 46° at these interfaces, respectively. Only the generated photons that strike these interfaces at angle within the critical angles can escape to the surrounding air,

others would be reflected back into devices. As a result, the majority of the generated photons are guided laterally through the air–GaN–sapphire waveguide structure and finally trapped in the semiconductor.

Several approaches have been proposed to solve this problem, including surface-roughening [3], [4], GaN growth on a patterned sapphire substrate [5]–[7], and the integration of two-dimensional photonic crystal patterns [8]–[10]. The idea behind these approaches is to interfere with the total internal reflection phenomenon using either the scattering or diffraction of light. Among these approaches, forming photonic patterns on the top of GaN devices is more difficult due to the precise sub-micron size controlling techniques. Huh et al. presented a method of making p-GaN micro-roughened to increase the light output efficiency by providing photons more opportunities to face escape cone. However, there are also some researches showing that the electrical characteristics of p-GaN would be deteriorated by dry etching [11].

In this chapter, a simple way to increase extraction efficiency of GaN-based LEDs without taking any other extra processing step is presented. A mesa structure formed by dry etch is utilized in GaN-based LEDs, and the exposed n-GaN surface could reveal various morphologies, such as smooth surface, nano-rods or hexagonal cavities dependent on etch conditions. LEDs with hexagonal cavities on exposed n-GaN layers are fabricated and characterized. The photons guided laterally through the air–GaN–sapphire structure would be partially interfered and extracted into the air through the hexagonal cavities. Therefore, the external quantum efficiency and power efficiency are enhanced.

7.2 Experimental

The InGaN–GaN multi-quantum-wells (MQWs) LED wafers were grown on c-face sapphire substrates by a metal-organic vapor phase epitaxy (MOVPE) reactor. The epitaxial structure consisted of 4-μm-thick n-GaN, 5 pairs of InGaN–GaN (MQWs) active layer, 0.2-μm-thick p-GaN, and a 10-nm-thick p-$In_{0.1}Ga_{0.9}N$ top layer. Moreover, the carrier concentrations of the p-GaN and n-GaN were 5 x 10^{17} cm^{-3} and 3 x 10^{18} cm^{-3}, respectively. A wafer with a peak wavelength at 460 nm was chosen and cut into two pieces. One piece was prepared for the LEDs with a smooth etched surface, and the other one was for LEDs with a hexagonal-pits etched surface.

SiO_2 layer was initially deposited on wafers by plasma enhanced chemical vapor deposition (PECVD) system as an etching mask, and the samples were subsequently etched to expose the n-type layer for electrode and cutting street regions by inductively coupled plasma (ICP) etcher. Proper tuning the working pressure, RF and ICP power of etching condition would make the surface smooth or hexagonal-pits morphology. The parameters of ICP etching utilized in this research are listed in table 7.1. Then, the samples were immersed in BOE, H_2SO_4 and NH_4OH solutions in sequence to strip SiO_2 mask, organic contaminants and native oxides followed by the deposition and patterning of indium tin oxide (ITO) films. The ITO films were evaporated on p-GaN layer as transparent conductive layers at 300°C in oxygen ambience with a partial pressure of 2 x 10^{-4} Torr by e-beam evaporation system. After patterning, these samples were subsequently annealed at 500°C in nitrogen ambience to achieve the optimal ohmic contact to p-GaN. Cr/Au (0.08 μm/0.8 μm) metallization films were employed for the n-type contact layer, p- and n- bonding pads. SiO_2 protection layer was deposited on the samples and patterned. Finally, the sapphire substrates were thinned to 90 μm thick by polishing, and the samples were scribed

and sliced into chips. 10 chips from each kind of samples were chosen to package into TO-Can forms.

The current-voltage (I-V) measurements were performed at room temperature by an HP4156 semiconductor parameter analyzer in wafer form. An IS CAS-140B optical analyze system was connected with a Keithley 2430 source meter to measure the current-power and current-luminescence characteristics of chips. Scanning electron microscopy (SEM) was used to justify the surface morphology of the exposed region and was performed by the model of JEOL JSM-6380.

Table 7.1 List of ICP dry etching conditions

Morphology	Cl_2/CH_4 (sccm/sccm)	Work pressure (mT)	RF Power (W)	ICP Power (W)	Etch Rate (nm/min)
Smooth	80 / 4	5	100	150	220
Hexagonal Pits	80 / 4	20	30	800	105

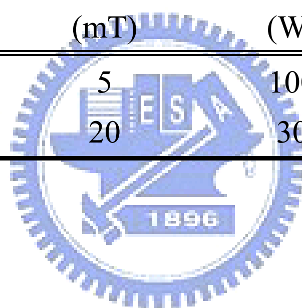

7.3 Results and discussion

Figure 7.1 shows the SEM and the microscopic emission pictures of the LEDs with smooth and hexagonal-pits n-GaN. The emission images are taken when the LEDs are operated under 0.1 mA-current-injections. From the SEM pictures, it can be clearly seen that the chip indeed reveals hexagonal pits on the exposed n-GaN layer by chemical reaction dominant dry etching. When the diodes are turned on, light spots can be observed in the diode with hexagonal-pits n-GaN layer but not in the diode with smooth layer. Therefore, the photons guided laterally through the air–GaN–sapphire structure are partially interfered and thus the photons can extract through the hexagonal cavities into the air.

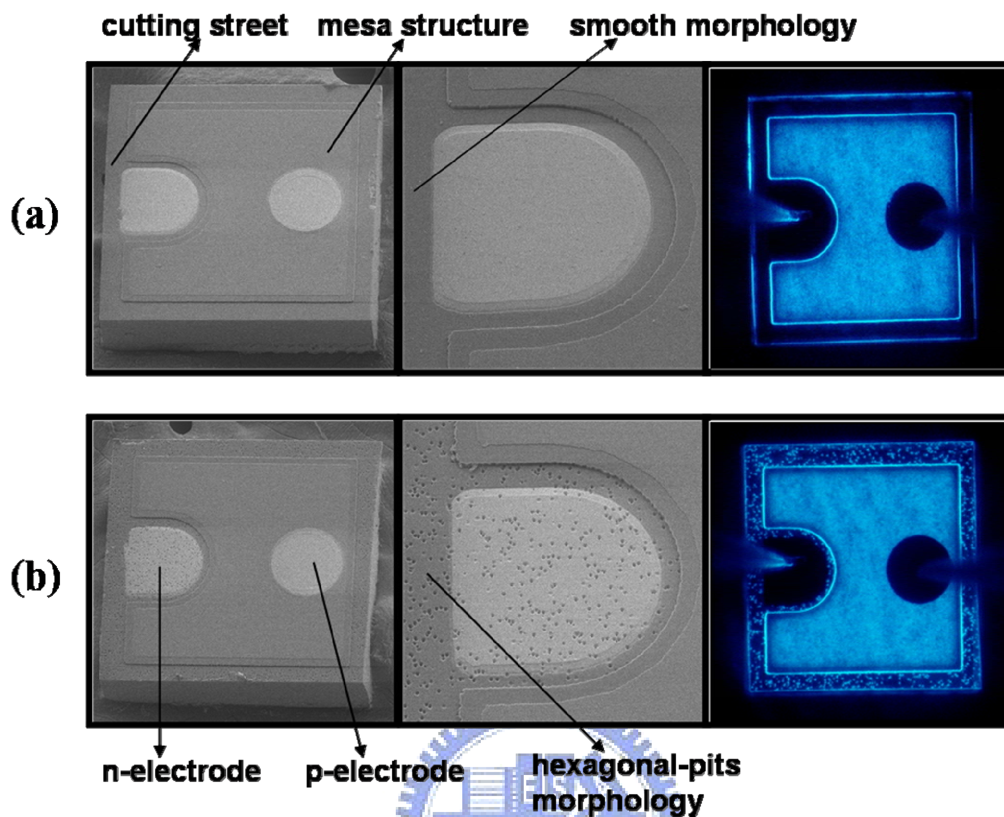

Fig. 7.1 SEM and Microscopic emission images of the LEDs with smooth and hexagonal-pits n-GaN.

Figure 6.2 plots the current-voltage characteristics of the LEDs with different exposed n-GaN surface. Both LEDs with smooth and hexagonal-pits n-GaN surface exhibit very similar forward and reverse electrical properties. The I-V curves of the smooth and hexagonal-pits devices are nearly coincident. From the result, the different dry etching condition to reveal hexagonal pits n-GaN would not do damage on the sidewall of mesas and deteriorate the n-type ohmic contacts, otherwise, the LEDs with hexagonal-pits n-GaN would show leakage current under reverse biased and a higher forward voltage as a current injected.

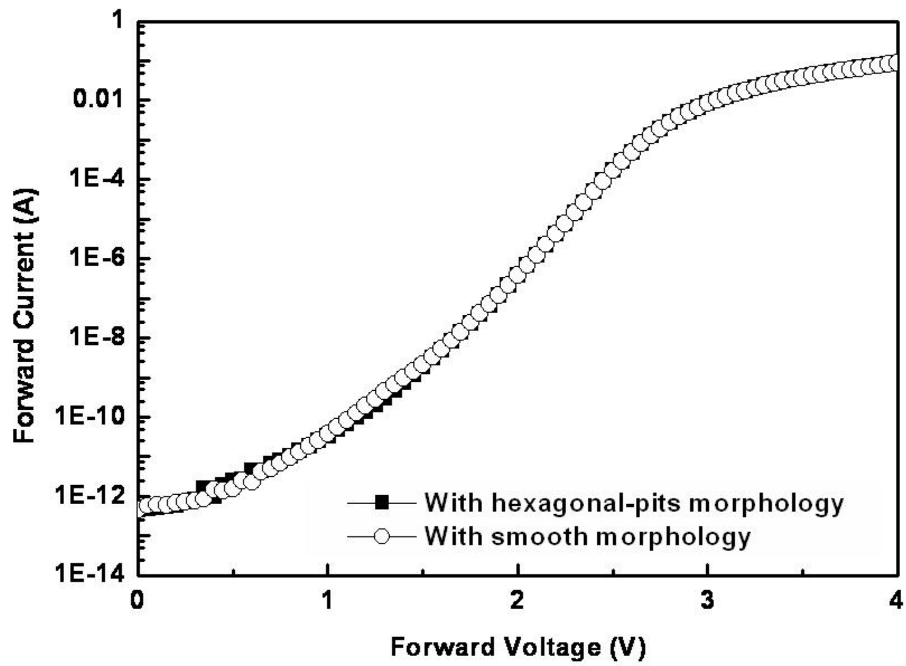

(a)

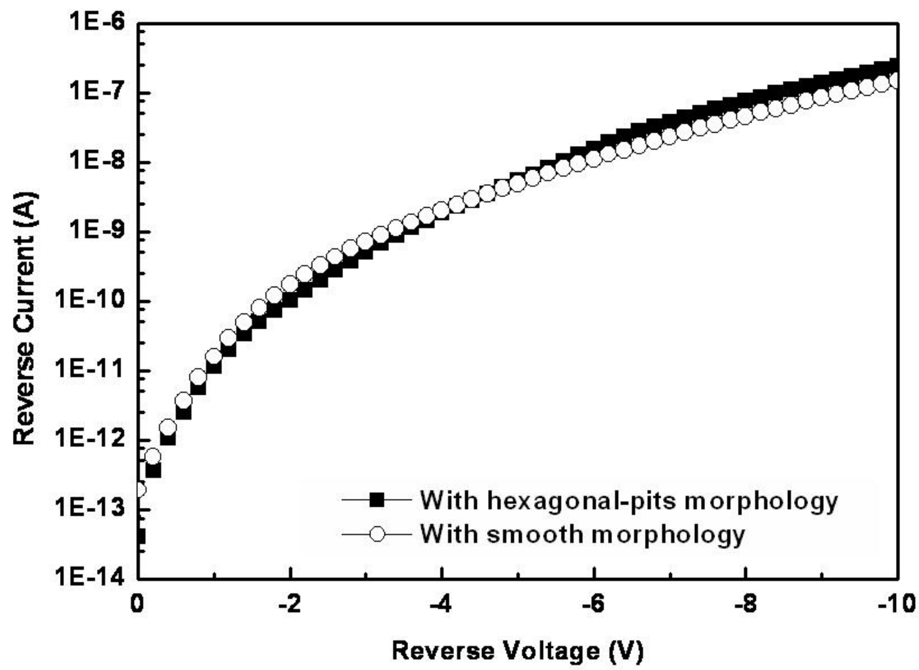

(b)

Fig. 7.2 (a) Forward and (b) reverse current-voltage characteristics of the LEDs with different n-GaN morphologies.

Figure 7.3 plots the current-luminescence and current-power relationships of LEDs. The LEDs with hexagonal-pits n-GaN exhibits the normal luminescence of 64.8 mcd and the output power of 5.45 mW at a 20-mA-current injection. The normal luminescence and the output power are enhanced by 27% and 13% respectively in comparison with that of LEDs with smooth surface.

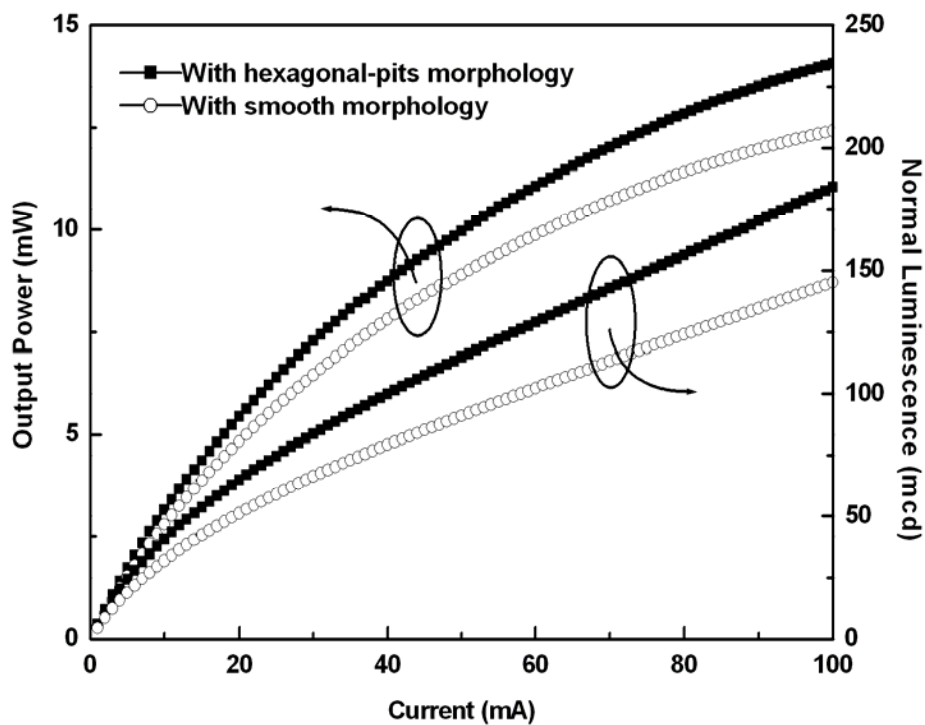

Fig. 7.3 Current-luminescence and current-power characteristics of the LEDs with different n-GaN morphologies.

Figure 7.4 also plots the ratio of normal luminescence to the output power of the LEDs with different n-GaN morphologies versus the injected currents. The ratio represents the concentration of the extracted light in the axial direction. The LEDs with hexagonal-pits n-GaN normally reveal a 12% higher ratio than that with smooth

surface. Therefore, the LED with hexagonal-pits n-GaN is more suitable for the application in surface mounting devices (SMD). The brightness improvement might be attributed to the increased scattering probability of the photons extracted through the exposed n-GaN region in the axial direction.

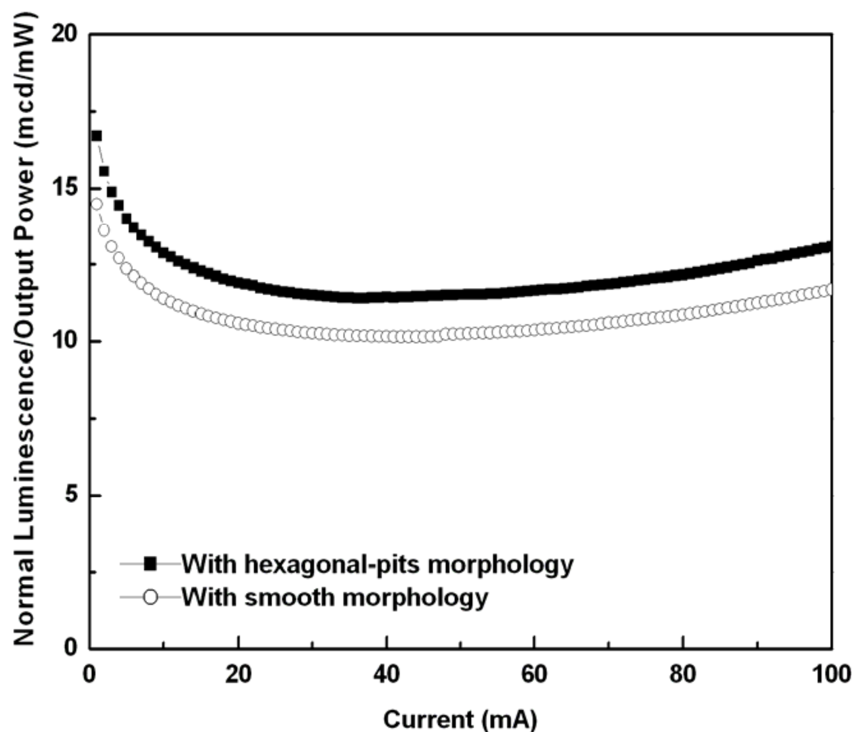

Fig. 7.4 Ratios of normal luminescence to output power the LEDs with different n-GaN morphologies.

Figure 7.5 schematically shows the possible paths of the photon guided laterally through the air–GaN–sapphire waveguide structure with roughened n-GaN. For a LED with rough n-GaN surface, the guided photons can escape the semiconductor through the hexagonal cavities. Therefore, the n-GaN with hexagonal-pits morphology can improve the probability of escaping the photons outside from the LEDs, thus, resulting in an increase in the light output power and luminescence.

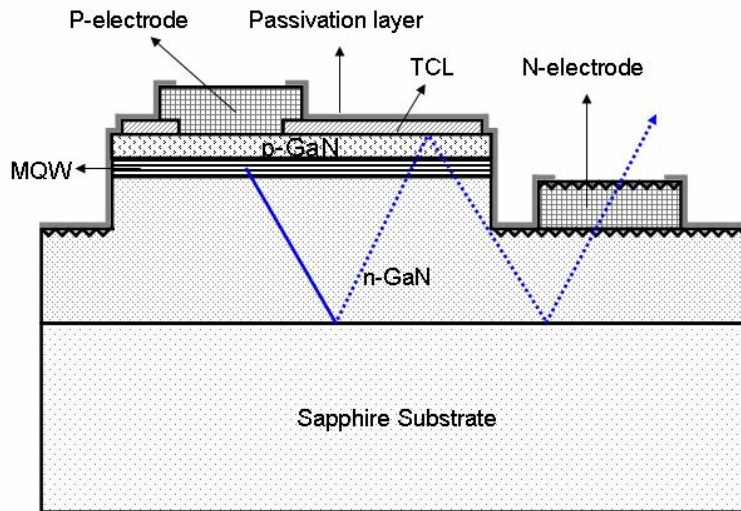

Fig. 7.5 Schematic diagram showing possible extraction paths of the photons laterally guided in the air-GaN-sapphire waveguide structure through hexagonal cavities.

7.4 Summary

In summary, we propose a simple way to increase extraction efficiency of GaN-based LEDs without taking any other extra processing step. Proper dry etching condition would result in smooth, hexagonal pits or nano-rods morphology. In this study, we employed the dry etch techniques to expose n-GaN with hexagonal pits rather than nano-rods morphology, because n-type bonding pads on n-GaN with a nano-rods surface would cause a peeling problem. From the current-voltage measurement results, LEDs with different n-GaN morphologies both show very similar electrical characteristics. The different dry etching condition to reveal hexagonal-pits n-GaN would neither do damage on the sidewalls of mesas nor deteriorate the n-type ohmic contacts. In the optical measurements, the LEDs with hexagonal-pits n-GaN exhibit the normal luminescence of 64.8 mcd and the output

power of 5.45 mW at a 20-mA-current injection. The normal luminescence and the output power normal luminescence are enhanced by 27% and 13% respectively in comparison with that of LEDs with smooth surface. Therefore, the power efficiency is increased by 13% by utilizing dry etching techniques to form hexagonal cavities in the exposed n-GaN layer.

References

[1] S. Nakamura, M. Senoh and T. Mukai, Jpn. J. Appl. Phys., vol. 32, pp. L8-L11, Jan. 1993.

[2] S. Nakamura, S. Pearton and G. Fasol, The Blue Laser Diode, Springer, New York, 2000.

[3] C. Huh, K. -S. Lee, E. –J. Kang, and S. –J. Park, J. Appl. Phys., vol. 93, pp. 9383-9385, Jun. 2003.

[4] L.W. Wu, S.J. Chang, Y.K. Su, R.W. Chuang, Y.P. Hsu, C.H. Kuo, W.C. Lai, T.C. Wen, J.M. Tsai, and J.K. Sheu, Solid-State Electronics, vol. 47, pp. 2027-2030, Nov. 2003.

[5] K. Tadatomo, H. Okagawa, Y. Ohuchi, T. Tsunekawa, Y. Imada, M. Kato, and T. Taguchi, Jpn. J. Appl. Phys., vol. 40, pp. L583-L585, Jun. 2001.

[6] M. Yamada, T. Mitani, Y. Narukawa, S. Shioji, I. Niki, S. Sonobe, K. Deguchi, M. Sano, and T. Mukai, Jpn. J. Appl. Phys., vol. 41, pp. L1431-L1433, Dec. 2002.

[7] J. Cho, H. Kim, H. Kim, J. W. Lee, S. Yoon, C. Sone, Y. Park, and E. Yoon, Phys. Stat. Sol. (c), vol. 2, pp. 2874-2877, Mar. 2005.

[8] T. N. Oder, K. H. Kim, J. Y. Lin, and H. X. Jiang, Appl. Phys. Lett., vol. 84, pp. 466-468, Jan. 2004.

[9] J. J.Wierer,M. R. Krames, J. E. Epler, N. F. Gardner,M. G. Craford, J. R. Wendt, J. A. Simmons, and M. M. Sigalas, Appl. Phys. Lett., vol. 84, pp. 3885-3887, May 2004.

[10] D.-H. Kim, C.-O. Cho, Y.-G. Roh, H. Jeon, Y. S. Park, J. Cho, J. S. Im, C. Sone, Y. Park, W. J. Choi, and Q.-H. Park, Appl. Phys. Lett., vol. 87, pp. 203508, Nov. 2005.

[11] K. -M. Chang, C. –C. Cheng, and J. –Y. Chu, J. Electrochemical Society, vol. 149, pp. G367-G369, Jul. 2002.

Chapter 8

Conclusion and Future Work

8.1 Conclusion

In Part 1, indium tin oxide (ITO) is employed to replace conventional Ni/Au contacts on p-GaN attributed to its high transparency characteristic. However, it is difficult to form an ohmic contact of ITO on p-GaN due to the large work function difference between ITO and p-GaN. A thin p-type $In_{0.1}Ga_{0.9}N$ layer is added as an intermediate layer to reduce the Schottky barrier height between ITO and p-GaN because p-$In_{0.1}Ga_{0.9}N$ is supposed to have a narrower band-gap than p-GaN. According to the variation of the contact resistivity with respect to the ambient temperature, the dominant transport mechanism of ITO/p-$In_{0.1}Ga_{0.9}N$/p-GaN interfaces varies with the post alloying temperature. The transport mechanism has a tendency from thermionic-field emission to thermionic emission as rising alloyed temperature from 400°C to 600°C. From the XPS, XRD and SIMS results, the out-diffusion of gallium atoms and the formation of Ga-O bonds would introduce gallium vacancies and increase the net concentration of carriers beneath the contact, which would make the ITO/p-$In_{0.1}Ga_{0.9}N$/p-GaN contact reveal ohmic characteristic.

Although ITO contacts with p-type $In_{0.1}Ga_{0.9}N$ intermediate layer does not reveal as good ohmic property as Ni/Au contacts on p-GaN, a contact resistivity of around 2.6 x 10^{-2} ohm-cm^{2} at a current density of 27 A-cm^{-2} is shown and the value is low enough for the application of LEDs. GaN-based LEDs with ITO contacts exhibit the

forward voltage of 3.43 V at an injection current of 20 mA. The forward voltage is a little higher than the conventional LEDs by 0.2 V, but the external quantum efficiency and power efficiency are raised by 46% and 36%, respectively. As for the life test, LEDs with ITO contacts annealed at 500°C exhibit a similar reliability as the LEDs with conventional Ni/Au contacts. Therefore, ITO contacts with p-$In_{0.1}Ga_{0.9}N$ intermediate layer can make GaN-based LED highly bright and reliable in practice.

GaN-based LEDs with various quarter wavelength thicknesses of ITO films are fabricated and characterized. Chips with various thicknesses of ITO films show nearly coincident output power-current curves and exhibit an enhancement of 30% as compared with Ni/Au contacts. At a current of 20 mA, the forward voltage is around 3.45, 3.42, and 3.32 V for devices with 60, 180, and 300-nm-thick ITO contacts, respectively. Thus, the power efficiency of LEDs with thicker ITO contacts is higher than that of devices with thinner ITO contacts because of the lower forward voltage. Moreover, from the simulation of current density distribution in devices, the LED chips with 60nm-thick ITO contacts present a worse uniformity and it is considered to cause a severe current crowding phenomenon and to introduce local hot spots when devices are operated. Consequently, the LED chips with 60nm-thick ITO contacts suffered an output power degradation of 48% after 1008-hour stress and the situation still went worse. On the other hand, LEDs with 300nm-thick ITO contacts exhibits a stable output after 1008-hour stress with merely 27% decay. Therefore, it is necessary to handle the lateral current conduction to alleviate local hot spots formation as devices operated especially for the conductive oxide material with low conductivity.

In Part 2, two structure modifications are proposed to increase the light extraction coefficient. First, a feasible method for fabricating micro-LEDs with ITO contact is demonstrated. The self-aligned micro-net LEDs are a least 10% brighter than the conventional structure in the normal direction without sacrifices of operating voltage

and leakage current. The ratio of luminescence to total output power is increased by 25% at a current density of 100 A/cm^2. Moreover, the peak value of external quantum efficiency can be increased by 5% by varying the dimensions and the density of the holes at a low current of 3 mA. With higher normal luminescence and external quantum efficiency, LEDs with such a structure are quite useful in surface-mounting and low-power-consuming devices.

Secondly, a simple way to increase extraction efficiency of GaN-based LEDs without taking any other extra processing step is presented. Different dry etching conditions would result in smooth, hexagonal pits or nano-rods morphology. LEDs with hexagonal cavities on exposed n-GaN layers are exhibited and characterized. From the current-voltage measurement results, chips with different n-GaN morphologies both show very similar electrical characteristics. The different dry etching condition to reveal hexagonal-pits n-GaN would neither do damage on the sidewalls of mesas nor deteriorate the n-type ohmic contacts. In the optical measurements, the LEDs with hexagonal-pits n-GaN exhibit the normal luminescence of 64.8 mcd and the output power of 5.45 mW at a 20-mA-current injection. The normal luminescence and the output power normal luminescence are enhanced by 27% and 13% respectively in comparison with that of LEDs with smooth surface. Therefore, the power efficiency is increased by 13% by utilizing dry etching techniques to form hexagonal cavities on the exposed n-GaN layer. The photons guided laterally through the air–GaN–sapphire structure are partially interfered and extracted into the air through the hexagonal cavities.

8.2 Future Works

The work presented in this dissertation is concentrated on the output power enhancement of GaN-based LEDs. There are substantial issues that are unresolved and some that were not investigated in this study. For high performance GaN-based light-emitting devices to be realized to the applications of solid-state lighting, further investigation must be conducted with the suggestions presented below.

Further investigation of the ohmic contact formation of ITO on p-GaN by adding a thin p-InGaN layer should be conducted. Although the formation of Ga-O bondings is confirmed, the role of p-InGaN is still not analyzed and discussed. After a more detailed understanding of p-InGaN is achieved, a better interface of ITO/p-GaN could be obtained and the corresponding specific contact resistivity would be reduced by the optimization of the intermediate layer. Optimization of the electrical and optical characteristics of GaN-based LEDs with ITO contacts present in this dissertation is a next step. ITO deposited by e-beam evaporation system is a kind of polycrystalline structure. The quality of ITO films would strongly affect the characteristics of transparency and electrical resistivity, and the post alloying condition would also influence the contact property of ITO on p-GaN. Therefore, it is necessary to optimize the evaporation condition of ITO films and the post alloy condition of ITO/p-GaN interfaces. Hence, the power conversion efficiency of GaN-based LEDs would be increased attributed to the less power consumption and high-brightness GaN-based LEDs can be obtained in the future.

In order to fulfill the requirements of solid-state lighting, one possible way to enhance the output power is to increase the extraction coefficient of LED chips just like studied in this dissertation. The other possible way to increase the LED output power is to increase the size of LED chips. Large size high power GaN-based LEDs

operated under high current injection would generate sufficient luminescence. Hence, high power LEDs with ITO contacts and surface structure modification should be fabricated and characterized in the future.